UAB
Universitat Autònoma de Barcelona

Doctoral Program in Medicine

Department of Medicine

DOCTORAL THESIS

TARGETED BIODEGRADABLE NANOPARTICLES OF SIMVASTATIN

AS NEW THERAPEUTIC TOOL FOR CHRONIC LIVER DISEASE

Doctoral Thesis for the PhD Degree of
Mar Gil Soler

Doctoral Thesis Supervisors:

María Martell Pérez-Alcalde, PhD

Diana Hide Alférez, PhD

Doctoral Thesis Academic Tutor:

Joan Genescà Ferrer, MD, PhD

Barcelona, 2023

Vall d'Hebron
Institut de Recerca

ACKNOWLEDGEMENTS

En primer lloc, vull agrair especialment a les meves directores, la María i la Diana, i al meu tutor, el Joan, totes i cadascuna de les fulles d'aquesta tesi, ja que sense ells aquest treball no hagués estat possible. Gracias María por haberme dado la oportunidad de trabajar en el laboratorio de Enfermedad Hepática Crónica Avanzada, abriéndome sus puertas de par en par, y haber confiado en mí para este proyecto, así como por haber sido mi guía en cada paso de este largo camino y hacerme sentir siempre orgullosa del trabajo realizado, donde en ocasiones menos es más. Diana, gràcies per tots els coneixements que m'has aportat, per la teva paciència al principi i la teva confiança al final, per haver-me ensenyat a ser una treballadora incansable i ser un exemple a seguir. I Joan, agrair-te el suport que m'has donat des d'un inici i que m'ha permès arribar fins aquí, aportant la teva gran experiència i ensenyament, veient sempre les coses des d'un punt de vista diferent i únic. De tot cor, moltes gràcies!

Seguint dins el laboratori, donar-los també una (i mil gràcies) a les altres dues persones que han estat clau al llarg d'aquest procés. A tu Imma, per ser la millor tècnic que una predoc com jo podria somiar, ajudant-me a mi (i a tots els que hem passat per allà, ho puc assegurar) en cadascun dels moments que t'he necessitat, i tot sempre amb un somriure a la cara (i mira que les hem vist de tots colors, sobretot amb el *superglue* jaja). No ho oblidi, ets el pilar d'aquest laboratori i agraeixo infinitament haver-hi coincidit amb tu! Y a ti Aurora, mi *partner in crime* desde el primer segundo. Empezamos en el máster juntas y desde entonces nuestros caminos han ido de la mano, llegando a un mismo final del cual no podría estar más orgullosa. Has sido mi apoyo en esta montaña rusa que llamamos doctorado, entendiéndome mejor que nadie y ayudándome para que me mantuviera siempre a flote. De verdad que no hubiera podido tener mejor compañera en los buenos y "no tan buenos" momentos que hemos vivido, por lo que solo deseo haber podido ser ese mismo apoyo para ti, ya que te lo mereces más que nadie. Así que a ti también, ¡enhorabuena por todo lo que has logrado Dra. Barberá!

principi, el grau de Ciències Biomèdiques. Reconec que no podria haver escollit millor carrera, i no ho dic tan sols pel camí on m'ha portat, sinó també per tota la gent meravellosa que em vaig endur d'aquells quatre anys a la UAB, on les hores i hores d'estudi ara se'm fan curtes si les comparo amb els bons moments que vaig gaudir, impossibles ja d'oblidar (perquè el que passa a les colònies... es queda al teu hipocamp!). Per tant, gràcies a tothom que hi va formar part, però especialment a les meves Irenes (a les tres xD), a l'Adri, la Blanca, la Carla i la Lídia, per haver compartit amb mi aquests moments tan de prop i fer-me sentir que no podria haver tingut unes millors companyes i company per a aquesta aventura biomed. Així que ara i sempre, ina, ina, ina... biomedicina!

Durant aquest temps, però, no tot ha sigut estudiar i treballar, ja que per sort també hi ha hagut moments per desconnectar i deixar anar les preocupacions i tensió acumulades. I quin millor lloc per fer-ho que dins una pista de pàdel? Doncs sí, la veritat que poder descarregar tot l'estrès d'un doctorat (que déu-n'hi-do) a cop de pala ajuda moltíssim, però encara més si ho pots fer rodejada d'un equip tan fantàstic com el meu, que ha arribat per donar-ho tot. Merci a totes, sou la puta Revolució!

I en aquesta llista no podia faltar un lloc especial per a tu. Carol, els estius a Calafell sempre estaran lligats al teu nom i encara que cada cop es facin més curts, sé que passi el temps que passi, estiguem on estiguem, la teva amistat perdurarà com el primer dia, esperant per posar-nos al dia amb totes les novetats fent un passeig per la platja a la vora del mar o recordant les nostres ximpleries de quan érem unes cries i tot semblava possible (qui no voldria ser una gota eh?!). Aquesta tesi també va dedicada a tu!

Evidentment, vull agrair a cadascun dels meus companys de pis la magnífica experiència d'haver compartit amb ells aquests anys frenètics a Barcelona. A tu Marc, per entendre'm tan bé i comprendre tot el que comporta el doctorat, que sabem ens ha fet riure i queixar-nos a parts iguals, però junts ho hem lluitat fins al final. Així que ara que et queda ben poc, donar-te molts ànims en aquest últim esforç, perquè et mereixes aquest títol més que ningú! A ti Mario, que doy las gracias por esas casualidades de la

vida y haberte encontrado ese día buscando piso en un edificio (del siglo XIII mínimo) en pleno centro de Pisa, ahora ya nuestra colmena. Desde entonces te he tenido siempre a mi lado y espero que siga así por muchos años más, ¡ya que no quiero ponerle fin a esta experiencia Erasmus! I a tu Mariona, la meva viatgera incansable, que sé que per molta distància que ens separi (mai se sap on aniràs a parar) la nostra amistat seguirà tan forta com sempre i que siguis on siguis arribaràs ben lluny amb el teu talent i la teva creativitat, ja que ets imparable. Mil gràcies als tres!

Antes de dejar Barcelona, pero, no me quiero olvidar de vosotros. De mi grupito de gallegos favorito, que me habéis hecho sentir una más (literal, mi acento lo puede corroborar) y me habéis hecho descubrir esta ciudad a otro nivel, siendo yo de aquí xD. Así que Igor, Mario y Héctor, moitas grazas de todo corazón!

De l'última etapa a Rubí no puc estar més agraïda tampoc. Us dono les gràcies, Sebas i Jana, per haver-me acollit a casa vostra, amb la Nala i la Syra, per descomptat, i haver-me abraçat com a una membre més de la vostra família de la forma més senzilla possible. No mentiria si dic que m'heu vist més hores que ningú davant de l'ordinador escrivint i sabeu tota la feina que hi ha darrere d'aquesta tesi, però heu aconseguit que dins d'aquesta voràgine trobés moments per gaudir de les petites coses quotidianes, com seure's al sofà a veure un, i dos i tres, capítols d'una sèrie o preparar el sopar tots junts mentre comentem el dia. De manera que espero poder-vos-ho compensar compartint molts més moments junts ara que això s'ha acabat! I dono les gràcies també pel fet que haver-me mudat a aquesta ciutat m'ha permès sentir més a prop que mai a una amiga com tu Júlia. Que naixéssim el mateix dia no crec que fos casualitat, i és que la connexió que sento amb tu ha de ser cosa del destí. No podríem ser més diferents, però a la vegada som tan iguals que realment fem un tàndem espectacular. Ets una persona única i t'agraeixo molt que hagis estat sempre al meu costat!

Per acabar, volia dir que aquests agraïments no tindrien cap mena de sentit si no les mencionés a elles, a les persones que considero la meva família. Primer de tot, a la família que un escull i que, en el meu cas, penso ha sigut l'elecció més fàcil i la més

encertada que hagi pogut fer. Amb la gran majoria he tingut la sort increïble de coincidir des de la infància, de manera que porten al meu costat tota una vida, i amb els que no, en fi, sento com si us conegués de sempre i així m'ho heu transmès. I que puc dir de tots ells? Doncs si em posés a mencionar cadascuna de les coses bones que m'han aportat podria passar-me hores escrivint i no acabaria mai. Han estat la meva àncora en els moments en què creia que el corrent se m'enduria i han estat el corrent pel qual deixar-se portar per poder continuar endavant. Tant se val si hem estat més a prop o més lluny, si havien passat uns dies o uns mesos, una quedada de les nostres i tot s'aturava per uns instants, recordant-me que qui té un amic té un tresor i que a mi m'ha tocat el més preuat. I no són poques les ocasions en què m'heu fet riure fins a plorar, rememorant una vegada i una altra (i no me'n cansaria mai) les nostres anècdotes, ja siguin d'una festa major, un Cap d'Any, la baixada del pi, un viatge d'estiu o de qualsevol de les mil i una calçotades, barbacoes, sopars... que hem arribat a fer per alguna ocasió especial o simplement pel plaer d'estar junts. No voldria fer-me pesada, però és que no trobo paraules suficients per descriure què ha significat per a mi poder comptar amb vosaltres en aquest període tan especial i tan bonic de la meva vida (i també tan dur, siguem clars), i saber que em porti on em porti ara, sense por a equivocar-me, puc estar tranquil·la, ja que hi seguireu estant per sempre. Sou la millor penya del món, així que us estaré eternament agraïda: Alba, Arola, Carlota i Rosa, perquè senzillament us estimo amb tot el meu cor; Blasi, López, Àlex, Jan i Arnau, perquè per molt que passin els anys sempre sereu els meus nens; Ilaria, Mireia, Laura, Júlia i Marta, perquè mai és tard per a una amistat de veritat; i a tots els nouvinguts i nouvingudes, perquè em fa feliç ampliar la nostra família.

Finalment, i si heu tingut paciència per arribar fins aquí, dir-vos que per ells esteu llegint això avui. I no em puc referir a ningú més que a la meva família de veritat, la que no s'escull, però a qui li importa si un té tanta sort com la meva. Semblaria la cosa més fàcil agrair-los tot el que han fet per mi al llarg d'aquests vint-i-set anys, però encara que es diu ràpid, no ho és tant. De fet, menteixo, perquè realment sé que qualsevol cosa que els pugui dedicar a ells els semblarà perfecte i estaran contents i feliços d'escoltar-la,

perquè no hi ha amor més gran i incondicional que el que puguin sentir els teus éssers estimats. Sé també que no podrien estar més orgullosos de mi per haver arribat fins on he arribat, per poder afirmar que m'he doctorat, però sincerament tant se val el títol, el sentiment d'orgull hagués estat el mateix fos quin fos el camí que hagués escollit, perquè sempre m'han recolzat en qualsevol decisió que he pres. Així mateix, ells m'han ensenyat a creure en mi en tot moment, a no posar mai en dubte el que valc, que si m'ho proposo, res em pot frenar i tot és possible. Us dono les gràcies per haver-me criat de la millor manera que heu sabut, per inculcar-me valors com l'amor mutu, l'amistat, la generositat, l'esforç, la perseverança, la valentia, la humilitat, l'empatia... i per ser un exemple de les persones que un dia vull arribar a ser. De moment soc com soc i estic aquí gràcies a vosaltres, per tant, aquesta tesi és tan meva com vostra. Mama, papa, iaia i tiet, l'orgull és meu per poder-vos dedicar aquestes paraules, i a tots els que hi van ser. Us estimo moltíssim! I a la Niula i la Tina també, que no me les podia deixar!

Gràcies a tots per formar part d'aquest procés i de la meva vida,

Res puc afegir aquí que no us hagi dit ja.

Agraïda pel suport de tota la gent amb qui he pogut comptar,

Crec que no us podria merèixer més i tenir amb més estima.

I tot i que aquesta etapa hagi arribat a la seva fi,

En el nou camí que està per començar

Sé ben segur que sempre us portaré amb mi!

Rubí, 4 de març de 2023

ABBREVIATIONS

The abbreviations are listed alphabetically.

ABC	Amphiphilic block copolymer/s
aHSC	Activated hepatic stellate cell/s
Akt	Protein kinase B, PKB
ALD	Alcoholic liver disease
ALP	Alkaline phosphatase
ALT	Alanine aminotransferase
Ang II	Angiotensin II
ANOVA	Analysis of variance
ARBs	Angiotensin receptor blockers
Arg	Arginine
ARG-1	Arginase-1, Arg1
Asp	Aspartic acid
AST	Aspartate aminotransferase
BDL	Bile duct ligation
BSA	Bovine serum albumin
CCL	Chemokine (C-C motif) ligand
CD	Cluster of differentiation
cDNA	Complementary deoxyribonucleic acid
CD31	Platelet endothelial cell adhesion molecule, PECAM-1
CD32b	Fc-gamma receptor IIb2, FcγRIIb2, SE-1
CD36	Thrombospondin receptor
cGMP	Cyclic guanosine monophosphate
CK	Creatine kinase
CLD	Chronic liver disease/s
CMC	Critical micelle concentration
CMT	Critical micelle temperature
COL1A1	Collagen type I alpha 1 chain
CYP3A4	Cytochrome P450 3A4
Cys	Cysteine
DALYs	Disability-adjusted life years
DAMPs	Damage-associated molecular patterns
DAPI	4',6-Diamidino-2-phenylindole
DCM	Dichloromethane
dH_2O	Distilled water
DIPEA	*N,N*-Diisopropylethylamine
DiR	1,1'-Dioctadecyl-3,3,3',3'-tetramethylindotricarbocyanine iodide, $DiIC_{18}(7)$
DLS	Dynamic light scattering

DMEM	Dulbecco's Modified Eagle's Medium
DMF	*N,N*-Dimethylformamide
DMSO	Dimethyl sulfoxide
dNTPs	Deoxynucleotide triphosphates
ECM	Extracellular matrix
EDC	1-Ethyl-3-(3-dimethylaminopropyl)carbodiimide
EE	Encapsulation efficiency
EGTA	Egtazic acid
eNOS	Endothelial nitric oxide synthase, Nos3
EPR	Enhanced permeability and retention
ET_A	Endothelin receptor type A, Ednra, ETA-R
ET-1	Endothelin-1, Edn1
ESI-MS	Electrospray ionization mass spectrometry
FBS	Fetal bovine serum
FcγR	Fc-gamma receptor
FFAs	Free fatty acids
FITC	Fluorescein 5-isothiocyanate
Fmoc	Fluorenylmethyloxycarbonyl protecting group
FPM	Functionalized polymeric micelle/s
FSC-A	Forward scatter area
FSC-H	Forward scatter height
FTIR	Fourier-transform infrared spectroscopy
GAPDH	Glyceraldehyde-3-phosphate dehydrogenase
GBSS	Gey's Balanced Salt Solution
GGPP	Geranylgeranyl pyrophosphate
GTP	Guanosine triphosphate
Gln	Glutamine
Gly	Glycine
HBV	Hepatitis B virus
HCC	Hepatocellular carcinoma
HCTU	*O*-(1*H*-6-Chlorobenzotriazole-1-yl)-1,1,3,3-tetramethyluronium hexafluorophosphate
HCV	Hepatitis C virus
HDL	High-density lipoprotein
H&E	Hematoxylin and eosin
HEPES	2-[4-(2-Hydroxyethyl)piperazin-1-yl]ethane-1-sulfonic acid
HMG-CoA	3-Hydroxy-3-methylglutaryl coenzyme A
HNF4	Hepatocyte nuclear factor 4 alpha, Hnf4a
HO-1	Heme oxygenase-1, Hmox1
HSC	Hepatic stellate cell/s
HVPG	Hepatic venous pressure gradient

ICAM-1	Intercellular adhesion molecule-1
IgG	Immunoglobulin G
IHC	Immunohistochemistry
IHVR	Intrahepatic vascular resistance
IL	Interleukin
IMDM	Iscove's Modified Dulbecco's Medium
IP	Intraperitoneal, intraperitoneally
I/R	Ischemia/reperfusion
IV	Intravenous, intravenously
KC	Kupffer cell/s
KLF2	Krüppel-like factor 2
LDL	Low-density lipoprotein
LOXL2	Lysyl oxidase-like 2
LSEC	Liver sinusoidal endothelial cell/s
Lys	Lysine
LYVE-1	Lymphatic vessel endothelial hyaluronan receptor-1
MAP	Mean arterial pressure
MHC	Major histocompatibility complex
mRNA	Messenger ribonucleic acid
MTD	Maximum tolerated dose
MWCO	Molecular weight cut-off
NAFLD	Non-alcoholic fatty liver disease
NASH	Non-alcoholic steatohepatitis
NCL	Native chemical ligation
NO	Nitric oxide
NQO1	Nicotinamide adenine dinucleotide phosphate quinone dehydrogenase-1
NSBB	Non-selective beta-blocker/s
OCT-1	Solute carrier family 22 (organic cation transporter) member 1, Slc22a1
OFA	Oncins France Strain A
O/N	Overnight
ox-LDL	Oxidized low-density lipoprotein
p-Akt	Phosphorylated protein kinase B
PBF	Portal blood flow
PBS	Phosphate-buffered saline
PDE-5	Phosphodiesterase-5
PDGFRB	Platelet derived growth factor receptor beta
PDI	Polydispersity index
PEG	Poly(ethylene glycol) or poly(ethylene oxide), PEO
p-eNOS	Phosphorylated endothelial nitric oxide synthase
PFA	Paraformaldehyde
PH	Portal hypertension

PM	Polymeric micelle/s
PP	Portal pressure
PPO	Poly(propylene oxide)
PRRs	Pattern recognition receptors
PVDF	Polyvinylidene difluoride
Q	Blood flow
qHSC	Quiescent hepatic stellate cell/s
qRT-PCR	Quantitative reverse transcription polymerase chain reaction
R	Resistance
RES	Reticuloendothelial system
RGD	Arginine-glycine-aspartic acid, Arg-Gly-Asp
RhoA	Ras homolog family member A
RIPA	Radioimmunoprecipitation assay
RNA	Ribonucleic acid
ROCK	Ras homolog family member A-associated protein kinase
ROS	Reactive oxygen species
RP-HPLC	Reversed-phase high-performance liquid chromatography
RPMI	Roswell Park Memorial Institute
RQ	Relative quantification
RT	Room temperature
SD	Standard deviation
SDS-PAGE	Sodium dodecyl sulfate polyacrylamide gels
SEM	Scanning electron microscopy / Standard error of the mean
Ser	Serine
SLCO1B1	Solute carrier organic anion transporter family member 1B1
SMABF	Superior mesenteric artery blood flow
SMAR	Superior mesenteric artery resistance
SOPF	Specific and opportunistic pathogen free
SPPS	Solid-phase peptide synthesis
TAA	Thioacetamide
TBS	Tris-buffered saline
TEM	Transmission electron microscopy
TFA	Trifluoroacetic acid
Thr	Threonine
TLRs	Toll-like receptors
TNF-α	Tumor necrosis factor alpha
TTBS	Tween®-Tris-buffered saline
TXA$_2$	Thromboxane A2
UATR	Universal Attenuated Total Reflectance
UPLC-MS/MS	Ultra performance liquid chromatography-tandem mass spectrometry
UV	Ultraviolet

VCAM-1	Vascular cell adhesion molecule-1
VEGF	Vascular endothelial growth factor
VLDL	Very-low-density lipoprotein
5-DTAF	5-([4,6-Dichlorotriazin-2-yl])aminofluorescein
α-SMA	Alpha-smooth muscle actin, Acta2
ΔP	Pressure gradient
Ø	Empty

TABLE OF FIGURES

15

TABLE OF TABLES

TABLE OF CONTENTS

ABSTRACT

Chronic liver disease (CLD) refers to any pathological state of the liver characterized by the progression from a state of fibrosis to the onset of liver cirrhosis or advanced CLD, one of the main complications being portal hypertension (PH). There are different causes that can induce liver injury, which can be life-threatening in case of liver failure, often requiring liver transplantation. There are currently very few treatments available to slow the progression of liver disease with PH. Statins have been one of the most extensively studied classes of drugs in recent decades, proving to be beneficial in the context of CLD, although causing certain adverse effects at the muscular and hepatic level.

To avoid the toxicity generated by statins in patients with this pathology, while increasing their therapeutic potential, this doctoral thesis is based on the development of nanoparticles as a drug delivery system for CLD and their study in experimental models of cirrhosis. Specifically, this work focuses on the use of polymeric micelles (PM) as nanodevices to encapsulate simvastatin, as the reference statin, and target it to liver sinusoidal endothelial cells (LSEC) due to the fundamental role played by these cells as sensors and drivers of CLD. Thus, the aim is to maintain the LSEC healthy phenotype to preserve the liver function. This thesis is divided into two studies: in the first study, two types of PM based on Pluronic® F127 and F108 polymers were evaluated for simvastatin delivery (PM-Sim) and tested in an advanced CLD model by bile duct ligation (BDL); in the second study, the PM-F127 was functionalized (FPM) by coupling peptide ligands of LSEC membrane receptors (CD32b, CD36 and integrin $\alpha_V\beta_3$ receptors) for active targeting of the nanoparticle to this cell type, and its efficacy was assessed in two experimental models of liver cirrhosis, by BDL and by thioacetamide (TAA) toxic induction.

PM-F127-Sim showed the highest cell internalization rates in isolated rat LSEC and significantly lower toxicity than free simvastatin, improving their cell phenotype *in vitro*. *In vivo* biodistribution of PM-F127 was mainly hepatic and after one week of

administration in the BDL model, PM-F127-Sim demonstrated a superior effect to free drug in reducing PH with no signs of toxicity. Functionalization of PM with different peptide ligands resulted in stable formulations with a greater degree of *in vivo* internalization in LSEC than untargeted PM. Administration of FPM-Sim in BDL rats reduced muscle and liver toxicity levels relative to free simvastatin, albeit with a moderate portal pressure lowering effect. In a less severe model of TAA-induced cirrhosis, treatment with the FPM-CD32b-Sim nanoparticle for two weeks significantly decreased portal pressure values, which was associated with a lower percentage of liver fibrosis, as well as stimulation of nitric oxide synthesis.

Altogether, the use of PM for simvastatin delivery is postulated as a safe and effective tool for the management of PH in non-decompensated CLD, being its functionalization with the peptide ligand CD32b a way to optimize its specific targeting to LSEC, improving the therapeutic potential of statins. Moreover, this delivery system could be used not only to encapsulate statins, but any beneficial drug or combination of them to improve dysfunctional LSEC.

RESUM

La malaltia hepàtica crònica (MHC) inclou qualsevol estat patològic del fetge caracteritzat per una fibrosi progressiva que condueix a l'aparició de cirrosi hepàtica o MHC avançada, sent una de les seves principals complicacions la hipertensió portal. Existeixen diferents causes que poden induir a una lesió hepàtica, la qual pot ser potencialment mortal en cas d'insuficiència hepàtica, sent necessari en molts casos un trasplantament de fetge. Actualment, existeixen molt pocs tractaments disponibles per a frenar la progressió de la malaltia hepàtica amb hipertensió portal. Una de les classes de fàrmacs més àmpliament estudiades en les últimes dècades són les estatines, que han demostrat ser beneficioses en el context de la MHC, tot i que poden provocar certs efectes adversos en l'àmbit muscular i hepàtic.

Per a evitar la toxicitat generada per les estatines en pacients amb aquesta patologia i augmentar-ne el potencial terapèutic, la present tesi doctoral es basa en el desenvolupament de nanopartícules com a sistema d'administració de fàrmacs per a la MHC i el seu estudi en models experimentals de cirrosi. En concret, aquest treball se centra en l'ús de micel·les polimèriques (MP) com a dispositius per a encapsular simvastatina, com estatina de referència, i dirigir-la a les cèl·lules endotelials sinusoidals hepàtiques (LSEC per les seves sigles en anglès, *liver sinusoidal endothelial cells*) a causa del paper fonamental que exerceixen aquestes cèl·lules com a sensors i impulsores de la MHC. En aquest sentit, la finalitat és mantenir el fenotip sa de les LSEC per a així preservar la funció hepàtica. La tesi es divideix en dos estudis: en el primer estudi es van avaluar dos tipus de MP basades en els polímers Pluronic® F127 i F108 per a l'administració de simvastatina (MP-Sim), i es van testar en un model de MHC avançada per lligadura del conducte biliar (BDL per les seves sigles en anglès, *bile duct ligation*); en el segon estudi la MP-F127 es va funcionalitzar (FMP) mitjançant l'acoblament de lligands peptídics de receptors de membrana de les LSEC (receptors CD32b, CD36 i integrina $\alpha_V\beta_3$) per a un adreçament actiu de la nanopartícula cap a aquest tipus cel·lular

i es va analitzar la seva eficàcia en dos models experimentals de cirrosi hepàtica, el de BDL i el d'inducció tòxica per tioacetamida (TAA).

La MP-F127-Sim va mostrar els majors índexs d'internalització cel·lular en LSEC aïllades de rata i una toxicitat significativament menor que la simvastatina lliure, millorant el seu fenotip cel·lular *in vitro*. La biodistribució *in vivo* de MP-F127 va ser principalment hepàtica i després d'una setmana d'administració en el model de BDL, la MP-F127-Sim va demostrar un efecte superior al del fàrmac lliure en la reducció de la hipertensió portal sense signes de toxicitat. La funcionalització de MP amb diferents lligands peptídics va resultar en formulacions estables amb un major grau d'internalització *in vivo* en LSEC que les MP no dirigides. L'administració de FMP-Sim en rates BDL va reduir els nivells de toxicitat muscular i hepàtica respecte a la simvastatina lliure, encara que amb un efecte reductor de la pressió portal moderat. En un model menys greu de cirrosi com l'induït per TAA, el tractament durant dues setmanes amb la nanopartícula FMP-CD32b-Sim va aconseguir rebaixar significativament els valors de pressió portal, la qual cosa es va associar amb un percentatge menor de fibrosi hepàtica, així com a l'estimulació de la síntesi d'òxid nítric.

En definitiva, l'ús de MP per a l'administració de simvastatina es postula com una eina segura i eficaç per al maneig de la hipertensió portal en la MHC no descompensada, sent la seva funcionalització amb el lligand peptídic de CD32b una manera d'optimitzar el seu adreçament específic cap a les LSEC, millorant el potencial terapèutic de les estatines. A més, aquest sistema d'administració podria ser utilitzat no tan sols per a encapsular estatines, sinó qualsevol fàrmac o combinació beneficiosa de fàrmacs per a millorar l'estat disfuncional de les LSEC.

1. INTRODUCTION

1. INTRODUCTION

1.1. Chronic liver disease

1.1.1. Epidemiology

Chronic liver disease (CLD) is defined as the final stage of a long period of inflammation that results in replacement of the healthy liver parenchyma with fibrotic tissue and regenerative nodules, leading to portal hypertension (PH). The disease evolves from an asymptomatic phase (compensated cirrhosis) to a symptomatic phase (decompensated cirrhosis), the complications of which often result in hospitalization, impaired quality of life, and high mortality. Progressive PH, systemic inflammation and liver failure drive disease outcomes. The management of liver cirrhosis is centred on the treatment of the causes and complications, and liver transplantation can be required in some cases[1–3] (Figure 1).
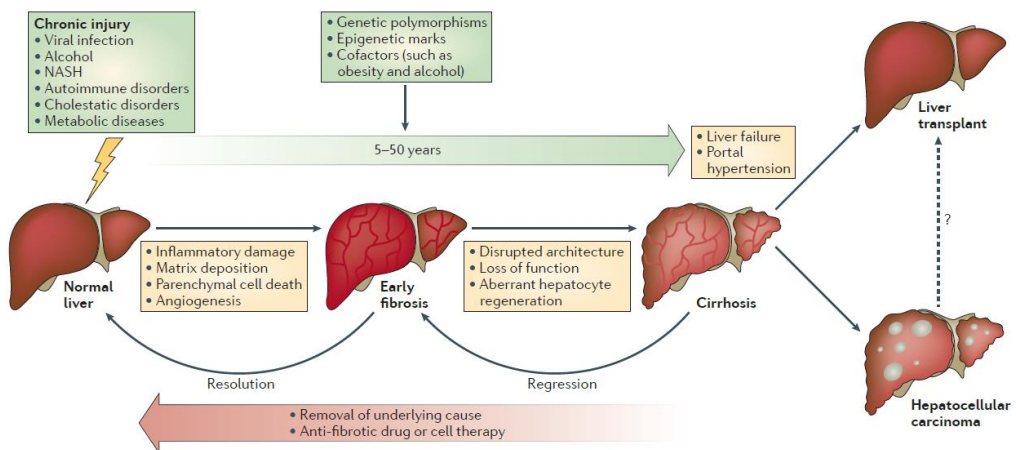
Figure 1. Natural history of CLD. NASH: non-alcoholic steatohepatitis. From Pellicoro A et al., Nat Rev Immunol 2014[2].

Cirrhosis is a leading cause of mortality and morbidity across the world. The Global Burden of Disease study in 2019[4,5] reported over 1.45 million deaths related to cirrhosis and other CLD, which was approximately 2.6% of all deaths worldwide, and 46.2 million disability-adjusted life years (DALYs), accounting for the 1.8% of global DALYs. Thus,

cirrhosis was the 10th leading cause of death and the 16th leading cause of DALYs. The prevalence of cirrhosis is difficult to assess and probably higher than reported, because the initial stages are asymptomatic so the disorder is undiagnosed[6], but the global prevalent cases of CLD (inclusive of any stage of disease severity) was estimated at 1.69 billion worldwide in 2019[4,5].

Cirrhosis can be a consequence of different causes, such as obesity, non-alcoholic fatty liver disease (NAFLD), alcoholic liver disease (ALD), hepatitis B (HBV) or C virus (HCV) infection, autoimmune diseases, cholestatic diseases, and iron or copper overload. Historically, viral hepatitis has been the leading etiology for CLD. However, improved prevention strategies (in the case of hepatitis B) and treatment (in the case of hepatitis C) have led to a change in trends in the primary etiology of CLD. In this sense, the most common causes of prevalent CLD are NAFLD (59%), HBV (29%), HCV (9%), and ALD (2%)[7–9].

1.1.2. Pathophysiology of PH

PH is a major complication of CLD and an important determinant of its disease course and prognosis, as almost 90% of the patients with cirrhosis eventually develop PH and this condition is a prequel to the majority of deaths in cirrhotic patients. In addition, PH can also develop in the absence of liver cirrhosis, which is called non-cirrhotic PH[10,11].

It is defined as increased pressure within the portal vein, the blood vessel connecting the outflow of the gastro-intestine and spleen (splanchnic organs), and the liver. CLD causes structural alterations of the liver via increased extracellular matrix (ECM) accumulation and turnover (fibrosis), and changes of the cellular phenotypes associated with dysfunction of liver sinusoidal endothelial cells (LSEC), activation of hepatic stellate cells (HSC) and inflamed resident or infiltrating macrophages. These changes induce a pathological increment in the intrahepatic vascular resistance (IHVR) to portal blood flow (PBF), which increases the portal pressure (PP) and is the initial step towards complications of CLD[12,13]. Secondary to the increase in IHVR, PH induces splanchnic and

systemic arterial vasodilation, leading to the development of a hyperdynamic circulatory syndrome and thereby aggravating and driving clinically detrimental complications[1,14] (Figure 2).
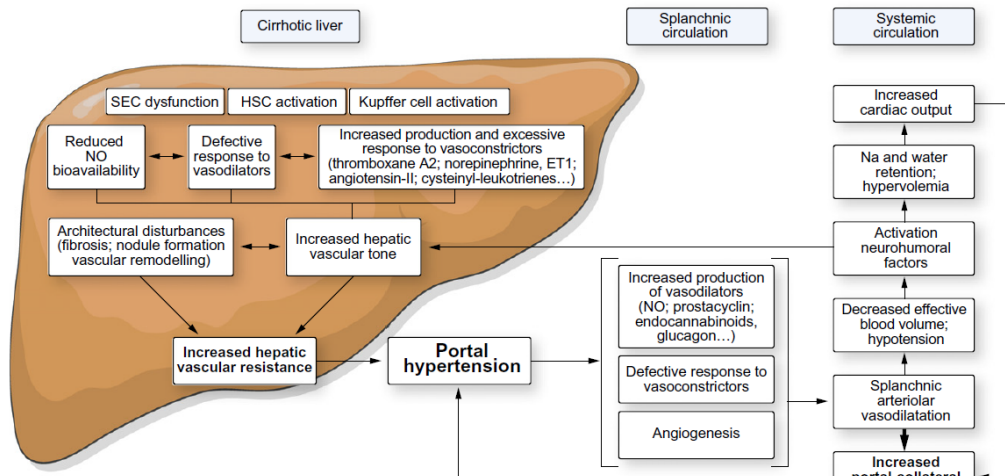
Figure 2. Pathophysiology of PH. ET1: endothelin-1, HSC: hepatic stellate cell, NO: nitric oxide, SEC: sinusoidal endothelial cell. From García-Pagán JC et al., J Hepatol 2012[15].

As mentioned, the natural history of CLD is characterized by an asymptomatic phase, termed compensated cirrhosis, followed by a rapidly progressive phase marked by the development of complications of PH, termed decompensated cirrhosis[16]. In the compensated stage, the development of clinically significant PH, defined by a hepatic venous pressure gradient (HVPG) of at least 10 mmHg, heralds the formation of portosystemic collaterals and oesophageal or gastric varices, what is associated with a worse prognosis. Decompensated cirrhosis is associated with the development of disease-related complications, such as ascites, variceal bleeding and hepatic encephalopathy, which require the HVPG to be elevated above 10 mmHg[14]. In this sense, HVPG is a good surrogate marker with a robust prognostic power for PH and, thus, for CLD[6,13,17,18].

The interaction between blood flow (Q) and resistance (R) determines the pressure gradient (ΔP) in the portal venous system. According to Ohm's law, in the context of

hemodynamics, this relationship is expressed as: $\Delta P = Q \times R$. Consequently, the development of cirrhotic PH can be due to the increased portal venous resistance, because of anatomical and functional changes in the intrahepatic circulation, and the increased portal venous flow as a result of splanchnic vasodilatation and increased cardiac output[10,14,19].

IHVR

The increase of IHVR is the prime determinant of PH in cirrhosis. IHVR results from the combination of structural disturbances associated with advanced liver disease (accounting for about 70% of total resistance) and of functional abnormalities leading to endothelial dysfunction and increased hepatic vascular tone[1,6].

Distortion of the liver vascular architecture is caused by collagen deposition, liver fibrosis, scarring and nodule formation, which distort the liver vascular anatomy and increase liver stiffness, capillarization of sinusoids and vascular occlusion[14]. The molecular mechanisms that induce these abnormalities are being delineated and represent new targets for therapy, mainly including an imbalance of vasodilator and vasoconstrictor compounds, the dysfunction of sinusoidal endothelium and the activation of HSC[6,20]. Among the hepatic cells that promote the increased IHVR, LSEC and HSC are directly involved. Thus, their modulation may both relieve the PP and, in the longer run, ameliorate PH and cirrhosis[12]. But it is not only these cells that play a major role in the development of CLD, as other cell types, such as Kupffer cells (KC) and hepatocytes, are involved and suffer damage throughout the course of the disease[21] (Figure 3).

To better understand the work done in this thesis, which mainly focuses on the use of LSEC as a target to direct the treatment of CLD, it is outlined below the crucial role of these cells in the pathogenesis of PH, as well as their crosstalk to the main liver cell types, that has a critical role in the development of the disease.
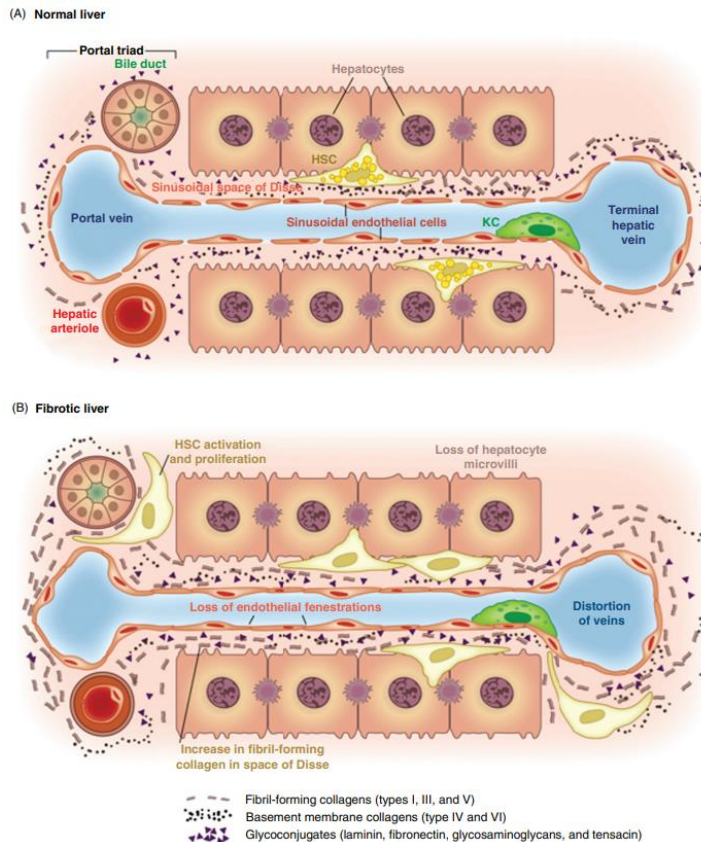
Figure 3. Matrix and cellular alterations in hepatic fibrosis. HSC: hepatic stellate cell, KC: Kupffer cell. From Puche JE et al., Compr Physiol 2013[22].

- **LSEC**

LSEC are one of non-parenchymal liver cells, form the wall of the liver sinusoids and represent approximately 15 to 20% of total liver cells, but only 3% of the total liver volume[23,24]. They differ morphologically and functionally from capillary endothelial cells of other organs, as they are a highly specialized and distinctive micro-vascular cell type with special features that are crucial for the regulation of the liver microenvironment[25,26]. Morphologically, LSEC contain fenestrae, which are non-diaphragmed pores that traverse the cytoplasm. The fenestrae are 50-300 nm in size, covering between 2 and 20% of the LSEC surface, and are clustered in groups that have been termed sieve plates[27,28] (Figure 4).
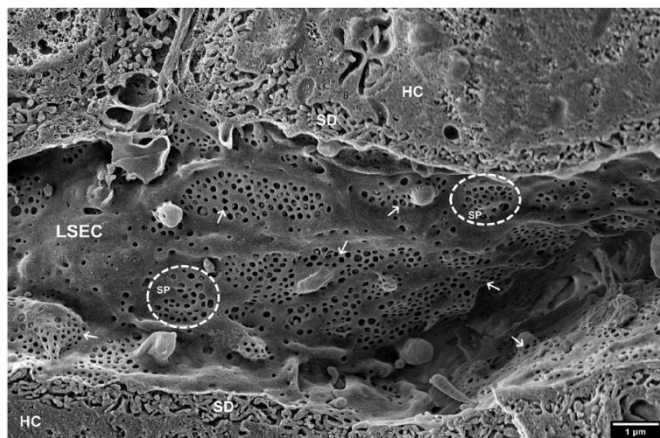
Figure 4. Scanning electron microscope (SEM) image of a hepatic sinusoid. Liver sinusoidal endothelial cells (LSEC) are covered in multiple fenestrations (arrows) arranged into sieve plates (SP, dotted line circles) distributed over the whole sinusoid. HC: hepatocytes, SD: space of Disse. From Szafranska K et al., Front Physiol 2021[28].

Different from other microvascular endothelial cells, LSEC also lack an organized basal lamina and only have an attenuated ECM, consisting mostly of fibronectin[25,29]. Thus, these cells have a morphologic phenotype that is unique in the mammal, with the combination of open fenestrae and lack of a basement membrane that creates open access for solutes between the sinusoidal blood and the space of Disse[27]. Because of these features, LSEC retain blood cells inside the vessel lumen, whereas small molecules, such as drugs, proteins, lipoproteins and small viruses, can pass this endothelial barrier via fenestrations to reach the surrounding hepatocytes, and *vice versa*[28,30]. Discontinuous sinusoidal endothelial cells also differ phenotypically from vascular or continuous endothelial cells, for instance in their failure to express factor VIII-related antigen, platelet endothelial cell adhesion molecule-1 (PECAM-1 or cluster of differentiation (CD)31), CD34 or E-selectin (also called CD62E), but instead express other differential receptors characteristic of a scavenger cell[25].

In this sense, one of the major functions of LSEC is the elimination of macromolecules and small particulates from the blood thanks to their active endocytosis receptors endowing the cells with an extraordinary high endocytic capability[31]. This ability makes

LSEC the body's most effective scavenger cells, clearing blood-borne macromolecules and nanosized compounds, thus contributing importantly to maintaining homeostasis and making them an important part of the hepatic reticuloendothelial system (RES), together with KC. This capability also gives LSEC a pivotal role in maintaining immune homeostasis within the liver through endocytosis, antigen presentation and leukocyte recruitment[23,29,32]. For this reason, LSEC express the endocytic Fc-gamma receptor (FcγR)IIb2 (CD32b), several pattern recognition receptors (PRRs), for example, various toll-like receptors (TLRs), as well as the mannose receptor and several scavenger receptors, of which stabilin-1 and stabilin-2 represent the most important (Figure 5). Interestingly, they also express the lymphatic vessel endothelial hyaluronan receptor-1 (LYVE-1) constitutively, a receptor predominantly restricted to lymphatic endothelial cells involved in uptake of hyaluronic acid and regulation of leukocyte adhesion or migration within the lymphatic circulation[29,33].
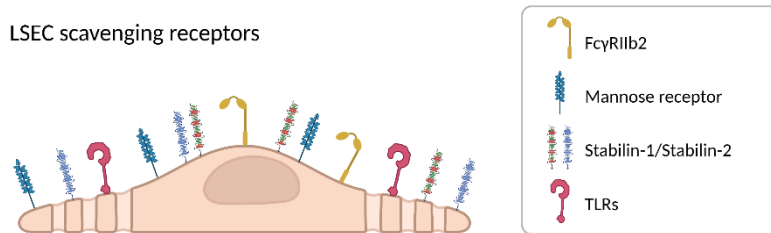
Figure 5. Scavenging receptors expressed by liver sinusoidal endothelial cells (LSEC). FcγRIIb2: Fc-gamma receptor IIb2, TLRs: toll-like receptors. Adapted from Bhandari S et al., Front Physiol 2021[32]. *Created with BioRender.com*.

CD32b, stabilin-2 and LYVE-1 are uniquely expressed by LSEC in adult liver and are to date the most reliable surface markers available for immune-identification of LSEC[33,34]. For this study, it is important to highlight the role of CD32b, the only FcγR expressed by LSEC[24]. Over 70% of CD32b in the body is expressed on the liver, mainly on LSEC, where it enables efficient endocytosis of small soluble immunoglobulin G (IgG)-antigen complexes[31,35]. Recent studies have revealed that CD32b is the main receptor for the efficient uptake of immune complexes in LSEC from rats via clathrin-mediated

endocytosis[36]. This FcγR-mediated uptake agrees with the dual cell principle of waste clearance in that small soluble immune complexes are cleared by LSEC, whereas larger immune complexes are phagocytosed by KC[29,35].

Beyond they great power of endocytosis, LSEC participate in the vascular tone regulation of hepatic sinusoids through the production of vasoactive molecules (vasoconstrictors and vasodilators). In this sense, the enzyme responsible for producing nitric oxide (NO), a gaseous vasodilator that is markedly reduced in cirrhotic livers, is the endothelial nitric oxide synthase (eNOS)[13,37]. It is constitutively expressed and produces small amounts of NO in response to stimuli such as flow shear stress and vascular endothelial growth factor (VEGF) to maintain the hemodynamics of liver capillaries[23,38]. In this cell type, eNOS expression has been shown to be regulated by the transcription factor Krüppel-like factor 2 (KLF2), a zinc finger protein sensitive to shear stress that is highly expressed in LSEC and induces the expression of different vasodilator, anti-thrombotic (e.g. thrombomodulin) and anti-inflammatory genes, and represses the expression of adhesion molecules, such as vascular cell adhesion molecule-1 (VCAM-1) and E-selectin[39,40] (Figure 6). Altogether, KLF2 is considered as a nuclear factor essential to maintain a functional endothelial phenotype[41,42].
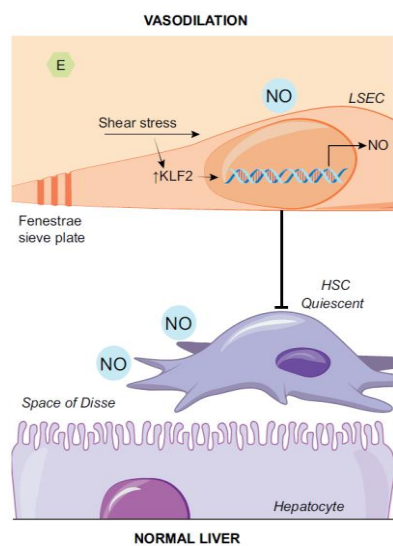
Figure 6. Role of liver sinusoidal endothelial cells (LSEC) regulating the vascular tone of hepatic sinusoids in normal conditions. HSC: hepatic stellate cell, KLF2: Krüppel-like factor 2, NO: nitric oxide. Adapted from Poisson J et al., J Hepatol 2017[24].

- Intercellular crosstalk: LSEC, HSC and KC

LSEC participate in fibrosis through the secretion of angiocrine signals that act as paracrine factors balancing the liver response to injury towards fibrosis or regeneration. LSEC have an important role in the early response to liver injury as they orchestrate the initial response to damage of the neighbouring hepatic cells. Thus, the development of liver fibrosis and progression from liver fibrosis to cirrhosis, or even to hepatocellular carcinoma (HCC), are closely related to this crosstalk between LSEC and other liver cells[21,23,43]. In this regard, a better understanding of the mechanisms implicated in the loss of LSEC functional capacity and their contribution to the initial response to damage is essential to find strategies able to halt or hamper fibrosis progression.

Due to their privileged situation and intimate contact with the blood stream, LSEC are the first liver cell type sensing the toxic stimuli. At very initial stages, LSEC lose their characteristic phenotype, which means that they gradually lose expression of their special markers (e.g. CD32b, LYVE-1) and revert to expressing common endothelial markers (e.g. CD31, CD34)[24]. The fenestrae also disappear and a basement membrane is formed, so it is no longer a discontinuous endothelium. This process of dedifferentiation, known as capillarization, is accompanied by the loss of characteristic LSEC functions, resulting in dysfunctional LSEC and endothelial dysfunction, a fact that has been identified as the initial trigger for the fibrotic response[25,26,44] (Figure 7).
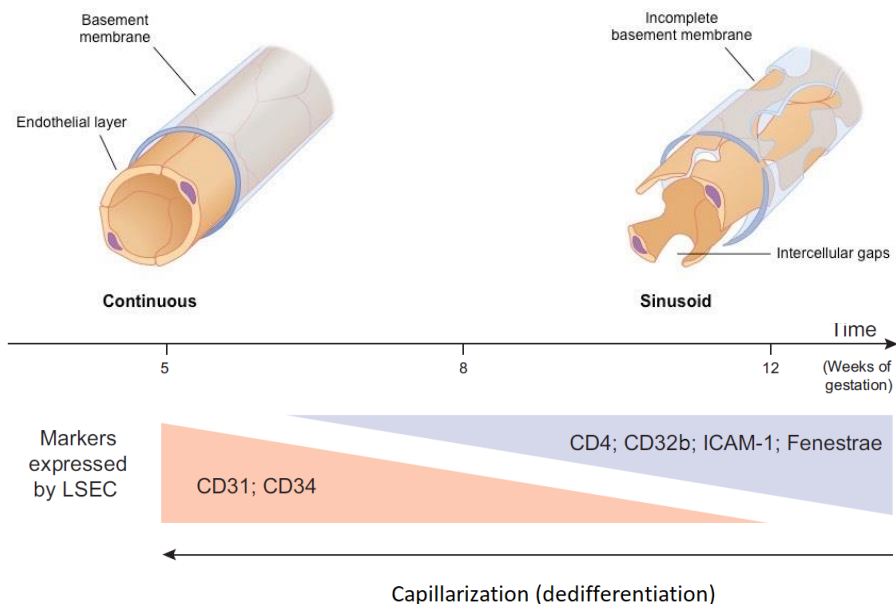
Figure 7. Differentiation and capillarization process of liver sinusoidal endothelial cells (LSEC) during embryogenesis. CD31: platelet endothelial cell adhesion molecule (PECAM-1), CD32b: Fc-gamma receptor IIb2, ICAM-1: intercellular adhesion molecule-1. Adapted from Poisson J et al., J Hepatol 2017[24].

Within this process, LSEC acquire a vasoconstrictor phenotype, characterized by elevated production of vasoconstrictors (e.g. endothelin-1 (ET-1), thromboxane A2 (TXA$_2$), angiotensin II (Ang II)) and reduced release of vasodilators (e.g. NO, prostacyclin)[15,23]. In CLD, this vasoconstrictive phenotype increases the IHVR and, subsequently, the PP. One of the reasons is because of the reduced eNOS activity, mainly due to the binding of eNOS to the inhibitory protein caveolin-1 in venous and sinusoidal endothelial cells of the cirrhotic liver[45], but also by the dysregulation of eNOS phosphorylation (p-eNOS) due to abnormal signalling by the regulator protein kinase B (PKB), also known as Akt, and the activation of Ras homolog family member A (RhoA)/Rho-associated protein kinase (ROCK), among other factors[46–48].

Moreover, there is a high NO-scavenging due to the elevated reactive oxygen species (ROS) present in the cirrhotic liver, so all this together leads to reduce the bioavailability of NO by the endothelium, in addition to the increased production of vasoconstrictive molecules such as ET-1 or TXA_2[15,49]. This imbalance does not only alter LSEC phenotype but also contributes to the contraction of different cells of the cirrhotic liver, like HSC, portal myofibroblasts and vascular smooth muscle cells, that leads to increased hepatic vascular tone and PP[26,43,49].

Regarding HSC (also referred to as Ito cell, fat-storing cell, lipocyte or perisinusoidal cell), they are one of the key non-parenchymal cell types of the liver. They are located in the space of Disse, the space between the liver plate and the sinusoids that contains ECM components, where they act as the main collagen synthesizers. In their quiescent state (qHSC) they mainly store lipids, specifically retinoids such as vitamin A, participate in the ECM metabolism, and help to maintain the architecture of the hepatic sinusoid interacting with the rest of liver cells[17,50]. In addition, qHSC produce various growth factors that modulate the function and proliferation of these cells and regulate the sinusoidal blood flow by their contractile capacity[43,51]. In this sense, when the hepatic microvasculature suffers some type of damage, qHSC are "activated" (aHSC) and undergo a transdifferentiation towards a proliferative and fibrogenic myofibroblast-like phenotype. This process is characterized by starting to express genes that encode contractile proteins and extracellular fibrogenic proteins such alpha-smooth muscle actin (α-SMA) and type I collagen, respectively. The consequence is that aHSC produce changes in intrahepatic vascular tone and increase IHVR through this hypercontractility, high response to endogenous vasoconstrictors (e.g. endothelins, Ang II) and augmented ECM production[17,39,50–54] (Figure 8).
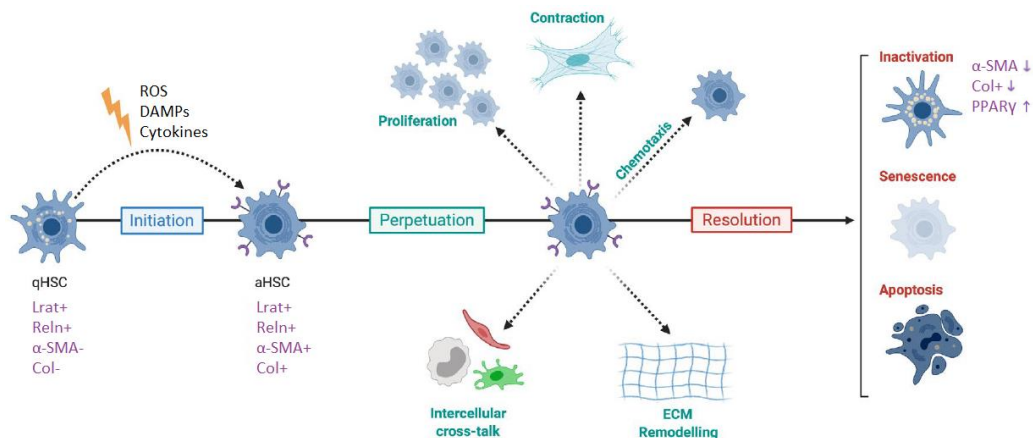
Figure 8. Phases of HSC activation and resolution. aHSC: activated hepatic stellate cell, Col: collagen, DAMPs: damage associated molecular patterns, ECM: extracellular matrix, Lrat: lecithin-retinol acyltransferase, PPARγ: peroxisome proliferator-activated receptor gamma, qHSC: quiescent hepatic stellate cell, Reln: reelin, ROS: reactive oxygen species, α-SMA: alpha-smooth muscle actin. From Kitto LJ et al., Hepatol Commun 2021[55].

Turning to LSEC, beyond their role in the vasoactive regulation of hepatic sinusoids, these cells also have a unique immunological role due to their privileged location as a barrier between the blood and the rest of the liver, making them an integral part of the hepatic RES[24,26,32,56]. Under physiological conditions, the liver has a unique potential to modulate immune response, especially through tolerance induction by modulating lymphocytes behaviour. LSEC express major histocompatibility complex (MHC) class I and class II, intercellular adhesion molecule-1 (ICAM-1), VCAM-1, and the costimulatory molecules CD80, CD86 and CD40 as professional antigen presenting cells, and play an important role in adaptive immunity[57,58].

On the other hand, due to their continuous exposure to bacterial-derived products from the gut, LSEC express anti-inflammatory cytokines to maintain the state of immune unresponsiveness, restricting the entry of circulating leucocytes into the liver tissue[24,31,59]. However, in presence of damaging stimuli (e.g. ROS), a robust immune response can be generated and LSEC become highly proinflammatory and start secreting a vast array of cytokines and chemokines (e.g. tumor necrosis factor alpha

(TNF-α), interleukin (IL)-6, IL-1β, chemokine (C-C motif) ligand(CCL) 2, initiating a robust intrahepatic inflammatory response capable of activating HSC and KC[20,26,60].

In this context of liver inflammation, the role of KC should also be highlighted, as they are the resident macrophages of the liver and because it has been described that LSEC dysfunction precedes KC activation[21,43]. In this tissue, macrophages can be broadly defined as either resident KC or monocyte-derived macrophages. KC predominate and are the largest population of resident macrophages in the body[61]. Importantly, they are located in the hepatic sinusoids, which enables them to directly sample the antigens that are transported from the gastrointestinal tract through the portal vein, ensuring early exposure to pathogenic bacteria, and to be in close contact with other circulating immune cells. Therefore, KC have a crucial homeostatic role in protecting the host, and can induce both immunogenic and tolerogenic immune responses[2]. M2-type KC are usually abundant in a healthy liver and are characterized by having a weak antigen-presenting ability and by counteracting the immune response by secreting potent immunosuppressive factors, such as IL-10[62].

But in response to hepatic injury, liver macrophage populations markedly change and KC adopt a more M1-type phenotype[62]. This change can be triggered by multiple inflammatory mechanisms by which these cells can act or participate as intermediaries during CLD development. Some of these pathways include the secretion of damage-associated molecular patterns (DAMPs) by apoptotic and/or necroptotic parenchymal cells, which stimulate the TLR4 receptor and cause the activation of KC, leading to the production of pro-inflammatory cytokines such as TNF-α, IL-1β, IL-6 and IL-8, initiating both hepatic and systemic inflammation[20,63,64]. The hepatic macrophage-derived pro-inflammatory cytokines TNF-α and IL-1β have more recently been shown to affect aHSC, and to promote the survival of HSC-derived myofibroblasts and the development of liver fibrosis[2,65]. Moreover, in the early response to injury, activated KC also secret chemokines, such as CCL2 and CCL5, which facilitate leukocyte recruitment to the site

of inflammation, thereby perpetuating the fibrotic response[2,66]. Finally, a further downstream effect of TLRs activation on these cells is the production of ROS, which directly interacts with NO leading to the formation of reactive nitrogen species[20,38] (Figure 9). Additionally, ROS stimulates eNOS "uncoupling" and decreased phosphorylation, as well as increases the formation of eNOS inhibitors, causing its dysfunction[67].
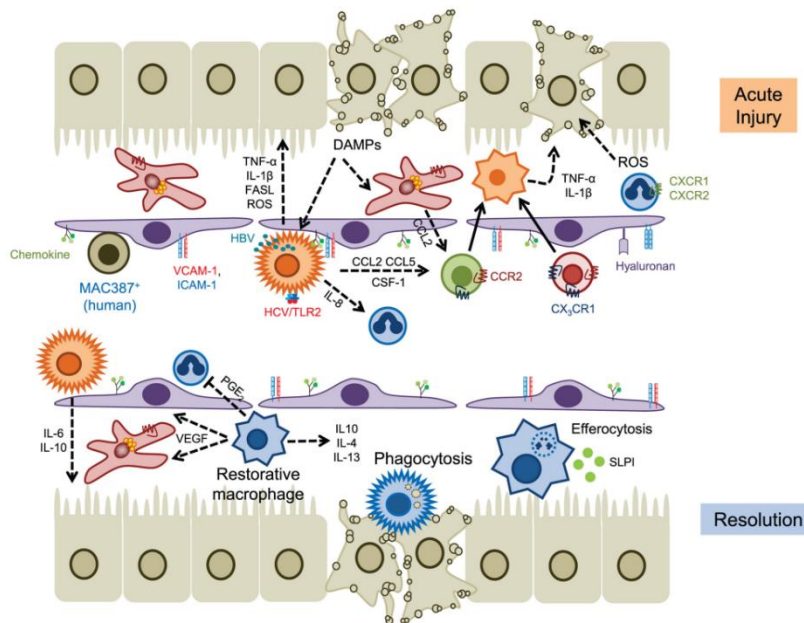
Figure 9. Activation and resolution of the inflammatory process in acute liver injury. CCL: chemokine (C-C motif) ligand, CCR2: CC chemokine receptor type 2, CSF-1: colony stimulating factor 1, CXCR: CXC chemokine receptor, DAMPs: damage-associated molecular patterns, FASL: Fas ligand, HBV: hepatitis B virus, HCV: hepatitis C virus, ICAM-1: intercellular adhesion molecule-1, IL: interleukin, PGE_2: prostaglandin E2, ROS: reactive oxygen species, SLPI: secretory leukocyte protease inhibitor, TLR2: toll-like receptor 2, TNF-α: tumor necrosis factor alpha, VCAM-1: vascular cell adhesion molecule-1, VEGF: vascular endothelial growth factor. From Weston CJ et al., Front Immunol 2019[68].

Splanchnic blood flow

As it has been mentioned above, pressure in the portal vein is determined by the interaction between vascular resistance and blood flow, so beyond increased IHVR, the other major trigger of PH is the increase of the portal venous flow. Under healthy conditions, PBF mainly changes after meals, which induce marked splanchnic vasodilation and subsequently increase portal vein inflow, which can also be achieved by volume expansion. In contrast, PBF is markedly decreased by stimulating adrenergic vasoconstriction[12,14].

In advanced PH, as an adaptive response to the changes in intrahepatic hemodynamics, it occurs a splanchnic vasodilatation with an increase in the inflow of blood into the portal venous system, and in more advanced liver cirrhosis this splanchnic vasodilatation is so intense as to generate a hyperdynamic systemic circulation (hyperkinetic syndrome)[13,69]. The fact is that this exaggerated vasodilatation of the splanchnic area induces a reduction in mean arterial pressure (MAP) that activates compensatory mechanisms, such as endogenous neurohumoral systems and sodium retention, to increase the plasma volume, leading to an increase in cardiac output that further rises splanchnic blood flow and PP, and thus, ascites and circulatory dysfunction[15].

This increased splanchnic blood flow is partly due to mesenteric arteriolar vasodilatation and decreased vascular responsiveness to endogenous vasoconstrictors. In contrast to the presence of endothelial dysfunction to vasodilators in hepatic vasculature, in cirrhotic splanchnic vessels vasodilatation is promoted by local over-production of vasodilators, which along with intrinsic vascular hypocontractility allows increased blood flow through the splanchnic vessels[10]. A wide variety of vasodilatory molecules play a role in inducing the vasodilatory state, but of all these molecules NO is the most important. Hyperactive splanchnic vascular endothelial cells over-produce NO mainly through eNOS in response to different stimuli such as shear stress, inflammatory cytokines and VEGF[19,20,39,45,69]. Furthermore, increased blood flow through the portal

system can only contribute significantly to PH when HVPG elevation is coupled with angiogenesis and portosystemic collateral formation. In decompensated cirrhosis, the amount of collateralized blood may exceed 90% of the total portal venous blood[14]. So, all in all, angiogenesis is also a pivotal feature in the splanchnic vasculature, worsening the hyperdynamic circulation.

Importantly, the majority of complications that occur in advanced cirrhosis, and even more in decompensated patients, are a consequence of the evolution of PH[70]. The development of decompensation events is associated with a reduction in the median survival of a patient to less than 2 years, from 12 years in a cirrhotic patient without these complications. Oesophageal and gastric varices, the most relevant portosystemic collaterals that develop in PH, are responsible for one of the most representative and severe complications of this condition, massive acute gastrointestinal bleeding[19,71]. Other consequence of the shunting of portal blood to the systemic circulation is the delivery of noxious substances from the portal circulation directly to the cerebral vasculature without hepatic detoxification, thus contributing to hepatic encephalopathy[72]. However, the list of clinical manifestations of decompensated cirrhosis does not stop here, but also includes ascites, increased susceptibility to spontaneous bacterial peritonitis and sepsis, and development of hepatorenal and hepatopulmonary syndromes due to exacerbation of the hyperkinetic circulation[10,12,18,70] (Figure 10).

Figure 10. Complications derived from PH evolution in decompensated cirrhosis.
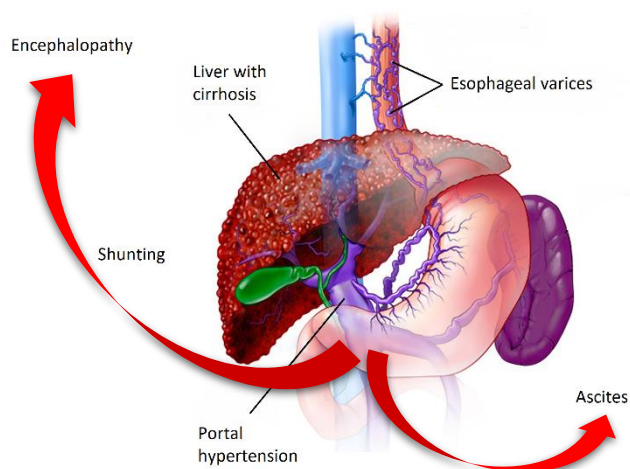
1.2. Treatment of CLD

There are few treatments available for patients suffering from advanced PH, as correcting PH has strong positive implications on patients' disease course and prognosis. This makes sense given that if we can prevent the PP gradient to exceed 10 mmHg, we could prevent complications of PH and decompensation of cirrhosis[14,19]. We have seen that during cirrhosis development, elevation in IHVR is the primary factor involved in increasing PP, leading to secondary splanchnic vasodilation and extrahepatic shunt formation, which further aggravate PH and liver dysfunction. Until recently, treatment strategies for PH and cirrhosis did not target the main underlying mechanisms but were stratified according to the complications of PH rather than the PH itself, with varices and ascites development being the two main complications linked to PH magnitude[19,73]. For this reason, non-selective beta-blockers (NSBB) are currently the most widely used drugs because of their ability to decrease splanchnic venous inflow and cardiac output by blocking the beta-1 adrenergic receptor, and to induce vasoconstriction in the splanchnic region by blocking the beta-2 adrenergic receptor, thereby decreasing PBF and preventing some of the aforementioned complications associated with PH caused by the hyperdynamic circulation[12]. In the last decade, carvedilol turned to be the most effective NSBB, as it can cause intrahepatic vasodilation due to an alpha-adrenergic vasodilator effect, causing a reduction in IHVR and thus, a more marked reduction in PP than traditional NSBB[71,74].

However, apart from NSBB, effective therapies to prevent the progression of PH or to treat its cause are missing due to the complexity of the pathogenesis of PH and the failure of clinical studies in humans. In this regard, in recent years it has emerged the idea that the "ideal drug" for PH should reduce PP maintaining or enhancing hepatic blood flow, and this aim would be achieved by decreasing IHVR caused by fibrosis or liver cirrhosis. Therefore, the basic mechanisms of LSEC and HSC dysregulation have been extensively studied, and potential therapeutic targets have been proposed, such as the reduced NO bioavailability, the increased vasoconstrictive response at the sinusoidal level or the increased synthesis of ECM components[12,15,75].

To begin with, one approach to decrease IHVR is to modulate the hepatic vascular tone and improve endothelial dysfunction through treatments aimed at increasing NO availability within intrahepatic circulation. For this purpose, there exist several therapeutic approaches, starting with NO donors[10,15,19,75,76], such as nitrates (e.g. isosorbide-5-mononitrate) or NCX-100, a liver specific NO donor which unexpectedly, failed to decrease HVPG in a phase II clinical trial[77]. Other strategies include the stimulation of endothelial NO synthesis by exogenous administration of the eNOS cofactor tetrahydrobiopterin[75,78] or the activation of its downstream mediators, such as soluble guanylate cyclase stimulators, that activate this intracellular NO receptor to catalyze the conversion of guanosine triphosphate (GTP) to cyclic guanosine monophosphate (cGMP), conferring a potent vasodilation[75,79,80]. In this line, there are other approaches aimed at potentiating the effects of cGMP by preventing its degradation by phosphodiesterase-5 (PDE-5). Thus, different PDE-5 inhibitors, like udenafil, showed lowering effects on PP in cirrhotic patients[75,80].

Related to this, reduction of ROS has also been found to be a key factor in alleviating liver inflammation and fibrosis. With this aim, we find antioxidants that compensate this oxidative stress by promoting the conversion of ROS into less reactive molecules. Among them, some have been studied for CLD therapy: sulfur-containing and some non-sulfur-containing antioxidants, vitamin E, ascorbic acid, silymarin, resveratrol or superoxide dismutase analogues, that mimic the action of this antioxidant enzyme catalysing the splicing of superoxide (O_2^-) and hydrogen peroxide (H_2O_2)[15,80–82].

Within the sinusoids, vasoconstrictive activity is up-regulated and for that reason, drugs aimed to reduce vasoconstriction are good options for the reduction of IHVR and PP[75,78,80,82]. One of the most potent vasoconstrictors that contributes to microvascular dysfunction in CLD is ET-1, so the use of antagonists targeting ET-1 receptors (either type A (ET_A), type B2 or both), like non-selective endothelin receptor antagonist bosentan and the selective ET_A receptor antagonist ambrisentan, showed improvements in the hepatic sinusoid and in liver fibrosis in preclinical models[83]. Based

on the same idea, there are eiconasoid inhibitors, blocking the action of the arachidonic acid-derived vasoconstrictors (e.g. TXA_2 receptor blockers terutroban or ifetroban)[84], and a variety of angiotensin-converting enzyme inhibitors, like captopril, and angiotensin receptor blockers (ARBs), such as losartan, candesartan and irbesartan, drugs that inhibit the Ang II action[85,86].

Lastly, another class of drugs to mention are antifibrotics, which aim to decrease the number and cellular activity of matrix-producing cells in the injured tissue, as well as acting directly on fibrosis to eliminate it. Among the most prominent options is the inhibitory monoclonal lysyl oxidase-like 2 (LOXL2) antibody AB0023, an antibody against a protein involved in collagen crosslinking and fibrotic matrix stabilization that was effective in preventing and reversing fibrosis in two mouse models of mild and advanced liver fibrosis, but did not show antifibrotic activity in patients with hepatic fibrosis in a recent phase II clinical trial with the anti-LOXL2 antibody simtuzumab[17,81,87]. A further possible strategy is to normalize HSC hypercontractility using a HSC-targeted ROCK inhibitor[54,88] or the peptide hormone relaxin[78].

But although many more options have been postulated (e.g. anti-inflammatories, antiangiogenics)[66,73,75,80,89], one group of drugs with more than 10 years of experimental and clinical evidence of use in the treatment of cirrhosis should be highlighted, being one of the main focuses of this thesis: statins[90].

1.2.1. Statins

Statins are one of the most prescribed drugs in clinical practice, originally designed to treat hypercholesterolaemia as specific inhibitors of the enzyme 3-hydroxy-3-methylglutaryl coenzyme A (HMG-CoA) reductase, blocking the conversion of HMG-CoA into mevalonate in cholesterol biosynthesis pathway[91,92]. However, statins possess multiple pleiotropic effects beyond reducing cholesterol levels that account for their anti-inflammatory, anti-proliferative, anti-thrombotic, anti-oxidative and immunomodulatory actions *in vitro* and *in vivo*[93–95] (Figure 11). The most studied beneficial effects of statins are on the cardiovascular system, being statin treatment a way to reduce cardiovascular-related morbidity and mortality in the case of patient with coronary artery disease, but also in patient without elevated cholesterol. Indeed, statins have demonstrated to reduce the risk of sudden cardiac death, deep vein thrombosis and fibrosclerotic aortic stenosis, and this is the reason why sometimes statins are considered for the primary prevention of cardiovascular diseases in patients who do not always have elevated cholesterol levels[96–98].
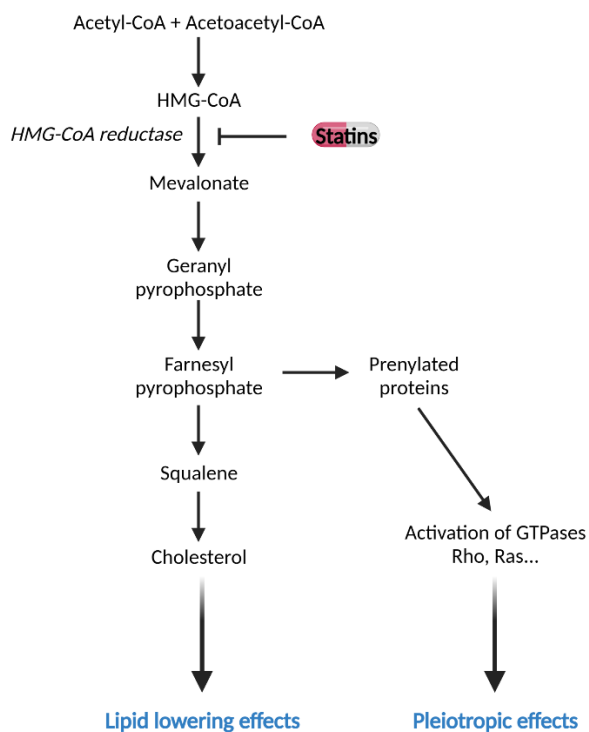
Figure 11. Effects of statins on the cholesterol biosynthesis pathway. CoA: coenzyme A, GTP: guanosine triphosphate, HMG: 3-hydroxy-3-methylglutaryl. Rho: Ras homolog family. Adapted from de Loecker I et al., Ann Intensive Care 2012[99]. *Created with BioRender.com*.

Beneficial effects in CLD

Beyond the known common effects, statins also exhibit a wide range of non-cardiovascular effects that have been shown to be favourable for the use of this type of drugs in the treatment of hepatic fibrosis and PH in CLD[93,100,101]. Due to these evidences, in the last few years there have been many researches aimed at discovering this potential. In different animal models of cirrhosis, the use of statins (e.g. simvastatin, atorvastatin) has shown to exert vasoprotective and antifibrotic effects in cirrhotic livers, improving LSEC dysfunction and reducing HSC activation, respectively, achieving hepatic fibrosis regression[48,76,94,102–107]. These remarkable beneficial effects were mainly dependent on the up-regulation of KLF2 in the hepatic cells after statins treatment[41,42,108] by enhancing the expression of their target genes, such as eNOS[76,95,109,110], or inhibiting the vasoconstrictive RhoA/ROCK axis[76,101,104,111], among other pathways. Also, in ischemia/reperfusion (I/R) injury, a major complication in clinical practice (e.g. liver resection surgery, liver transplantation) that may lead to liver failure, some studies in animal models have aimed to investigate the hepatoprotective role of a simvastatin pretreatment in order to improve the viability of livers from donors after circulatory death. Their results have demonstrated that, through a KLF2-dependent mechanism, this kind of pretreatment significantly reduces hepatic damage and apoptosis, preserves the hepatic endothelial phenotype and decreases KC activation by inducing a M2 polarization, generating therefore a protective effect against hepatic I/R injury[40,112–114]. Finally, regarding their lipid-lowering effect, statins can reduce liver triglycerides, and thus, ameliorate hepatic steatosis. Of this, there are diverse studies showing that statins effectively improve lipid profile, inflammation and oxidative stress, reducing steatosis, liver fibrosis and carcinogenesis in rat models of non-alcoholic steatohepatitis (NASH)[83,94,109,115–117].

Now, regarding clinical research, it has been seen that statins use has a potentially positive effect on the natural history of cirrhosis[90,116–118]. Focusing on simvastatin, there are clinical trials in patients with CLD demonstrating that simvastatin treatment lowers PP most likely through a reduction in IHVR[119,120]. In the BLEPS study[121], a double-blind

parallel trial of 158 patients with cirrhosis after variceal bleeding receiving standard prophylaxis to prevent rebleeding, it has been shown that simvastatin increased survival in these decompensated cirrhotic patients, but it did not prevent further complications of PH. And more recently, in another randomized controlled trial assessing the effect of simvastatin on hemodynamics in 40 patients with cirrhosis and PH it was demonstrated that, compared to placebo, simvastatin significantly decreased PH and hepatic resistance, and improved liver perfusion without harmful effects on systemic circulation after 30 days of treatment[122]. However, even though there are results indicating that simvastatin has a clear potential for the treatment of PH in patients with cirrhosis, the beneficial effects of this statin need to be confirmed in long-term clinical trials.

Until now, it has been seen that simvastatin decreases HVPG without significantly modifying hepatic blood flow, which is in accordance with the concept that this drug exerts its PP-lowering effect through a decrease in IHVR[48,95,107]. But the underlying mechanisms that might explain the hepatic vascular protection observed in these studies are not completely understood. In an attempt to elucidate them, the main pathways that have been investigated and discovered, and that could explain the beneficial effects of simvastatin in CLD and PH, are outlined below.

- Enhanced bioavailability of NO

The major part of the pleiotropic effects of simvastatin can be attributed to effects on endothelial function, being the most important one the increase in endothelium-derived NO bioavailability[40,109,119,120]. As an example, it was observed that simvastatin rapidly induces the phosphorylation of Akt (p-Akt) at serine (Ser) residue 473, which increases its protein kinase activity, and it is involved in Akt-mediated phosphorylation of eNOS on Ser residue 1177, leading to NO production and promoting endothelial cell survival in an Akt-dependent manner[95,98,107,110].

- **Expression of KLF2**

This transcription factor is expressed in all hepatic cell types, but one of the cell types that most expresses it are LSEC, where it was identified as a key component acting as a defence mechanism in response to damage that occurs during the progression of liver cirrhosis. As mentioned above, KLF2 confers vasoprotection to LSEC inducing the expression of vasodilator, anti-inflammatory and antithrombotic genes, including eNOS and thrombomodulin, and repressing the expression of adhesion molecules, like VCAM-1 and E-selectin. Moreover, another point in favour of KLF2 is that, when it is expressed in endothelial cells, it helps to inhibit oxidative stress-mediated cell injury and apoptosis[41,42,108]. Experimental studies in different models of hepatic damage have demonstrated that KLF2 expression can be induced by exogenous administration of simvastatin, and other statins, maintaining a functional phenotype in LSEC thanks to the stimulation of these vasoprotective pathways, which contribute to the beneficial effects of simvastatin in cirrhosis[40–42,108,111,112,115,123].

- **Reduced formation of isoprenoids**

Like all statins, simvastatin lowers cholesterol by inhibiting HMG-CoA reductase, the rate-limiting enzyme of the mevalonate pathway for *de novo* synthesis of cholesterol. But this general inhibitory action also results in depletion of the downstream intermediate products of this pathway, such as farnesyl pyrophosphate and geranylgeranyl pyrophosphate (GGPP), necessary for proper function of small GTPases, such as Ras proteins. In the case of GGPP, it is known that this isoprenoid serves as a lipid membrane anchor for proteins of the Rho GTPase family, especially RhoA[48,95,101,104,111]. Thus, in the case of aHSC, statins treatment inhibits the production of GGPP, avoids RhoA translocation to the membrane and disrupts RhoA/ROCK downstream signalling, resulting in decreased contraction of these cells, reduced deposition of ECM, less liver fibrosis, and thereby, lower IHVR and PP[48,105,106].

- ### Link between Rho GTPases and KLF2

Some studies emphasize the link between Rho GTPases and KLF2 in liver cirrhosis, previously described only for cirrhotic endothelium[108]. One of the works demonstrated that collagen production, activation and contraction of aHSC are dependent on KLF2 expression and are potentially other downstream effectors of RhoA besides ROCK[48]. This might be supported by previously published data, showing that statins reduced HSC activity, turn-over and induced senescence in these cells, improving experimental liver fibrosis through the activation of the endothelial KLF2-NO pathway and other pathways, such as the reduction in α-SMA production and the inhibition of HSC contraction by counteracting the activation of the RhoA/ROCK pathway[105,106] (Figure 12).
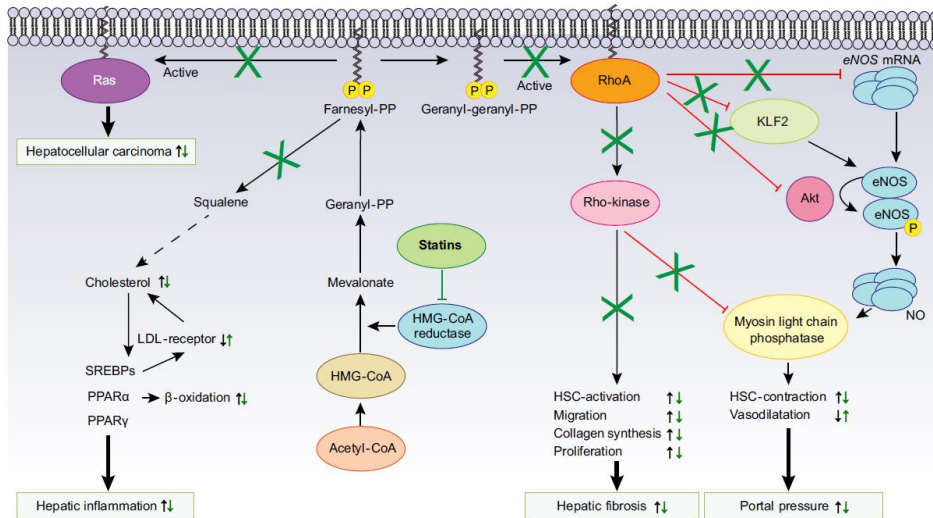
Figure 12. Pleiotropic effects of statins in the liver. Akt: protein kinase B (PKB), CoA: coenzyme A, eNOS: endothelial nitric oxide synthase, HMG: 3-hydroxy-3-methylglutaryl, HSC: hepatic stellate cell, KLF2: Krüppel-like factor 2, LDL: low-density lipoprotein, mRNA: messenger ribonucleic acid, NO: nitric oxide, PP: pyrophosphate, PPAR: peroxisome proliferator-activated receptor, Rho: Ras homolog family, SREBPs: sterol regulatory element-binding proteins. From Pose E et al., J Hepatol 2019[93].

Adverse effects

Statins are currently considered the most promising drugs to slow down or stop the molecular mechanisms that lead to a progressive liver inflammation and fibrosis in CLD, due to its numerous beneficial intrahepatic effects. However, and although statins have been widely used for lipid-lowering purposes with a good safety profile, like any medication they are not free of adverse effects[90,124].

The most significant undesirable effect of statins is muscle toxicity, ranging from myalgia to rhabdomyolysis, leading to elevated creatine kinase (CK) values[125–129]. In this regard, in the BLEPS study mentioned above, 2 patients receiving simvastatin along with standard therapy for the prevention of variceal rebleeding experienced significant muscle toxicity at a much higher rate than in the normal population, reporting an episode of rhabdomyolysis and forcing the withdrawal of the drug. Then, in the LIVERHOPE-SAFETY trial[130], the maximum dose of simvastatin tested (40 mg/day) had an increase in CK final value and generated muscle toxicity in 3 of 16 patients treated compared with no patients in the lower simvastatin dose (20 mg/day) or placebo groups. In this case, it is worth mentioning that despite sharing a mechanism of action, the risk of developing muscle symptoms depends on the statin used and its dose, and can be increased substantially when statins are used in combination with other drugs that affect their metabolism (in particular, inhibitors of cytochrome P450) and in certain types of patients (e.g. polymorphisms in the solute carrier organic anion transporter family member 1B1 (SLCO1B1) gene)[92,126,131]. Thus, it seems that statins metabolized by the cytochrome P450 3A4 (CYP3A4) (e.g. simvastatin, atorvastatin, lovastatin) would have a greater risk of interaction that would reinforce their toxic effect[91,126,132], being simvastatin the one with the greatest incidence of muscle toxicity in clinical trials[121,126,130] (Figure 13). In addition to this, statins have also been shown to cause certain liver toxicity, inducing an elevation of hepatic aspartate aminotransferase (AST) and alanine aminotransferase (ALT)[90,117,121,130,132]. All in all, these side effects limit the effectiveness of statins, especially in populations with a higher risk of toxicity such as patients with advanced CLD.

At the experimental level, in a previous experience of our research group, the model of secondary biliary cirrhosis by bile duct ligation (BDL), paradigm of advanced liver disease with cholestasis, showed a very high toxicity to statins, specifically more to simvastatin than to atorvastatin, with significant weight loss, a higher mortality rate and both muscle and hepatic toxicity[76,106]. Furthermore, other results from our laboratory show that rats with NAFLD-NASH, obtained through a model fed with a high fat diet combined with a high glucose-fructose beverage, treated with simvastatin or atorvastatin, exhibited mild muscle toxicity[115].
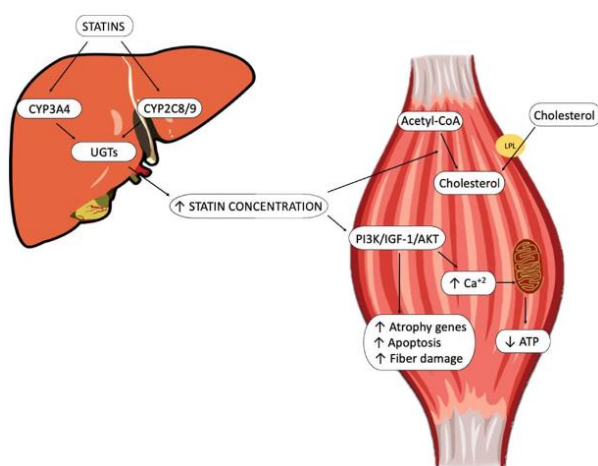
Figure 13. Potential mechanisms for the development of statin-associated muscle symptoms. Acetyl-CoA: acetyl coenzyme A, AKT: protein kinase B (PKB), ATP: adenosine triphosphate, Ca^{+2}: calcium, CYP: cytochrome P450, IGF-1: insulin-like growth factor 1, LPL: lipoprotein lipase, PI3K: phosphoinositide 3-kinase, UGTs: uridine 5'-diphospho-glucuronosyltransferase s. From Ward NC et al., Circ Res 2019[133].

Therefore, seeing these adverse effects, one of the options that has been proposed to avoid the toxicity of statins like simvastatin is the use of nanoparticles for their more targeted administration, which has already been successfully tested in animal models of different pathologies such as myocardial infarction[134], colorectal cancer[135], ischemic stroke[136] and, more recently, HCC[137].

1.3. Nanoparticle treatment

In the last decade, the field of nanotechnology has advanced exponentially and many products containing nanoparticles are now used in various applications such as in food science, cosmetics and pharmaceuticals[138]. Focusing on the latter, recent advances in engineered nanomaterials have hold significant promise to improve disease diagnosis and treatment specificity, as they exhibit a range of properties that could help overcome the limitations of conventional drug delivery, including nano-range size, improved solubility, protection of cargo from early degradation, sustained and controlled drug release, and targeted delivery that can increase the therapeutic index of medicines[139,140].

The most typical form of nanomedicines are nanoparticles, which have generated promising results *in vitro* and in small animal models[139]. However, the number of nanomedicines available to patients is drastically below projections for the field, with only 51 nanomedicines approved by the United States Food and Drug Administration (FDA or USFDA) till 2018[141,142], partially because of a translational gap between animal and human studies, and due to the lack of specific regulatory guidelines[140]. Nanoparticles are defined as particles with one dimension ranging between 1 and 100 nm, typically comprised of therapeutic entities, such as small-molecule drugs, peptides, proteins and nucleic acids, and components that assemble with the therapeutic entities, such as lipids and polymers, to form the nanoparticle. These devices, including polymeric nanoparticles, nanoemulsions, liposomes or inorganic nanoparticles, are suggested to have potential clinical applications depending on different parameters, like their physical and chemical properties (e.g. size, shape, zeta potential (surface charge), mechanical strength, hydrophilicity), drug loading efficiency, drug release and, most importantly, low or no toxicity of the carrier itself[138,143]. In this sense, it is important to stand that nanoparticles have been specially used to lower the overall systemic dose and damage that toxic and potent drugs may produce by spatially localizing their release to specific therapeutic sites. But, in order for a drug delivery device to achieve these desired benefits, it must be present in the bloodstream long enough to reach or

recognize its therapeutic site of action, and the opsonization or removal of drug nanocarriers from the body by the RES is a major obstacle, even more when dealing with particles larger than 200 nm in diameter[144,145]. To solve this problem, some methods have been developed for camouflaging or masking nanoparticles to bypass recognition by the RES and increase their blood circulation half-life. One of the main systems is the use of poly(ethylene glycol) (PEG), also known as poly(ethylene oxide) (PEO), and PEG-containing surface treatments, because that interfere with the binding of opsonin proteins to the particle surface as a means of imparting stealth or RES-avoidance characteristics to nanoparticles[146].

Another remarkable property of nanoparticles, which has led to their main use in cancer therapies, is the fact that as their size normally ranges from 10 to 100 nm, the lower bound avoids premature first-pass elimination by the kidneys, and the upper bound leads to the passive accumulation of nanodrugs within tumor sites allowed by the enhanced vascular permeability of the intratumoral vessels together with a defective lymphatic drainage, the so-called "enhanced permeability and retention (EPR) effect". This effect triggers a higher drug concentration at the tumor site and decreased toxic side effects compared with systemic administration[143,144,147–149] (Figure 14). Beyond this effect, at these diameter parameters nanoparticles are still able to access the liver, as entities up to 100-150 nm can pass through LSEC fenestrae, as explained before[30].

Figure 14. General properties of nanoparticles as a drug delivery system. From Mitchell MJ et al., Nat Rev Drug Discov 2021[139].
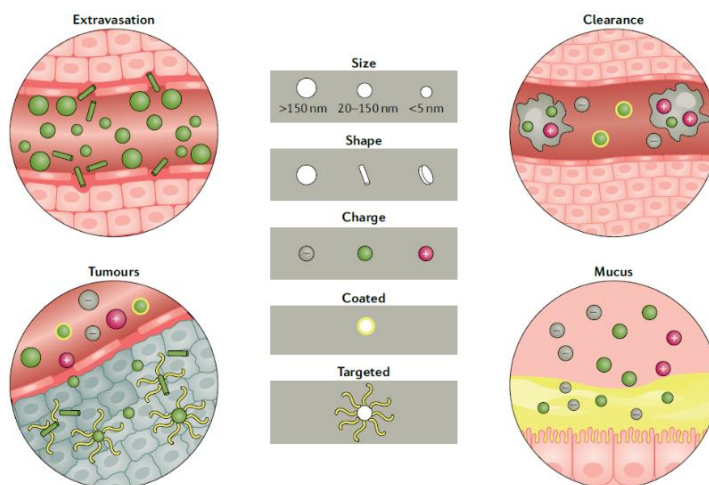
Taking advantage of all these factors, the use of nanoparticles has been postulated as a good option for the treatment of CLD to target drugs to the liver[150]. In line with this, nanoparticulate systems have gained much attention for the treatment of liver fibrosis and we can find some examples of nanodevices developed in recent years for this purpose, like guided liposomes directed to aHSC, that were able to effectively inhibit HSC activation and alleviate fibrosis[151]; inorganic nanoparticles of cerium oxide (CeO_2), which proved to be an effective antioxidant capable of mitigating oxidative stress and proinflammatory activity in cirrhotic rats[152]; and polymeric nanoparticles decorated with vitamin A for the specific and controlled delivery of NO to HSC, that demonstrated to downregulate the profibrogenic and contractile activity of these cells *in vitro*, and to reduce PH in BDL rats[153].

1.3.1. Polymeric micelles

Among the several types of nanoparticles that have been developed, one of the most prominent are polymeric micelles (PM), which have recently gained significant attention as a carrier system for drug administration to overcome the low solubility, bioavailability and biodistribution of hydrophobic drugs, as well as to enable a precise targeting and controlled drug release, which ultimately modifies the efficiency and decreases systemic side effects[137,154–156]. PM have a small size (10 to 100 nm) and are characterized by a core-shell structure, formed by hydrophilic and hydrophobic polymeric blocks that self-assemble in an aqueous environment in such a way that the hydrophobic block forms the internal core and the hydrophilic block acts as a surrounding shell. This phenomenon occurs when the critical micelle temperature (CMT) or concentration (CMC) of so-called amphiphilic block copolymers (ABC) is exceeded. Therefore, the CMT or CMC are defined as the minimum temperature or concentration, respectively, at which single polymer chains (unimers) self-assemble to form thermodynamically stable micelles[155,157–159] (Figure 15). The inner hydrophobic domain can act as a storage for lipophilic drugs, as would be the case for simvastatin, in order to increase their solubility

and improve drug bioavailability. For its part, the hydrophilic surrounding shell provides steric stability assuring the integrity of micelles in an aqueous environment and, if properly selected, prevents rapid uptake by the RES, resulting in prolonged circulation time in the body[145,155,158,160]. In addition, this hydrophilic surface can be easily functionalized with active-targeting ligands to further improve drug targeting to the organ or cell of interest[149].
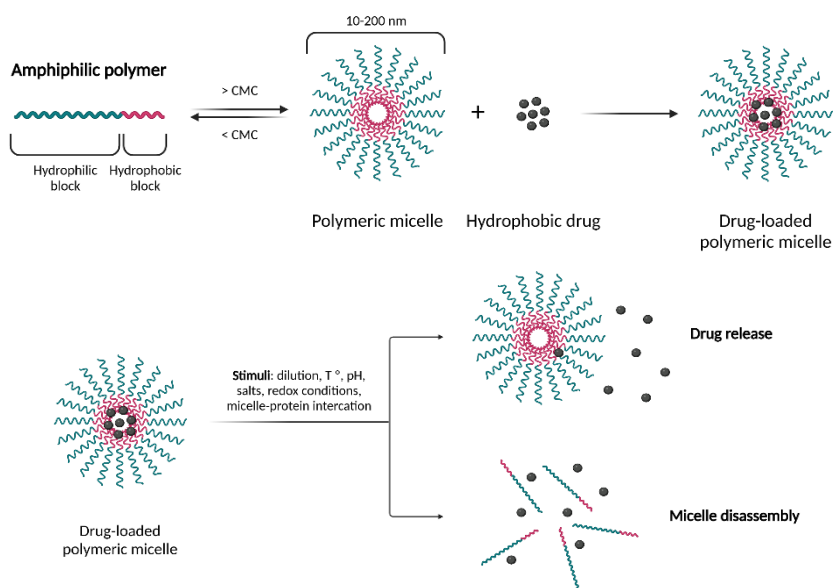
Figure 15. Schematic representation of polymeric micelles formation and drug release. CMC: critical micelle concentration. Adapted from Ghezzi M et al., J Control Release 2021[161]. *Created with BioRender.com*.

On the one hand, most commonly used polymers for hydrophobic core formation are poly(propylene oxide) (PPO), poly(lactide), poly(lactide-co-glycolide), poly(ε-caprolactone), poly(L-aspartate) and poloxamers. The stability of PM, determined by their CMC, depends on the type and molecular weight of the hydrophobic block, and in general, the more hydrophobic and the higher the molecular weight, the lower the CMC[149,156,161]. Moreover, hydrophobic interactions between the drug and the core of these nanoparticles are a key factor in solubilizing poorly soluble drugs, as well as retarding their release rate[162]. On the other hand, some of the widely accepted

hydrophilic copolymers used to wrap the hydrophobic core in PM include PEG, the most common, poly(oxazolines), chitosan, hyaluronic acid and dextran. For all these molecules, the surface density and molecular weight, among other physicochemical properties, need to be considered because they are closely related to the systemic circulation time, biodistribution and stability of PM *in vivo*[157,161].

Pluronic®-based PM

In this way, it is possible for researchers to explore various polymeric combinations, differing in functionalization and flexible chemistry. Among them, the most used and studied polymers are a type of ABC called poloxamers consisting of PEG and PPO blocks arranged in a basic triblock A-B-A copolymer structure: PEG_x-PPO_y-PEG_x. This arrangement results in an amphiphilic copolymer in which the number of hydrophilic PEG (x) and hydrophobic PPO (y) units can be altered, forming various compositions that are commercially available under the name Pluronics® (BASF, Ludwigshafen, Germany)[159,163]. The Pluronic®-based PM have been shown to be very promising and have gained substantial attention over conventional block copolymers due to their advantageous properties, such as being non-ionic and having high surface-activity, high loading capacity, low-toxicity, low immunogenicity, and an excellent biocompatibility and biodegradability[164,165]. Thus, some of the Pluronics® have been approved by FDA to be used as injectable nanomedicines in human body in various biomedical application like anticancer drug delivery, gene therapy, diagnostics, scaffold synthesis for tissue engineering, and separation and purification of proteins[157]. Examples of these are Pluronic® F127 (PEG_{100}-PPO_{65}-PEG_{100}) and Pluronic® F108 (PEG_{133}-PPO_{50}-PEG_{133}), belonging to the category of hydrophilic Pluronics®, which not only have good hydrophilicity but also have excellent biocompatibility[166]. In addition, Pluronic® F127 is the most widely polymer used due to its diverse nature, having a major potential in pharmaceutical applications[155,167–169].

1.3.2. Functionalization

Finally, one of the outstanding properties of PM, and therefore of micelles made of Pluronics®, is their ability to be functionalized (FPM) by adding peptide or protein molecules for active targeting to their hydrophilic surface to enhance drug delivery to specific sites in the body or specific receptors on cells, thereby maximizing the therapeutic efficacy of the cargo while reducing systemic toxicity compared with untargeted micelles[139,170,171]. The concept behind this approach is based on the proposition that Pluronic® PM internalize in cells via receptor-mediated endocytosis, as it has been shown that Pluronics® can be internalized by caveolae-mediated endocytosis (unimers), as well as transported through cell membrane via clathrin-mediated endocytosis (micelles). When ligands conjugated to PM bind to their specific receptors on the cell membrane, endocytic internalization of those FPM is promoted. In this way, active targeting results in higher intracellular drug concentrations and less systemic toxicity[172–174] (Figure 16).
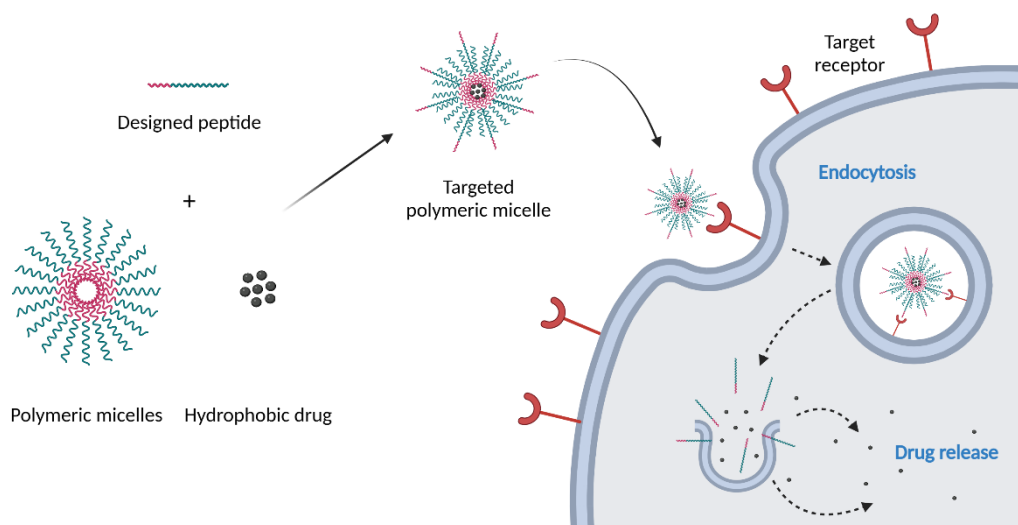
Figure 16. Active targeting of PM and endocytic uptake. Adapted from Nag OK et al., Pharmaceutics 2019[175]. *Created with BioRender.com*.

Usually, incorporation of hydrophilic proteins into Pluronic® micelles involves covalent attachment of the ligand to the free terminal hydroxyl groups (-OH) at the ends of the hydrophilic blocks, so that ligands are exposed on the surface and are available for tissue-specific binding. Among the many possibilities we find peptide binding, but other molecules can also be bound to the shell-forming block, such as organic compounds, oligosaccharides, vitamins or antibodies[164,176]. On this subject, peptide ligands resemble protein-protein interactions with advantages over protein ligands. Peptides have a greater ability to penetrate cells than proteins and are easier to synthesize in large scales. Compared with small molecule ligands, peptides have higher binding specificity and affinity to receptors. On the other hand, peptide stability is considered a hardship, but can be solved by methods that increase it, including cyclization of peptides by disulfide bonds or amide bonds, or via synthesis of peptides containing D-amino acids[177]. Lastly, it is worth mentioning that drugs or nanoparticles functionalized with peptides are usually administered parenterally and rarely orally, and an important reason for this is to avoid proteolytic enzymes found in the digestive system[178].

In summary, in this thesis we wanted to explore the development of a nanoparticle targeting the liver, and specifically LSEC because of their crucial role in the development of CLD and their very accessible biological location, for the delivery of one of the types of drugs that have shown most potential for improving PH and fibrosis in recent years, statins, but which have also generated unwanted toxic effects, especially simvastatin. In this endeavour, the functionalization of a Pluronic®-based PM emerges as a possibility to optimize the delivery of this nanodevice for active targeting to LSEC by using peptide ligands with affinity for receptors expressed on the cell membrane of these cells. As will be explained later in the Methods section (see section 4.1.3, *Selection of target receptors on LSEC and their peptide ligands*), a series of criteria were used to choose the following three cell membrane receptors in LSEC for PM targeting:

CD32b

CD32b is a low-affinity FcγR that belongs to the family of IgG-scavenger receptors, being the only inhibitory FcγR. It plays a crucial role in immune responses, emerging as one of the critical regulatory receptors in immune homeostasis, controlling both the threshold and the extent of immune activation by maintaining immune tolerance. As a result, it is expressed in various cell types including monocytes, phagocytes, basophils, mast cells, B lymphocytes[179,180]. Moreover, as explained before, CD32b has a noteworthy role is the clearance function of LSEC acting as a scavenger receptor from the peripheral blood mediating the endocytosis of small soluble IgG-antigen complexes. LSEC express this receptor in physiological conditions and it has been used as one of the differential markers for these endothelial cells[25,181,182]. Conversely, CD32b expression is affected by the capillarization process of LSEC in situations of liver damage and is gradually lost as these cells become dysfunctional, along with other receptors specific to the fenestrated endothelium[115,183].

Thrombospondin receptor

The so-called thrombospondin receptor (CD36), which belongs to the class B scavenger receptors acting as a cell-cell and cell-matrix adhesion molecule, is a transmembrane glycoprotein expressed on the surface of a wide variety of cells like platelets, adipocytes, monocytes, hepatocytes and most vascular endothelial cells. It is a multifunctional signalling molecule with several known ligands such as thrombospondin-1, long-chain free fatty acids (FFAs), the native high-density lipoprotein (HDL), low-density lipoprotein (LDL) and very-low-density lipoprotein (VLDL), and modified lipoproteins (e.g. oxidized LDL (ox-LDL))[184–186]. CD36 is strongly expressed on LSEC, where it has multiple functions including acting as a scavenger receptor for ox-LDL[33,34,186–188]. Anyhow, microvascular endothelial cells also appeared to constantly express CD36, which behaves like a collagen receptor. The level of expression of this cell-matrix adhesion protein detected on the endothelial lining of portal vessels and centrilobular veins is comparable to that of LSEC. In this line, CD36 expression is maintained throughout the capillarization

process of LSEC, where these cells adopt a more common endothelial phenotype, as it is a baseline marker present on capillary vessel cells[186–188].

Integrin $\alpha_V\beta_3$

Integrins belong to a large family of cell surface receptors that regulate cell attachment and respond to ECM, playing an important role in normal physiological development by cell signalling, cell-to-cell adhesion, apoptosis, and cell-matrix interactions. Integrins are transmembrane heterodimeric molecules composed of α and β subunits, generating multiple combinations that have led to the description of at least 24 distinct integrins[151,189]. Each combination has its own binding specificity and signalling properties, but a common feature of integrins is that they bind to ECM proteins by way of the three amino acid sequence of arginine-glycine-aspartic acid (Arg-Gly-Asp, RGD), forming an integrin-binding motif[190–192]. Integrin $\alpha_V\beta_3$ is strongly expressed by microvascular endothelial cells, but only faintly detectable along the sinusoidal wall[187]. This fact changes when we talk about capillarized LSEC, as it has been proved that they express high levels of integrin $\alpha_V\beta_3$[193]. In turn, this integrin also becomes expressed by HSC during their activation and promotes their proliferation and survival[194]. Finally, as respect to hepatocytes, integrin $\alpha_V\beta_3$ has been reported to be overexpressed in carcinoma tissue and mediates the invasion and metastasis of HCC cells[189]. Thus, in general terms, the hepatic expression of integrin $\alpha_V\beta_3$ has been demonstrated to be increased along with the development and progression of liver fibrosis[189,191,195], being explored as a target unit of drug delivery systems for the treatment of liver fibrosis and PH[151,193].

2. HYPOTHESIS

2. HYPOTHESIS

Although CLD is a major cause of mortality and morbidity, affecting approximately 1.7 million people worldwide, the available treatments for PH, one of its main consequences, are currently limited. Reducing HVPG/PP has been shown to have beneficial effects in preventing complications of PH and decompensation of cirrhosis. In this regard, over the last decades, statins have played a crucial role as a potential treatment for CLD, demonstrating beneficial vasoprotective and antifibrotic effects at the hepatic level. However, this class of drugs has also shown adverse effects, mainly muscle and liver toxicity.

The use of nanoparticles as drug delivery systems has been widely studied in recent years thanks to advances in nanotechnology, specially used to lower the overall systemic dose and damage that toxic and potent drugs may produce by spatially locating their release to specific therapeutic sites. Regarding this, there are formulations that have shown promising results in ameliorating liver fibrosis, as well as nanocarriers that have been used to encapsulate statins. But the use of simvastatin-loaded nanodevices specifically targeting LSEC in models of CLD has not been addressed so far.

For this reason, this doctoral thesis focuses on the election of LSEC as the cellular target for simvastatin-loaded PM nanoparticles because of their accessible location forming the liver vascular wall and their leading role in CLD pathophysiology, while taking advantage of their outstanding endocytic capability thanks to the expression of multiple receptors for active endocytosis, which can be used as a target for FPM.

Altogether, the main hypothesis of this thesis is that the use of PM as nanocarriers for simvastatin reduces the hepatotoxicity and side effects caused by the free drug in the treatment of CLD. Furthermore, the active targeting of PM by functionalizing them with peptides that are ligands for surface receptors expressed on LSEC improves the delivery of simvastatin to this cell type, maximizing its effectiveness and safety.

3. OBJECTIVES

3. OBJECTIVES

The main objective of this doctoral thesis is to develop a drug delivery system as a safe and effective therapeutic tool for CLD, based on a biodegradable PM loading simvastatin and targeting LSEC as one of the initial sensors of liver injury.

The specific aims are:

- To develop a PM with a good stability, an efficient encapsulation of simvastatin and an elevated internalization rate in LSEC.
- To functionalize our PM with peptide ligands for different membrane receptors of LSEC in order to achieve efficient active targeting to these cells and optimize simvastatin delivery.
- To demonstrate the efficiency of PM and FPM when loading simvastatin in ameliorating liver disease progression, and reducing PP and drug toxicity in different rat models of cirrhosis.

4. METHODS

4. METHODS

4.1. Design and production of PM and FPM

4.1.1. Simvastatin activation

Prior to encapsulation or *in vitro* treatment, commercial simvastatin (Sigma-Aldrich, Merck KGaA, Darmstadt, Germany) had to be activated by simulating the metabolic process that occurs in the intestinal wall, liver and plasma when it is administered orally. The drug is in the form of an inactive lactone that is hydrolyzed after ingestion to produce its β-hydroxyacid form, which is the active agent. For this purpose, the protocol for simvastatin activation provided by Merck KGaA was followed. Briefly, 8 mg of simvastatin (0.019 mM) were dissolved in 0.2 ml of pure ethanol, with subsequent addition of 0.3 ml of 0.1 N sodium hydroxide (NaOH). The solution was heated at 50 ºC for 2 h and neutralized with hydrochloric acid (HCl) to pH 7.0. The resulting solution was brought to a final volume of 1 ml with distilled water (dH$_2$O), and aliquots were stored at -80 ºC until use or lyophilized using a VirTis BenchTop Freeze-Dryer (SP Industries, Warminster, USA).

4.1.2. Synthesis of micelles

The synthesis of micelles (both PM and FPM) was based on the thin-film hydration technique, as previously described[169], using Pluronic® F127 and F08 polymers (BASF, Germany). Polymers were weighed and dissolved in an organic mixture of methanol:ethanol (1:1) (Panreac Química SLU, Castellar del Vallès, Spain). Then, the organic solvent was removed under vacuum in a rotary evaporator and the formed thin-film was left to dry overnight (O/N) at room temperature (RT) to eliminate any remaining solvent. In the next step, the film was hydrated with phosphate-buffered saline (PBS; Biowest, Nuaillé, France) pH 7.4 at RT, and the aqueous solution was vortexed for 5 min, allowing polymers to self-assemble to form micelles (Table 1).

Synthesis of drug-loaded micelles

For the formation of simvastatin-loaded micelles (PM/FPM-Sim), activated simvastatin was dissolved, at the desired concentration (20 or 40 mg/ml), in the organic solution of the thin-film hydration technique together with F127 and F108 polymers before the solvent evaporation step.

Synthesis of fluorescently-labelled micelles

F127 and F108 polymers were fluorescently conjugated with 5-([4,6-dichlorotriazin-2-yl])aminofluorescein (5-DTAF; Sigma-Aldrich, Merck KGaA, Germany) in an aqueous medium via nucleophilic aromatic substitution by an addition-elimination mechanism[196]. Briefly, a stock solution of 20 g/L 5-DTAF in dimethyl sulfoxide (DMSO; Sigma-Aldrich, Merck KGaA, Germany) was diluted in 0.1 M sodium hydrogencarbonate (NaHCO$_3$) (pH 9.3) and added to a 6% (w/v) polymer solution in 0.1 M NaHCO$_3$ to a final molar ratio of 1:2 (polymer:5-DTAF). The reaction proceeded O/N in the dark at RT. The 5-DTAF-labelled polymer was purified from the excess of unreacted 5-DTAF by dialysis using Spectra/Por® 2 Dialysis Membranes (MWCO 12-14 kDa; Spectrum Laboratories, Inc., Rancho Dominguez, USA) against dH$_2$O. The dialyzed polymer solution was lyophilized and stored in a closed container protected from light until use. In this case, for internalization studies (see section 4.4.1), fluorescent micelles were synthesized with a 10% of 5-DTAF-labelled polymer (Table 1) using the same technique as non-fluorescent micelles.

On the other hand, for the biodistribution study (see section 4.2.2), another type of fluorescent micelle was generated by loading PM with the tracer 1,1'-dioctadecyl-3,3,3',3'-tetramethylindotricarbocyanine iodide, DiIC$_{18}$(7) (DiR; Invitrogen™, Thermo Fisher Scientific, Waltham, USA), which was introduced into the organic mixture of the micelle synthesis process at a concentration of 1.5% (percentage with respect to polymer).

Synthesis of carboxylated micelles

To allow the PM to be functionalized, Pluronic® F127 needed to be carboxylated (F127-COOH) to assist with the peptide ligand conjugation, and it was done by the maleic anhydride method[170]. F127 polymer and maleic anhydride (1:11 ratio) (Sigma-Aldrich, Merck KGaA, Germany) were dissolved in distilled chloroform and the solution was allowed to react for 24 h under stirring at 70 ºC in a condensation system to avoid any loss of solvent. The solution was concentrated and poured twice into an excess amount of iced cold diethyl ether to precipitate the reaction product. Then, F127-COOH was dried by vacuum dehydration and collected as a white powder for use in the production of carboxylated micelles prepared for functionalization. For this purpose, micelles were synthesized with a mixture of F127 and F127-COOH polymers (8:2 ratio) (Table 1) using the aforementioned thin-film hydration technique.

Table 1. Polymer composition of the different types of micelles synthesized.

Micelle	Polymer composition
PM	100% unlabelled polymer
FPM	80% unlabelled polymer + 20% carboxylated polymer
5-DTAF-PM	90% unlabelled polymer + 10% 5-DTAF-labelled polymer
5-DTAF-FPM	70% unlabelled polymer + 20% carboxylated polymer + 10% 5-DTAF-labelled polymer

FPM: functionalized polymeric micelle, PM: polymeric micelle, 5-DTAF: 5-([4,6-dichlorotriazin-2-yl])aminofluorescein.

4.1.3. Functionalization of PM

Selection of target receptors on LSEC and their peptide ligands

The first step in generating PM specifically aimed at LSEC by functionalizing them was to choose receptors present in the cell membrane of these liver cells to act as target units for the FPM, and then design peptide ligands that interact with those receptors to be used as the peptide elements for functionalization. Through a literature search using the free search engine PubMed (National Institute of Health (NIH), Bethesda, USA), accessing primarily the MEDLINE database, we sought to find a specific marker to differentially identify LSEC in their physiological state, as well as throughout the pathological process of capillarization, but the lack of exclusive markers to these endothelial cells in all these situations led to the establishment of selection criteria whereby the selected receptor (1) was a specific marker of functional LSEC, (2) was expressed in all LSEC, both functional and dysfunctional, and (3) was over expressed in dysfunctional LSEC in pathological situations (Table 2). The rational of these criteria was to select receptors expressed on the cell membrane of LSEC at different levels depending on their state, covering different stages of the pathology. The receptors finally selected were (1) CD32b, (2) CD36 and (3) integrin $\alpha_V\beta_3$.

Table 2. Comparison of the expression level of selected membrane receptors by normal and cirrhotic LSEC, and capillary endothelial cells[25,182,186–188].

Receptor	Normal LSEC	Cirrhotic LSEC	Capillary endothelial cells
CD32b	+++	–/+	–
CD36	+++	+++	+++
Integrin $\alpha_V\beta_3$	+	++	+++

CD32b: Fc-gamma receptor IIb2, CD36: thrombospondin receptor, LSEC: liver sinusoidal endothelial cell. – (undetectable); –/+ (detected on a few cells), + (faintly detected), ++ (moderate labelling intensity), +++ (strong labelling intensity).

Once receptors were chosen, the existing literature was searched again to find ligand proteins for each of the receptors and then, the amino acid sequences of the selected proteins were used to design peptides containing the recognition sequences for the receptor binding sites (Table 3). In the case of CD32b and CD36, these amino acid sequences were determined from literature based on the interaction between ligand proteins and human receptors. For their translation to this study performed in rats, the Basic Local Alignment Search Tool (BLAST; NIH, USA) was used to compare the amino acid sequences of interest (called query) with a library of sequences based on *Rattus norvegicus*. The peptide ligands designed were called (1) CD32b, (2) CD36 and (3) ITGB3.

Table 3. Recognition sequences included in the peptide ligands designed for binding LSEC membrane receptors.

Receptor	Ligand	Peptide ligand (Recognition amino acid sequence)	Reference
CD32b	IgG1	CD32b (TPEVTCVVVDVSHEDP)	180,197–199
CD36	Thrombospondin	CD36 (SVTCG)	200–204
Integrin $\alpha_V\beta_3$	RGD motif	ITGB3 (RGD)	205,206

CD32b: Fc-gamma receptor IIb2, CD36: thrombospondin receptor, IgG1: immunoglobulin G1, RGD: arginine-glycine-aspartic acid.

As a negative control to verify the specificity of the ligand-receptor interaction for the correct targeting of FPM towards LSEC, a scrambled version of the CD32b and CD36 peptide ligands was used to generate FPM with a hindered interaction capacity. To this end, the original amino acid sequence of both designed peptide ligands was used to create a scrambled peptide through a sequence permutation by introducing it at the Scrambled Libraries Tool from the online website of Mimotopes (Mimotopes Pty Ltd., Victoria, Australia).

Synthesis, purification and characterization of peptide ligands

All processes related to the synthesis, purification and characterization of peptide ligands were carried out in the laboratory of Dr. Norman Metanis at the Institute of Chemistry of The Hebrew University of Jerusalem (HUJI, Jerusalem, Israel).

- ### Solid-phase peptide synthesis

All peptides were prepared using solid-phase peptide synthesis (SPPS) technique[207] (Figure 17), either manually or automatically, using a CS136X peptide synthesizer (CSBio, Menlo Park, USA). The peptide synthesis was done on a 2-chlorotrityl chloride resin support (Chem-Impex, Wood Dale, USA), typically on 0.25 mmol scales, using standard fluorenylmethyloxycarbonyl protecting group (Fmoc)-L-amino acids (CSBio, USA; and Matrix Innovation Inc., Quebec, Canada) (Table 4). Fmoc deprotection was done twice by dissolutions with 20% piperidine in *N,N*-dimethylformamide (DMF) (Bio-Lab Ltd., Jerusalem, Israel) for 5 min. The carboxylic acid functional group (-COOH) present at the C-terminus of each amino acid was activated with 4 equiv of coupling reagent *O*-(1*H*-6-chlorobenzotriazole-1-yl)-1,1,3,3-tetramethyluronium hexafluorophosphate (HCTU; Luxembourg Bio Technologies Ltd., Ness Ziona, Israel) in the presence of 8 equiv *N,N*-diisopropylethylamine (DIPEA; Bio-Lab Ltd., Israel) for 5 min and added to the resin for coupling with constant shaking during 30 min at RT. After coupling, the resin was washed trice with DMF and dichloromethane (DCM; Bio-Lab Ltd., Israel), dried and cleaved with a cocktail of trifluoroacetic acid (TFA)/trisopropylsilane/water (94:3:3 ratio) (Bio-Lab Ltd., Israel). After cleavage, the resin was removed by filtration, washed twice with neat TFA and bubbled with nitrogen for TFA removal. Afterwards, cold diethyl ether was added to precipitate the peptide, which was centrifuged (4,000 rpm, 10 min) and diethyl ether was decanted. Cleaved peptide was dissolved in 0.1% TFA in guanidinium chloride (GndCl) (Apollo Scientific Ltd., Stockport, UK) and lyophilized.
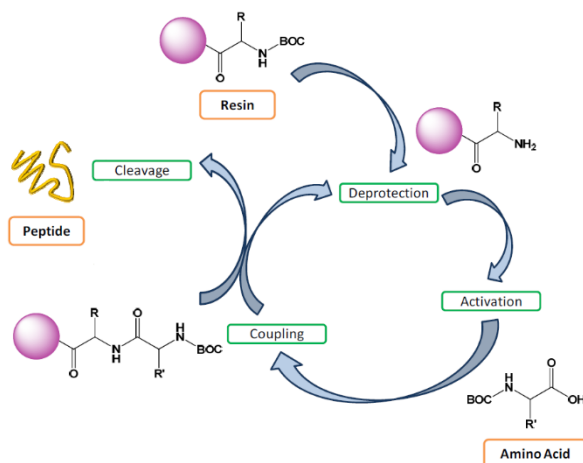
Figure 17. Schematic representation of SPPS. BOC: *tert*-butyloxycarbonyl, R: radical. From Duro-Castano A et al., Polymers 2014[208].

Table 4. Fmoc-L-amino acids used for SPPS.

Fmoc-L-amino acid	Side chain protecting group
Arginine (Arg)	2,2,4,6,7-Pentamethyl-2,3-dihydrobenzofuran-5-sulfonyl (Pbf)
Aspartic acid (Asp)	*tert*-Butyl (*t*Bu)
Cysteine (Cys)	Trityl (Trt)
Glutamine (Gln)	Trityl (Trt)
Glycine (Gly)	2,4-Dimethoxybenzyl (Dmb)
Lysine (Lys)	*tert*-Butyloxycarbonyl (Boc)
Lysine (Lys)	Allyloxycarbonyl (Alloc)
Serine (Ser)	*tert*-butil (*t*Bu)
Threonine (Thr)	*tert*-butil (*t*Bu)

Fmoc: fluorenylmethyloxycarbonyl protecting group. Fmoc-L-amino acids were from CSBio, USA; and Matrix Innovation Inc., Canada.

- ### Synthesis of fluorescently-labelled peptides

For the synthesis of fluorescent peptides, it was coupled Fmoc-L-Lys(Alloc)-OH on the C-terminus of the amino acid chain to label them with fluorescein 5-isothiocyanate (FITC; Sigma-Aldrich, Merck KGaA, Germany), because this fluorescent tracer is known to best react with the amine (NH_2) residue of Lys. To ensure a selective labelling of the FITC on Lys, it was used an orthogonal protecting group Alloc, as orthogonal protecting groups have special and different deprotection conditions. In this line, to perform the deprotection of Lys and get the free NH_2 of it to react with FITC, the peptide-resin was swelled in argon-sparged DCM in a glass reaction vessel and the Alloc group was removed by adding 20 equiv phenylsilane ($PhSiH_3$) and 0.35 equiv tetrakis(triphenylphosphine)palladium(0) ($Pd(PPh_3)_4$) in 5 ml. The reaction vessel was covered using aluminium foil and swelled for 4 h. After deprotection completion, the peptide resin was washed four times with DIPEA in DMF (1:200 ratio) for 2 min. Then, the compound was washed with 20 mM sodium diethyldithiocarbamate trihydrate ($NaS_2CN(C_2H_5)_2 \cdot 3H_2O$) in DMF (0.225 gr in 50 ml DMF) by four sequential treatments of 2 min each. Last washings were with DMF followed by DCM, each four times during 2 min. Peptide was then cleaved from the solid support, precipitated in cold diethyl ether and lyophilized. After lyophilization, FITC labelling was done using 4 equiv FITC, 8 equiv DIPEA and a little of DMF, and the reaction vessel was swelled for 2 h for coupling completion.

- ### Purification and characterization of peptides

The lyophilized crude peptides were dissolved in acetonitrile (Bio-Lab Ltd., Israel) in water with 0.1% TFA and purified by reversed-phase high-performance liquid chromatography (RP-HPLC) done on a LC Prep 150 System, with 220 and 280 nm ultraviolet (UV) detection, using a XSelect CSH C18 column (5 μm, 130 Å, 30 x 250 mm) (Waters Corporation, Milford, USA). According to the UV absorption, RP-HPLC peaks were collected and characterized by electrospray ionization mass spectrometry (ESI-MS) performed on a LCQ Fleet™ Ion Trap Mass Spectrometer (Thermo Scientific™,

Thermo Fisher Scientific, USA). Peptide masses were calculated from the experimental mass-to-charge ratios (*m/z*) from all the observed multiply charged species of peptides.

Synthesis of FPM

First, for the functionalization of PM, nanoparticles needed to be generated with a mixture of F127 and F127-COOH polymers, as explained above (see section 4.1.2, *Synthesis of carboxylated micelles*), and once synthesized, they were incubated with 1-ethyl-3-(3-dimethylaminopropyl)carbodiimide (EDC; Sigma-Aldrich, Merck KGaA, Germany) dissolved in water (PM:EDC ratio 1:1.5) and stirred for 30 min at RT to activate the carboxylic acid groups of all modified polymers (20% of total polymer). Second, synthesized peptide ligands were modified by adding a Cys residue at the N-terminus of the peptide chain in order to be used in the conjugation reaction with the activated carboxyl groups of PM, which was done by the native chemical ligation (NCL) technique[209], based in creating a natural amide bond. For this reaction, modified peptides were solubilized in PBS, added to the activated PM solution (peptide:PM ratio 1:100) and incubated under stirring for 2 h at RT. The obtained dispersion of PM or FPM was filtered through a 0.22 µm syringe filter (Gilson Inc., Middleton, USA) for sterilization and to remove eventual aggregates. Once filtered, all types of nanoparticles were lyophilized for long-term storage at RT until use.

4.1.4. Physicochemical characterization of micelles

Regarding functionalization, each batch of FPM synthesized was analyzed by Fourier-transform infrared spectroscopy (FTIR) to confirm the correct conjugation of peptide ligands to the hydrophilic surface of these micelles. FTIR was carried out in the Preparation and Characterization of Soft-Materials Services at Institut de Ciència de Materials de Barcelona (ICMAB-CSIC, Barcelona, Spain) using a Spectrum One FT-IR Spectrometer (energy range: 450-4,000 cm^{-1}) (PerkinElmer, Inc., Waltham, USA), equipped with the Universal Attenuated Total Reflectance (UATR) accessory.

Particles mean hydrodynamic diameter and polydispersity index (PDI) were measured by dynamic light scattering (DLS), and zeta potential by laser Doppler micro-electrophoresis using a Zetasizer Nano (Malvern Instruments, Malvern, UK) with an angle of 173 º in a measurement range of 0.3 nm - 10 µm and sensitivity of 0.1 mg/ml.

Particle shape and size were observed by transmission electron microscopy (TEM) using the high performance and high contrast 120 kV JEM-1400Flash Electron Microscope (JEOL Ltd., Tokyo, Japan) from the Electron Microscopy Service at Univeristat Autònoma de Barcelona (UAB, Cerdanyola del Vallès, Spain). For their visualization, samples were placed on a copper carbon-coated grid and negatively stained with uranyl acetate for 1 min at RT. Gatan software (Gatan, Inc., Pleasanton, USA) was used to process information and get measures from TEM images.

Drug encapsulation

To assess the encapsulation percentage of simvastatin for each formulation produced, the encapsulation efficiency (EE; %) of the loaded drug was calculated by equation 1. From the total amount of drug added to the aqueous solution in the micelle synthesis technique, the free drug that was not encapsulated was obtained by centrifuging the samples (10,000 rpm, 10 min, 4 ºC) in a Nanosep® Centrifugal Device with Omega™ Membrane 10K (Pall Corporation, Port Washington, USA), a membrane pore which does not allow micelles to pass through, and analyzing the filtrate by ultra performance liquid chromatography-tandem mass spectrometry (UPLC-MS/MS) on a Xevo™ TQ Absolute mass spectrometer (Waters Corporation, USA). All experiments were performed in triplicate at 20 ºC, and the total area of the peak was used to quantify the free drug.

Equation 1. Determination of EE of loaded simvastatin in nanoparticles.

$$\text{EE (\%)} = \frac{\text{Total amount of simvastatin} - \text{Free simvastatin in filtrate}}{\text{Total amount of simvastatin}} \times 100$$

In vitro drug release assay

In vitro release profile of simvastatin from micelles was assessed using the regular dialysis method[210]. Briefly, PM/FPM loaded with 20 mg/ml of simvastatin were placed inside a dialysis device Spectra/Por® Float-A-Lyzer® G2 (MWCO 20 kDa; Spectrum Laboratories, Inc., USA) immersed in a PBS pH 7.4 solution (1:100 dilution). The system was maintained at 37 ºC under magnetic stirring and at predetermined time intervals (0.25, 0.5, 1, 3, 6, 9, 12, 24, 48 and 72 h) a 500 µl sample of released media was collected for simvastatin quantification by UPLC-MS/MS (Xevo™ TQ Absolute). This volume was replaced with fresh buffer. All formulations were analyzed in duplicate.

4.2. Animal experimentation

All animal procedures were conducted in accordance with European Union legislation on the protection of animals used for scientific purposes (Directive 2010/63/EU revising Directive 86/609/EEC), approved by the Animal Research Ethics Committee (CEEA) of the Vall d'Hebron Institut de Recerca (VHIR, Barcelona, Spain) (approved file numbers: 10374 (first study), 11014 and 11427 (second study)) and conducted in the animal facilities of VHIR.

Male Sprague-Dawley® rats of Oncins France Strain A (OFA) and CD® strains (Charles River Laboratories, Saint-Germain-sur-l'Arbresle, France) were used in the first and second study, respectively, to generate two models of CLD with PH and cirrhosis. All animals were housed under a constant temperature of 22 ± 2 ºC and 50% humidity in a controlled 12/12 h light/dark cycle. They were fed *ad libitum* with a grain-based chow (SAFE® 150; SAFE® Complete Care Competence, Rosenberg, Germany) and had free access to water.

In addition, male BALB/cAnNRj mice (Janvier Labs, Le Genest-Saint-Isle, France) aging 5-6 weeks were used for the maximum tolerated dose (MTD) assay of the second study, performed at Cellvax facilities (Villejuif, France) (see section 4.2.4). Animal health status was specific and opportunistic pathogen free (SOPF), and they were housed in

polyethylene cages (< 5 mice/cage) in a climate and light controlled environment in accordance with Cellvax approved standard operating procedures.

4.2.1. Experimental animal models of PH

BDL model

Intrahepatic PH caused by secondary biliary cirrhosis was induced by common BDL for a period of 4 weeks on male Sprague-Dawley OFA and CD rats weighing 200-220 g.

Before starting the surgery, a 0.01-0.05 mg/kg dose of analgesia (Bupaq® Multidose 0.3 mg/ml; Richter Pharma AG, Wels, Austria) was administered subcutaneously (25G needle) to prevent painful stimulus. At the time of surgery, the rat was anaesthetized by inhalation of isoflurane (5% for induction and 2% for maintenance; Baxter International Inc., Deerfield, USA). The abdomen was shaved and the skin was disinfected with 70% ethanol. The effect of the anaesthesia was checked by foot and eye reflex before starting the procedure. The animal was placed on a heating pad (Homeothermic Monitoring System; Harvard Apparatus, Holliston, USA) to control the body temperature, and the operation was started by making a 4 cm incision in the skin and muscle layer with the help of blunt-tipped scissors, so as not to damage any internal organs. The common bile duct was then dissected from the underlying fat and occluded by double ligation (3 knots each one) with 4-0 non-absorbable silk suture (Perma-Hand®; Ethicon Inc., Johnson & Johnson, New Brunswick, USA), with the subsequent resection of a portion of the duct between the two ligatures to avoid repermeabilization. At the end of the procedure, the muscle layer was sutured continuously with a 4-0 resorbable silk (VICRYL®; Ethicon Inc., Johnson & Johnson, USA) and a thin layer of antiseptic and disinfectant skin solution (Furacín®; SEID Lab, Lliçà de Vall, Spain) was applied to the area to prevent its contamination and infection. Then, the skin was sutured discontinuously, to prevent the rat from completely opening the suture, with the same 4-0 resorbable silk. Finally, povidone-iodine was applied to the suture to prevent skin infections.

Once surgery was completed, 10 mg/kg of prophylactic antibiotic treatment (Gobemicina®; Laboratorios Normon, Tres Cantos, Spain) were given promptly by intramuscular route (27G needle), and analgesic treatment (0.01-0.05 mg/kg) was continued with subcutaneous injections every 8 h for 48 h. Moreover, an 8 mg/kg dose of vitamin K_1 (Konakion®; Cheplapharm, Greifswald, Germany) was administered intramuscularly weekly during the 4-week generation period of the model because, due to BDL, bile acids cannot be released into the duodenum and this prevents the absorption of fat-soluble dietary substances such as vitamin K, which is essential for the synthesis of clotting factors. Therefore, this administration was intended to prevent hemorrhage and decrease the mortality of the model.

Thioacetamide model

Intrahepatic PH was induced by intraperitoneal (IP) injection of 250 mg/kg of thioacetamide (TAA) with a 25G needle, 2 days/week over a period of 8 weeks (16 total injections), to Sprague-Dawley CD rats weighing 125-150 g at baseline. Animals were weighed weekly to adjust the dose to the weight gain.

One hour prior to IP injection, TAA powder (Sigma-Aldrich, Merck KGaA, Germany) was weighted and diluted in 0.9% sodium chloride (NaCl) (XalabarderFarma, Barcelona, Spain) to obtain a solution at a 125 mg/ml concentration. As TAA was in powder form, this process was performed under a fume hood, as it is a toxic and carcinogenic substance. The solution was vortexed for a few minutes until the TAA was completely dissolved and kept at RT until use.

Each rat received twice its weight by volume (e.g. 600 µl to a 300 g rat) of the 125 mg/ml TAA solution to administer a dose of 250 mg/kg. After receiving the 16 total injections, all animals developed histological features of cirrhosis.

4.2.2. Biodistribution study

PM-F127 loaded with DiR were intravenously (IV) injected (25G needle) to healthy and BDL rats (n = 3 animals/group) at a dose of 0.8 mg/kg of DiR. Rats were monitored over time using a non-invasive IVIS® Spectrum *in vivo* imaging system (PerkinElmer Inc., USA), taking serial images from 0 to 2 h. At the end of the experiments, nanoparticle accumulation in tissues *ex vivo* was analyzed by fluorescence imaging and quantified as radiant efficiency (Living Image® 4.3.1 software; PerkinElmer Inc., USA).

Following imaging studies, samples of harvested liver, muscle and kidney tissues were collected and snap frozen in liquid nitrogen. Slices of 6-7 µm were obtained with a Leica CM3050 S cryostat (Leica Biosystems, Wetzlar, Germany), fixed with acetone -20 ºC for 10 min and washed in PBS (3 x 5 min) at RT. Samples were then stained for 5 min with 4',6-diamidino-2-phenylindole (DAPI; Thermo Scientific™, Thermo Fisher Scientific, USA) in a 1:1,000 dilution in PBS, washed again with PBS in triplicate and mounted with VECTASHIELD® Antifade Mounting Medium (Vector Laboratories, Inc., Newark, USA). After drying, slices were visualized under a FV1000 spectral confocal microscope (Olympus Corporation, Shinjuku, Japan) for DiR-PM localization taking images of 60x magnification.

In a different set of animals, detection of PM accumulation in the liver at different time points was performed. A single dose of 5-DTAF-labelled PM-F127 (100 mg/kg of polymer) was administered IV to healthy rats and liver tissue was obtained at three time points: 4, 24 and 48 h (n = 3 animals/group) for 5-DTAF-PM detection by confocal microscopy, as explained above.

4.2.3. Determination of simvastatin in muscle tissue

For simvastatin detection in muscle, healthy rats were treated with different formulations of the drug at 20 mg/kg to compare their accumulation in this tissue. Treatments were as follows: oral (inactive) and IV (active) simvastatin, PM-Sim, FPM-CD32b-Sim, FPM-CD36-Sim and FPM-CD32b-CD36-Sim (n = 3 animals/group). After 10

h, a sample of quadriceps femoris muscle was obtained, snap frozen and ground to a fine powder. A sample of ground muscle was then dissolved with a buffer composed of methanol and dH_2O (1:1 volume, final concentration 0.2 g muscle/ml) and sonicated for 15 sec three times. The homogenate was centrifuged at 13,000×g for 10 min at 4 ºC and the supernatant was stored at -20 ºC until simvastatin extraction was performed as previously described[136]. To this end, 50 µl of muscle homogenate supernatant were mixed with 125 µl of acetonitrile and vortexed for 30 sec. Following, 25 µl of 5 M ammonium formate (NH_4HCO_2) buffer (pH 4) were added and the mixture was vortexed again. Finally, the sample was centrifuged at 13,000×g (10 min, 4 ºC) and the supernatant was analyzed by UPLC-MS/MS (Xevo™ TQ Absolute) for quantification of active simvastatin.

4.2.4. MTD
To study the safety profile of simvastatin-loaded nanoparticles, a MTD assay was performed to determine the highest tolerated dose that would not produce significant toxicity when assessing the *in vivo* efficacy of these formulations. This assay was conducted in both healthy rats (first study) and healthy mice (second study).

First study: MTD of PM-F127-Sim and PM-F108-Sim
PM-F127-Sim and PM-F108-Sim were administered IV (25G needle) to healthy rats at 5, 10 and 20 mg/kg of simvastatin, and compared with oral drug administration at the maximum dose of 20 mg/kg (n = 3 animals/group). As control, a vehicle group was performed by giving IV PBS. Treatments were administered 3 days/week for 2 weeks. Body weight and animals' behaviour was controlled during treatment, and blood samples were collected at days 0, 2, 5 and 10.

Second study: MTD of FPM-Sim

For the second study, the MTD assay was outsourced and conducted by the preclinical contract research organization Cellvax, as abovementioned. In this case, to determine the MTD and administration schedule of FPM-Sim, the trail was divided into three sequential phases where acute toxicity (phase 1 and phase 2) and subacute toxicity (phase 3) of treatment with FPM-CD36-Sim formulation, as the reference FPM-Sim, were evaluated. For the different phases, various doses and administration schedules were used as shown in figures 18 and 19. All phases were performed in healthy mice, and the weight and condition of the animals were monitored throughout the process.

- ### Acute toxicity: Phase 1 and phase 2

In phase 1 of the acute toxicity study, different doses of encapsulated simvastatin (10, 20 and 50 mg/kg), determined on the basis of doses used in previous studies with free simvastatin and PM-Sim (first study), were tested by administering a single IV dose (25G needle) and drawing samples at different times (4 h, 48 h and 1 week) post-treatment (n = 2 animals/group). This phase was used to determine the dose that showed neither toxicity nor mortality. Control group was performed in animals that did not receive any kind of treatment.

The selected dose in phase 1 (FPM-CD36-Sim 10 mg /kg) was further evaluated in a second acute toxicity phase (phase 2), where it was IV given 3 days/week during 2 weeks to see the cumulative effect of the drug on the animals for up to 14 days compared to the control condition (n = 5 animals/group) (Figure 18).
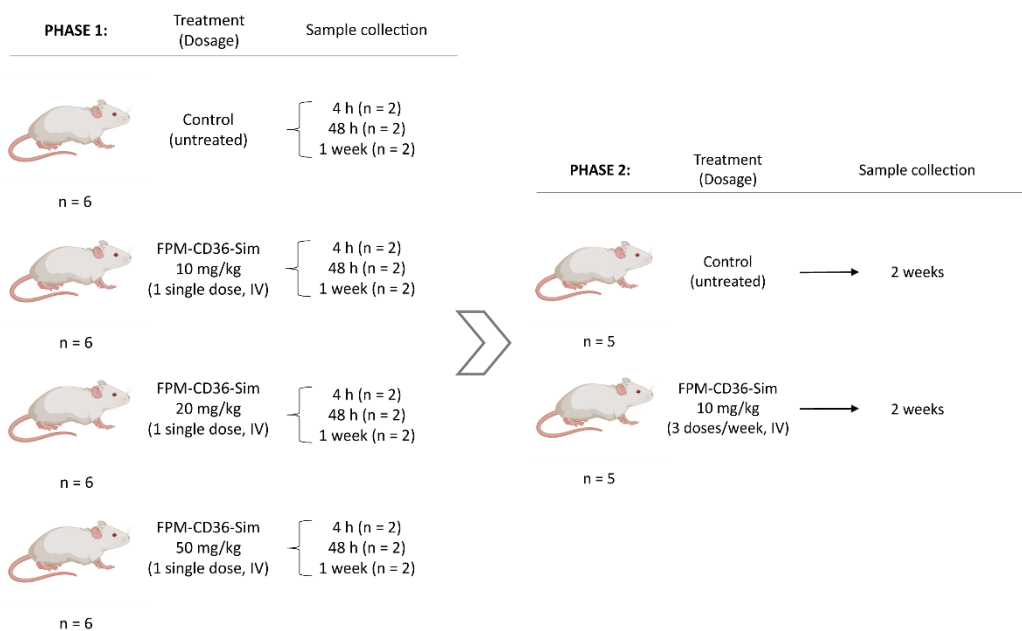
Figure 18. Study design of the acute toxicity study (phase 1 and phase 2) from the MTD assay of FPM-Sim. FPM: functionalized polymeric micelle, IV: intravenous, Sim: simvastatin.

- Subacute toxicity: Phase 3

In the subacute toxicity phase, 10 mg/kg FPM-CD36-Sim were administered 5 days/week during 3 weeks, simulating a longer treatment situation. For this phase, a vehicle group receiving IV saline injections was conducted as control. For each group, 10 mice were used (Figure 19).
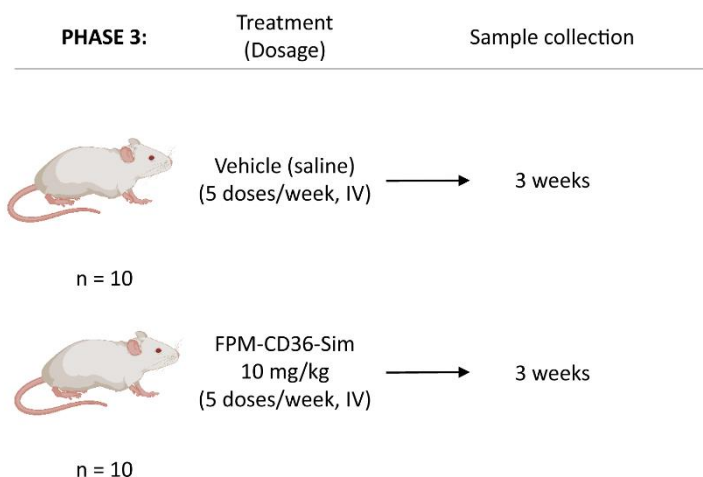
Figure 19. Study design of the subacute toxicity study (phase 3) from the MTD assay of FPM-Sim. FPM: functionalized polymeric micelle, IV: intravenous, Sim: simvastatin.

- **Sample collection: Serum and liver tissue**

Once the treatment was completed in each of the phases, serum and liver tissue samples were obtained from the animals, and sent to our facilities for biochemical and histological analysis, respectively.

4.2.5. *In vivo* efficacy study

Animal treatment

For all efficacy studies, treatment with simvastatin (Ratiopharm, Ulm, Germany) was administered orally by *gavage* with a polyurethane feeding tube of 13ga for rats (Instech Laboratories, Inc., Plymouth Meeting, USA), and treatment with simvastatin-loaded nanoparticles was administered IV (25G needle). Animals were weighed daily to administer the doses established in each study.

For oral administration of simvastatin, a solution was prepared at a concentration of 10 mg/ml by dissolving 100 mg of simvastatin powder (from 10 crushed tablets, 10 mg/tablet) in 10 ml of water suitable for animal consumption, provided by the Laboratory Animal Service (LAS) of VHIR. The solution was kept at 4 ºC and vortexed

before use. The volume (in µl) of *gavage* administered corresponded to the weight of the animal (in g) for a 10 mg/kg dose.

For administration of encapsulated simvastatin, vials were prepared with lyophilized micelles containing 100 mg/ml Pluronic® polymer, 20 mg/ml simvastatin and, in the case of functionalized nanoparticles, 1 mg/ml peptide ligand. These vials were resuspended in 250 µl of water for injections and diluted in saline (Fresenius Kabi, Bad Homburg, Germany) to obtain the desired concentrations of PM/FPM-Sim: 1 or 5 mg/ml. The micelles solution was filtered through a 0.22 µm filter and a volume (µl) corresponding to the animal weight (g) (e.g. 300 µl to a 300 g rat) was injected IV in order to administer a dose of 1 or 5 mg/kg simvastatin, respectively.

- **First study: *In vivo* efficacy of PM-F127-Sim**

To evaluate the therapeutic effect of PM-Sim compared to oral simvastatin, cirrhotic rats developed by 3 weeks of BDL were randomly distributed among the following groups: vehicle (oral dH$_2$O) (n = 11), oral simvastatin 10 mg/kg (n = 9), PM-F127-Sim 1 mg/kg (n = 7) and PM-F127-Sim 5 mg/kg (n = 13). All treatments started at day 22, when cirrhosis had already developed, and were daily administered during 7 days (Figure 20).

- Second study: *In vivo* efficacy of FPM-Sim
    - BDL model

In order to assess the pharmacological effect of FPM-Sim on the hepatic hemodynamics, rats were treated from day 22 of BDL and administered daily for 7 days, comparing the effect of functionalized versus non-functionalized micelles and oral simvastatin. BDL rats that did not receive any treatment were used as controls. Rats were randomly assigned to each of the study groups: control (untreated) (n = 9), oral simvastatin 10 mg/kg (n = 15), PM-Sim 5 mg/kg (n = 9), FPM-CD32b-Sim 5 mg/kg (n = 9), FPM-CD36-Sim 5 mg/kg (n = 14) and FPM-CD32b-CD36-Sim 5 mg/kg (n = 10) (Figure 20).
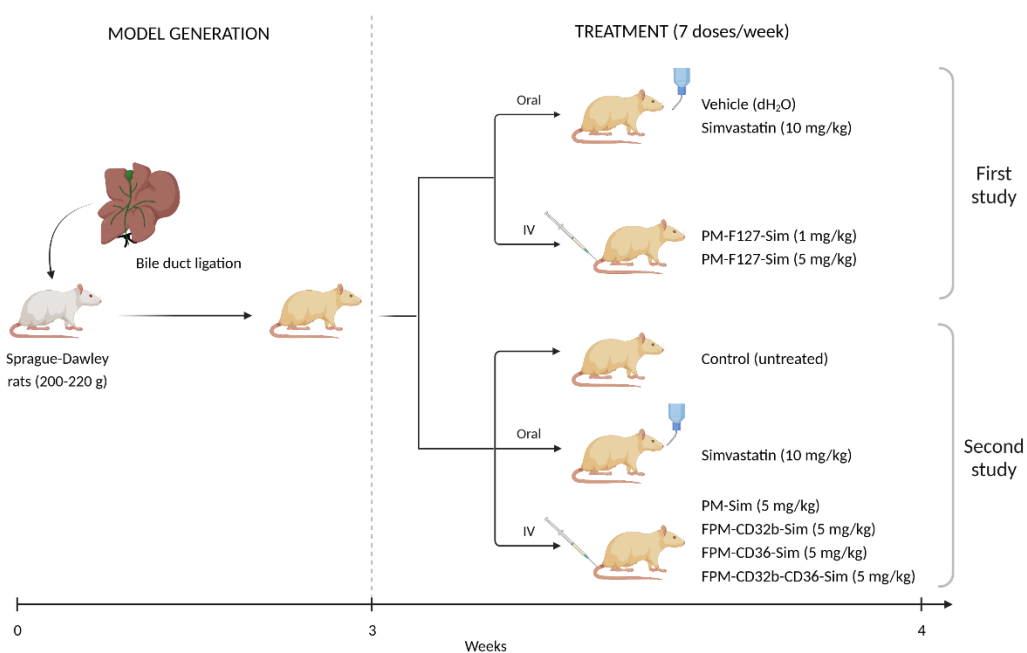
Figure 20. Schematic representation of the BDL model performed on Sprague-Dawley rats and treatments administered for the evaluation of *in vivo* efficacy in the first and second study. dH$_2$O: distilled water, FPM: functionalized polymeric micelle, IV: intravenous, PM: polymeric micelle, Sim: simvastatin. *Created with BioRender.com*.

○ TAA model

To study the effect of FPM-Sim on PP, and other hemodynamic and biochemical parameters, in the TAA model, rats were treated during the last 2 weeks of the 8-week model generation, receiving a total of 10 doses (5 doses/week). The study groups to be compared were the same as for the efficacy study in the BDL model, with animals randomly distributed to each group: control (untreated) (n = 9), oral simvastatin 10 mg/kg (n = 10), PM-Sim 5 mg/kg (n = 10), FPM-CD32b-Sim 5 mg/kg (n = 10), FPM-CD36-Sim 5 mg/kg (n = 10) and FPM-CD32b-CD36-Sim 5 mg/kg (n = 10) (Figure 21).
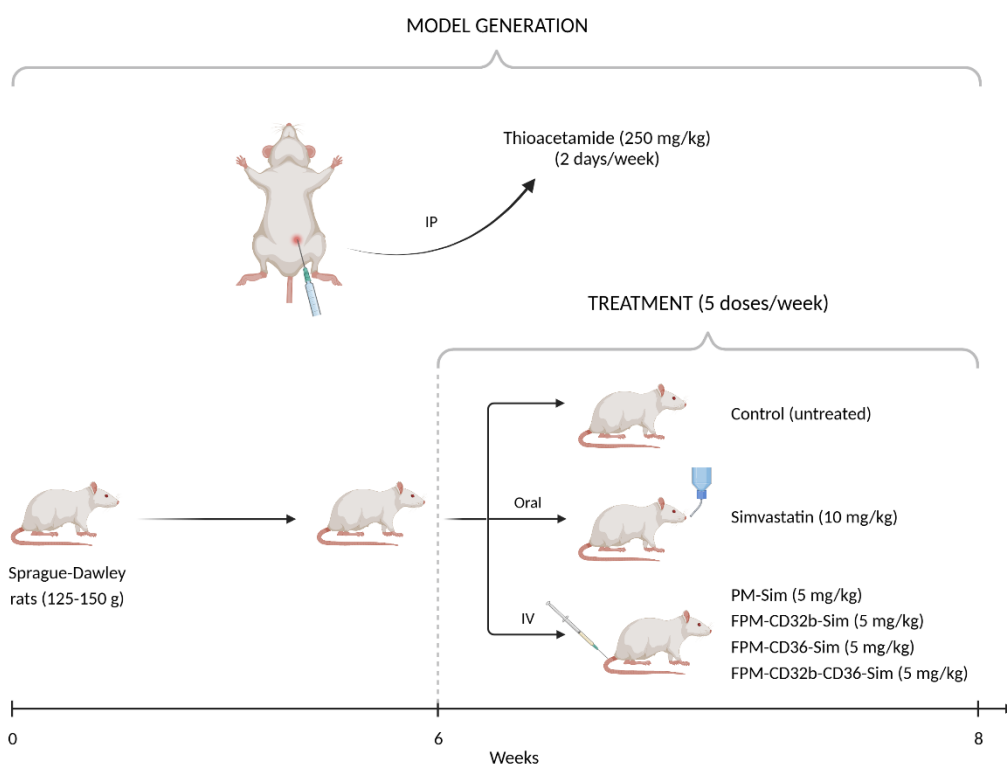
Figure 21. Schematic representation of the TAA-induced cirrhotic model performed on Sprague-Dawley rats and treatments administered for the evaluation of *in vivo* efficacy in the second study. FPM: functionalized polymeric micelle, IP: intraperitoneal, IV: intravenous, PM: polymeric micelle, Sim: simvastatin. *Created with BioRender.com*.

Hemodynamic study

The measurement of hemodynamic parameters was performed under fasting conditions (O/N) 90 min after the last dose of drug or vehicle administered. The dose of anaesthesia was adjusted according to the experimental model used and the condition of the animal to prevent breathlessness and bradycardia. Thus, starting from a dose of 100 mg/kg ketamine (Ketolar®; Pfizer, New York, USA) and 5 mg/kg midazolam (Laboratorios Normon, Spain) for healthy rats, BDL animals received 2/3 of the anaesthesia and in the TAA model, 80%. In all cases, anaesthesia was administered IP with a 25G needle. Throughout the process, the animal was monitored for deep anaesthesia using the foot and eye reflex, and in those cases where necessary, an additional dose (a maximum of 0.15 ml ketamine and midazolam, 2:1 or 1:1 ratio) was administered for complete anaesthesia. Once the animal was asleep, the fur was shaved from the abdominal area and the inner part of both legs (for surgical approach), and the animal was placed in the supine position. During the whole process the temperature of the animal was maintained at 37 (± 5) ºC by means of a rectal probe associated to a heating pad (Homeothermic Monitoring System). For the recording of hemodynamic parameters, it was used a PowerLab data acquisition device associated with the physiological data analysis software LabChart 5.0 (ADInstruments, Dunedin, New Zealand).

- ## MAP and heart rate

To determine MAP (mmHg) and heart rate (BPM) a cut on the left inner leg of the animal was made, and the muscle and connective tissue was dissected to expose the femoral triangle, the bundle formed by the femoral artery, vein and nerve. The femoral artery was then separated from the rest of the tissues using forceps and, once the vessel was isolated, a small hole was made with a 23G needle. To cannulate the artery, a polyethylene catheter (BD Intramedic™ Polyethylene Tubing PE 50; BD, Franklin Lakes, USA), connected to a highly sensitive-pressure transducer from the PowerLab device, was introduced through the hole and secured by tying two knots with a 3-0 silk suture

(Silkam®; B. Braun, Melsungen, Germany). From this point on, the MAP was recorded and, through this, the beats per minute (bpm) to determine the HR. These two parameters were monitored at all times to control the state of consciousness of the animal.

- **PP**

In order to cannulate the ileocolic vein to measure PP (mmHg), an incision was made in the lower abdomen and the abdominal cavity was opened through the linea alba to avoid bleeding. At this point where the abdomen was opened, before cannulating the ileocolic vein, the presence or absence of ascites in the cirrhotic animals was determined, as well as the volume of fluid in the affirmative case. In the latter case, the fluid was withdrawn with a syringe. Once this was done, the intestines were removed, and the ileocolic vein was exposed and cannulated with another PE-50 catheter connected to the PowerLab system to initiate PP recording. To immobilize the catheter, 1 or 2 drops of superglue were applied to the area.

- **Superior mesenteric artery blood flow**

With the abdominal cavity opened, the superior mesenteric artery was isolated from the surrounding connective tissue and clamped with a 1.0 mm diameter ultrasonic perivascular flowprobe connected to a TS420 Perivascular Flow Module (Transonic Systems Inc., Ithaca, USA) to measure superior mesenteric artery blood flow (SMABF; [ml/min]·100 g). To facilitate signal transmission, ultrasound gel was applied to the flowprobe beforehand.

- **PBF**

Using the same perivascular flowprobe with ultrasound gel applied to it, the dissected portal vein was clamped to record PBF ([ml/min]·100 g).

- ## Superior mesenteric artery resistance

Superior mesenteric artery resistance (SMAR; [mmHg·min]/[ml·100 g]) was calculated by the following formula:

$$SMAR = \frac{(MAP - PP)}{SMABF}$$

- ## IHVR

IHVR ([mmHg·min]/[ml·100 g]) was calculated by the following formula:

$$IHVR = \frac{PP}{PBF}$$

Sample collection: Blood and liver tissue

Once the hemodynamic study was completed, blood and liver tissue samples were collected from the rat in order to assess the efficacy of *in vivo* treatment by biochemical, and histological and molecular analysis, respectively. First, with the abdomen exposed, the inferior vena cava was sought and a fasting blood sample was obtained (25G needle) and collected in an anticoagulant-free tube (BD Vacutainer® SST™ II Advance Tubes; BD, USA) for subsequent biochemical analysis. After blood sampling, the animal was rapidly euthanized by exsanguination through the inferior vena cava and the liver was harvested. The organ was weighed whole and then a small sample was placed in an embedding cassette for fixation in 4% paraformaldehyde (PFA; Panreac Química SLU, Spain) for 24 h before being paraffin-embedded for histological analysis. The rest of the organ was perfused with physiological saline (Grifols S.A., Barcelona, Spain) to remove any residual blood and cut into pieces (less than 0.5 cm thick). Some of the pieces were snap-frozen in liquid nitrogen and stored at -80 ºC, and others were preserved in RNA*later*™ Stabilization Solution (Invitrogen™, Thermo Fisher Scientific, USA) for 1 week at 4 ºC before being stored at -80 ºC. These perfused liver samples were used for gene expression and protein analysis, respectively (see sections 4.4.4 and 4.4.5).

4.2.6. Biochemical analysis

The biochemical analysis of blood and serum samples was carried out with standard methods at the Hospital Universitari Vall d'Hebron (HUVH) Core Lab (Barcelona, Spain). The parameters determined were creatinine and total bilirubin, AST, ALT, alkaline phosphatase (ALP) and CK enzymes, total cholesterol, triglycerides and albumin.

Liver and muscle toxicity of in vivo efficacy studies

The mean and standard deviation (SD) of ALT and CK enzyme levels of the vehicle group (first study) and the control group (second study) were used to determine a threshold for assessing the potential simvastatin-induced liver and muscle toxicity, respectively, using equation 2. In this way, values above this threshold were considered toxic. The results of the hemodynamic study of animals showing liver toxicity were discarded for the final analysis.

Equation 2. Calculation of the threshold value for determining liver and muscle toxicity of *in vivo* efficacy studies.

$$\text{Liver toxicity} = \text{ALT} > \text{Mean} + (\text{SD} \times 3)$$

$$\text{Muscle toxicity} = \text{CK} > \text{Mean} + (\text{SD} \times 3)$$

4.2.7. Histological analysis

Hematoxylin and eosin staining

The extracted liver tissue samples were fixed in 4% PFA (in embedding cassettes) for 24 h and then preserved in 50% ethanol solution, all under cold conditions (4 ºC), until they were taken to the Pathological Anatomy Department of HUVH, where samples were processed for histological analysis by hematoxylin-eosin (H&E) stain. They were dehydrated (by a sequential treatment with increasing % alcohol solutions and xylene), embedded in paraffin blocks, cut into 4 µm-thick sections and placed into Poly-L-lysine

treated slides for H&E stain. The stained samples were analyzed blindly by an expert liver pathologist from the Hepatology Department of HUVH, who assessed the degree of lobular inflammation according to the scoring system criteria described in table 5.

Table 5. Scoring system for lobular inflammation[211].

Histologic feature	Definition	Score
Lobular inflammation	None	0
	<2 foci per 20x field	1
	2-4 foci per 20x field	2
	>4 foci per 20x field	3

Sirius Red staining

In order to detect liver fibrosis, Sirius Red staining was performed to stain collagen fibres in 4 µm-thick sections of paraffin-embedded liver. The sample was first kept at 60 ºC for 1 h in a hybridisation oven (SHEL LAB®, Sheldon Manufacturing, Inc., Cornelius, USA) to remove paraffin and then underwent a hydration process (Table 6). Once hydrated, the sample was dried and stained with 0.1% Picro-Sirius Red (see Appendix, section 10.1) for 1 h at RT under gentle agitation. It was then washed twice with acidified water (see Appendix, section 10.1) for 5 min and dried. Sample was then dehydrated (Table 7) and mounted with DPX rapid mounting medium (Panreac Química SLU, Spain). For this, the excess xylene was dried from the slides and a drop of DPX was placed on top of the sample with a plastic Pasteur pipette. A coverslip was dropped on top of the slide and lightly pressed to allow the medium to cover the entire tissue sample. Finally, the slides were left to dry O/N in a fume hood.

Table 6. Hydration process of deparaffined liver sections.

Solution	Time (min)
Citrosol	20
Ethanol 100%	5
Ethanol 95%	5
Ethanol 70%	5
dH$_2$O	5

dH$_2$O: distilled water. Citrosol is a xylene substitute.

Table 7. Dehydration process of deparaffined liver sections.

Solution	Time (min)
Ethanol 70%	0.25
Ethanol 95%	0.25
Ethanol 100%	0.25
Xylene	5

The samples were viewed under a BX61 optical microscope (Olympus Corporation, Japan) and images were taken to analyze the fibrotic area. Ten images (10x magnification) were randomly taken of each tissue sample and the ratio of red-stained area to total area was quantified using ImageJ software (NIH, USA). Briefly, RGB colour images were split in three channels (red, green and blue) and after stacking them, the analysis was done in the green colour stack. A threshold of the grayscale (from 0 to 120) was set up and adjusted manually if necessary. The area fraction (%) was measured for each image as the proportion of the grey area regarding the total area.

4.3. Isolation and culture of primary rat liver cells

Primary liver cells were obtained from animals under anaesthesia with 100 mg/kg of ketamine and 5 mg/kg of midazolam by IP puncture (25G needle). Cirrhotic animals received 2/3 of this anaesthesia. After checking the animal's state of sedation through the foot and eye reflex, the abdomen was shaved and disinfected with 70% ethanol, and the animal was placed in the supine decubitus position to begin the procedure. For this, the skin of the abdomen was clamped and with scissors an incision was made in order to find the linea alba and cut in this direction the entire belly of the animal up to the diaphragm. The abdominal cavity was then opened by two lateral cuts and the intestines were removed to expose the portal vein and the inferior vena cava. The area around the incision was covered with sterile gauze to avoid contamination of the liver with bacteria and/or yeast from the skin and hairs. A 3-0 silk suture (Silkam®) was then passed through the infrahepatic inferior vena cava and the portal vein, in the latter case one in the most distal part of the liver and another in the most proximal part, leaving a space for cannulation. Next, 0.5 ml of 1% heparin (Laboratorios Farmacéuticos ROVI, Madrid, Spain) were injected through the inferior vena cava and then the distal silk of the portal vein was closed with a knot. Immediately afterwards, a cannula (20G needle) (BD Venflon™ Pro Safety Needle Protected IV Cannula; BD, USA) was introduced through the portal vein and secured by means of two knots of the proximal and distal silk. Once secured, the cannula was connected to the tubing of a peristaltic pump system (Minipuls 3®; Gilson Inc., USA), the inferior vena cava was cut below the kidneys, and perfusion of the liver was started in a non-recirculating fashion with 200 ml of buffer (the appropriate buffer for each cell type) to remove blood.

4.3.1. LSEC and KC

To isolate LSEC and KC, the liver was perfused through the portal vein for 10 min at a flow rate of 20 ml/min at 37 ºC with 200 ml of Hanks I buffer (see Appendix, section 10.1) divided in 4 centrifuge tubes. Just before starting the perfusion, 0.9 ml 1% heparin

were added into the two first centrifuge tubes (0.5 ml to the first tube and 0.4 ml to the second tube). After removal of all blood from the liver, this was perfused with collagenase A (10 mg/ml; Roche, Merck KGaA, Germany) at a concentration of 0.15 mg/ml (healthy liver) or 0.2 mg/ml (cirrhotic liver) in 200 ml Hanks II buffer (see Appendix, section 10.1) at 37 ºC. The first 50 ml were allowed to flow at a flow rate of 10 ml/min, and approximately 5 min later, the flow rate was lowered to 5 ml/min and the silk of the inferior hepatic cava vein was closed with a knot to perfuse the remaining 150 ml to perform the *in vivo* liver digestion. The resultant digested liver was excised and mechanically disrupted, and *ex vivo* digestion was performed with the same buffer at 37 ºC for 10 min in constant agitation. The cells were passed through 100 μm nylon filters (VWR®, Avantor, Inc., Radnor, USA). The filtrate was divided in 4 centrifuge tubes containing 25 ml of cold Krebs' buffer (see Appendix, section 10.1) and centrifuged at 50×g for 3 min at 4 ºC. Once the centrifugation was finished, the supernatant containing the non-parenchymal cells was stored in 4 new centrifuge tubes; the pellet containing the hepatocytes was discarded. This centrifugation was performed a second time to correctly eliminate the hepatocytes (after the second centrifugation the hepatocyte pellet is much smaller). The supernatant was then centrifuged at 800×g for 10 min, and the obtained pellet was resuspended in PBS and centrifuged again at 50×g (3 min, 4 ºC), to completely eliminate the hepatocytes that were in the pellet. The subsequent supernatant was then centrifuged at 800×g for 10 min, and the obtained pellet was resuspended with PBS to a final volume of 10 ml. The resulting solution was centrifuged at 800×g for 25 min through a two-step 25-50% Percoll® gradient (Sigma-Aldrich, Merck KGaA, Germany) at 4 ºC (in the centrifuge, acceleration in half and deceleration without brake). The interface of the gradient was enriched in LSEC and KC. This cell fraction was collected, rinsed with PBS and centrifuged at 800×g (10 min, 4 ºC). The cell pellet was resuspended in tempered Roswell Park Memorial Institute (RPMI) medium correctly supplemented (see Appendix, section 10.1), seeded into a plastic culture dish and incubated for 30 min at 37 ºC in humid atmosphere with 5% CO_2. This step was done in order to separate KC from LSEC by the selective adherence of KC, which were then

washed twice with PBS and maintained in RPMI at 37 ºC, 5% CO_2. The supernatant containing the non-adherent LSEC was collected, seeded into a culture dish coated with a 100 µg/ml collagen solution (see Appendix, section 10.1) and incubated for 45 min (37 ºC, 5% CO_2). After this time, the medium was discarded and adhered cells were washed twice with PBS to remove non-adherent erythrocytes and cell debris, and maintained in RPMI (37 ºC, 5% CO_2).

4.3.2. Hepatocytes

With the same procedure of perfusion and digestion used in section 4.3.1, after centrifuging the digested liver filtrate at 50×g for 3 min at 4 ºC, we found hepatocytes in the pellet. This centrifugation was repeated and the second pellet containing hepatocytes was resuspended in approximately 25 ml of PBS. This step was repeated 2-3 times to rinse the cells from cellular debris. Once a clean pellet was obtained, the supernatant was decanted and each pellet was resuspended in 15 ml of supplemented Dulbecco's Modified Eagle's Medium (DMEM) (see Appendix, section 10.1). The cell suspension of each centrifuge tube was filtered with a 100 µm filter to eliminate residues of liver tissue remaining in the pellet (e.g. fat, connective tissue). Then, hepatocytes were counted by Trypan Blue Solution (Gibco™, Thermo Fisher Scientific, USA) method (1:5 dilution), using a Neubauer counting chamber. Hepatocytes were planted and incubated in culture dishes treated with collagen (100 µg/ml) at 37 ºC and 5% CO_2. After 4 h the cells were already attached, so they were gently washed with tempered PBS and cultured in maintenance DMEM medium (see Appendix, section 10.1).

4.3.3. HSC

The HSC isolation method used was based in the perfusion of the rat liver through the portal vein with 150 ml of Gey's Balanced Salt Solution (GBSS; Sigma-Aldrich, Merck KGaA, Germany), divided in 3 centrifuge tubes, at a flow rate of 20 ml/min at 37 ºC. Just before starting the perfusion, 0.9 ml 1% heparin were added into the two first centrifuge tubes (0.5 ml to the first tube and 0.4 ml to the second tube). After removing the blood, the liver was perfused with 1.5 mg/ml pronase E (Roche, Merck KGaA, Germany), 0.15 mg/ml (healthy liver) or 0.2 mg/ml (cirrhotic liver) collagenase A, and 0.05 mg/ml (healthy liver) or 0.065 mg/ml (cirrhotic liver) DNase I (10 mg/ml; Roche, Merck KGaA, Germany) in 200 ml GBSS solution at 37 ºC. The first 50 ml were allowed to flow at a flow rate of 10 ml/min, and approximately 5 min later, the silk of the inferior vena cava was closed and the liver was digested *in vivo* with the remaining solution (150 ml), at a flow rate of 5 ml/min. The digested liver was excised, mechanically disrupted with a scalpel and incubated in 100 ml of GBSS solution containing 0.4 mg/ml pronase E, and 0.1 mg/ml (healthy liver) or 0.13 mg/ml (cirrhotic liver) of both collagenase A and DNase I to perform an *in vitro* digestion at 37 ºC for 10 min stirring. The resulting suspension was filtered through a 100 µm nylon filters, collected in 2 centrifuge tubes, and centrifuged at 50×g for 4 min at 21 ºC. The supernatant was centrifuged at 800×g for 5 min and the obtained pellet was resuspended in 25 ml GBSS. This step was repeated 2-3 times until the supernatant was clear. After that, the pellet was resuspended with GBSS to a final volume of 7.5 ml and the resulting dispersed cells were fractionated by density gradient centrifugation using Optiprep™ Density Gradient Medium (11.5%) (Sigma-Aldrich, Merck KGaA, Germany) at 1,400×g for 21 min (in the centrifuge, acceleration in half and deceleration without brake). The interface of the gradient was enriched in HSC and this cell fraction was collected, rinsed with GBBS and centrifuged at 800×g for 5 min. The obtained pellet of HSC was resuspended in tempered Iscove's Modified Dulbecco's Medium (IMDM) correctly supplemented (see Appendix, section 10.1), seeded into an uncoated plastic culture dish and incubated O/N at 37 ºC in a humidified atmosphere with 5% CO_2. The next day, when HSC were attached to the

plate, the medium was discarded and cells were washed twice with PBS and maintained in IMDM (37 ºC, 5% CO_2) until the relevant studies were performed, usually the same day to avoid the activation and subsequent transdifferentiation of HSC that occurs when these cells contact with plastic.

4.4. Cellular and molecular biology techniques

4.4.1. Cellular internalization

The uptake of fluorescent peptide ligands and micelles by liver cells was assessed quantitatively by flow cytometry and qualitatively by confocal microscopy, both in cell culture and after *in vivo* treatment.

In vitro internalization

- Internalization by flow cytometry

For the peptide ligands and PM/FPM *in vitro* internalization protocol by flow cytometry, primary rat liver cells were seeded into a 96-well plate in a final volume of 100 µl/well (one plate was prepared for each cell line). The next day, or two days later for HSC, 15 µl of FITC-peptide ligands (0.75 mg/ml) or 10 µl of 5-DTAF-labelled PM/FPM (100 mg/ml of polymer) were added to the plate at different time-points: from 1 min to 1 h (peptide ligands) or 4 h (PM/FPM). For each time-point, three wells of the 96-well plate were treated; as the positive control for settings, three wells were treated for the maximum time with fluorescent ligands/micelles, and as the negative control there were three other wells that did not perceive any treatment. At the end of all incubation time-points, the plate was prepared for flow cytometry analysis as follows: the medium was aspirated and cells were washed once with PBS. Then, in order to lift them, cells were incubated with 30 µl of trypsin 10X (or 1X for hepatocytes) (Biowest, France) for 5-10 min at 37 ºC. When the cells were already detached, 120 µl of PBS at 5% fetal bovine serum (FBS; Biowest, France) with DAPI (1:1,000 dilution) were added per well to inactivate the trypsin and have a fluorescent stain of cell viability, respectively. In the

case of HSC, the labelling was not done with DAPI, but with propidium iodide solution (1 mg/ml; Sigma-Aldrich, Merck KGaA, Germany) in a 1:50 dilution, because of the autofluorescence of these cells in UV length caused by their lipid droplets. Next, cells from the positive and negative control wells were placed in tubes for analysis to establish the cytometer settings. Viable cells were sorted by DAPI/propidium iodide staining, and doublets and aggregates were excluded from analysis based on the forward scatter height (FSC-H) and area (FSC-A) profile. Voltages were based on unstained cells from negative controls and compensation was set using single-stained positive controls. When all settings were established, the plate was read by flow cytometry on a BD LSRFortessa™ Cell Analyzer (BD, USA). One determination was made in each of the three wells per condition studied.

- Internalization by confocal microscopy

The day of isolation, primary rat liver cells were seeded into an open μ-Slide chambered coverslip with 8 wells (Ibidi, Gräfelfing, Germany) in a final volume of 300 μl. The next day the medium was removed, and 5-DTAF-PM were added in a 1:10 dilution and incubated with cells during 1 or 2 h. After this time, cells were washed twice with PBS, and membranes were stained with CellMask™ Deep Red Plasma Membrane Stain (Invitrogen™, Thermo Fisher Scientific, USA) for 10 min at 37 ºC (1:1,000 dilution). Finally, the wells were washed twice and 300 μl of new culture medium, without phenol red (Biowest, France), were added to kept living cells at 37 ºC and 5% CO_2 before visualizing them under a FV1000 spectral confocal microscope. To obtain the photomicrographs it was established a zoom factor of 1.8 to show representative high-power fields (60x magnification). Images were processed using ImageJ software.

METHODS

In vivo internalization

- ## Internalization by flow cytometry

To study the *in vivo* cellular internalization of micelles, healthy rats received an IV dose (25G needle) of 5-DTAF-labelled PM or FPM (100 mg/kg of polymer). Untreated rats were used as negative controls. The following day, the four main types of liver cells (LSEC, KC, HSC and hepatocytes) were isolated and cultured. Once the cells were attached to the plate, medium was removed and the culture dish was washed twice with tempered PBS. To lift the cells, trypsin 10X, or 1X for hepatocytes, was added for 5-10 min at 37 ºC and, once lifted, 3 ml of supplemented medium was added to inactivate the trypsin. Cells were then collected and centrifuged at 800×g for 5 min, and the pellet was resuspended in PBS at 5% FBS with DAPI (1:1,000 dilution), or propidium iodide (1:50 dilution) for HSC. Cells were analyzed by flow cytometry, as explained above in the *in vitro* internalization section, to detect the percentage of positive cells for the fluorescent labelling of nanoparticles. Results were obtained from cells isolated from three or five animals for each of the study groups, with three determinations per sample.

- ## Co-localization by confocal microscopy

For co-localization immunohistochemistry (IHC), a single dose of 5-DTAF-labelled PM-F127 (100 mg/kg of polymer) was administered IV to BDL rats. Livers were harvested 16 h after PM administration, snap frozen and processed with Leica CM3050 S cryostat to obtain 6-7 μm liver cryosections. Sections were fixed with acetone at -20 ºC or 4% PFA at RT for 10 min and washed with PBS (3 x 5 min). Samples fixed with PFA were then permeabilized with 0.1% Triton™ X-100 (Sigma-Aldrich, Merck KGaA, Germany), 10 min at RT. Afterwards, all cryosections were blocked with 5% goat serum (Sigma-Aldrich, Merck KGaA, Germany) for 1 h at RT and rinsed again with PBS trice. Specific antibodies for LSEC (SE-1), KC (CD68) and HSC (desmin) were used according to the specifications in table 8.

Table 8. Primary antibodies for immunofluorescence staining of liver cell types.

Cell type	Primary Ab	Manufacturer (Code)	Dilution	Incubation
LSEC	SE-1	Novusbio (NB110-68095)	1:200	1 h, RT
KC	CD68	BioRad (MCA341R)	1:100	1 h, RT
HSC	Desmin	Thermo Fisher Scientific (MA5-13259)	1:50	O/N, 4 ºC

Ab: antibody, CD68: cluster of differentiation 68, HSC: hepatic stellate cell, KC: Kupffer cell, LSEC: liver sinusoidal endothelial cell, O/N: overnight, RT: room temperature, SE-1: Fc-gamma receptor IIb2 (CD32b). Primary antibody dilution was made in PBS. For CD68 and desmin IHC, sections were permeabilized with 0.1% Triton™ X-100 in PBS before incubation with the primary antibody.

After the incubation, PBS washes were done (3 x 5 min) and 2 drops of goat anti-mouse Alexa Fluor® 594 secondary antibody (Invitrogen™, Thermo Fisher Scientific, USA) were diluted in 1 ml of PBS to incubate it 10 min at RT. After this time, washes were repeated and the cryosection slides were mounted using VECTASHIELD® Antifade Mounting Medium. Samples were imaged using a FV1000 spectral confocal microscope (as in the *in vitro* internalization section).

4.4.2. Cell viability assay

To study the toxicity of simvastatin-loaded micelles, freshly isolated liver cells were cultured O/N (37 ºC, 5% CO_2) in 96-well plates in 100 µl of the corresponding mediums containing activated simvastatin or micelles loaded with simvastatin at ten different concentrations (0.05, 0.5, 5, 50, 100, 250, 500, 1,000, 2,500, and 5,000 µM). Positive control cells only received medium and negative control cells were incubated with 50% DMSO. After O/N treatment, cell viability was determined using PrestoBlue® Cell Viability Reagent (Invitrogen™, Thermo Fisher Scientific, USA). This cell viability indicator was added directly to cells in culture medium (10 µl/well) and incubated for 6 h (37 ºC, 5% CO_2). Next, light absorbance was detected at a wavelength (λ) of 570 and 600 nm (reference wavelength for normalization) by a Synergy™ Mx Microplate Reader

associated to Gen5™ Version 2.0 Data Analysis Software (BioTek, Agilent Technologies, Inc., Santa Clara, USA) for data collection, analysis, exporting and reporting. Each treatment was tested at least in three individual wells and three independent animals.

The relative cell viability was determined by the amount of PrestoBlue® irreversibly reduced to the pink coloured and highly red fluorescent resorufin. The optical density of resorufin formed in the positive control cells was taken as 100% viability, while that of the negative control cells was considered as 0%. Cell viability was determined using the following equation:

Equation 3. Calculation of cell viability.

$$\text{Cell viability (\%)} = \frac{(\lambda 570 - \lambda 600 \text{ exposed cells}) - (\lambda 570 - \lambda 600 \text{ positive control})}{(\lambda 570 - \lambda 600 \text{ negative control}) - (\lambda 570 - \lambda 600 \text{ positive control})} \times 100$$

4.4.3. Scanning electron microscopy

Scanning electron microscopy (SEM) was performed on LSEC cultured on collagen-coated 12 mm coverslips (150 µl/coverslip), placed inside a 6/12-well plate, that were treated O/N with free or encapsulated simvastatin at a concentration of 5 µM. Control LSEC did not receive any treatment. After incubation, cells were washed twice with tempered PBS and were fixed with 1 ml of 2% PFA fixative (see Appendix, section 10.1) during 30 min at RT. Fixed cells were maintained at 4 ºC until their analysis. If samples had to be stored for more than 1 week, the standard fixative was replaced by a maintenance fixative (see Appendix, section 10.1), allowing storage for up to 2 months at 4 ºC. SEM processing of samples was carried out by the Electron Microcopy Service within the Scientific and Technological Centres of the University of Barcelona (CCiTUB, Barcelona, Spain), where cells in coverslips were osmicated with 1% osmium tetroxide (OsO$_4$) in 0.1 M sodium cacodylate buffer (Na(CH$_3$)$_2$AsO$_2$·3H$_2$O), dehydrated in an ethanol gradient to 100% and incubated for 2 min in hexamethyldisilazane to dry them. Coverslips were mounted on stubs, sputter-coated with 10 nm of gold and examined

using a JSM-6380 Scanning Electron Microscope (JEOL Ltd., Japan). Images were taken to analyze fenestrae frequency (nº of fenestrae/nm^2) and porosity (% of area covered by fenestrae) of LSEC. Ten images of each coverslip were taken at 5,000x magnification and were analyzed using ImageJ software.

First of all, the scaling of the images was measured to determine the pixels corresponding to a distance of 1 µm and the total area (nm^2) of observed cells was calculated. The area of each fenestra was then measured, based on the longest diameter (nm), and summed to give a total fenestrae area. The number of fenestrae per cell was also counted. From these parameters, the frequency of fenestrae and the porosity of these cells were determined (Equation 4). For all calculations, the area of the gaps, considered as holes with a diameter greater than 300 nm, was discarded.

Equation 4. Determination of fenestrae frequency and porosity of LSEC.

$$\text{Fenestrae frequency} = \text{Nº of fenestrae}/(\text{Total area} - \text{Gaps area})$$

$$\text{Porosity (\%)} = \frac{(\text{Fenestrae area} - \text{Gaps area})}{(\text{Total area} - \text{Gaps area})} \text{ x } 100$$

4.4.4. Gene expression analysis
Ribonucleic acid extraction
- From cells

For ribonucleic acid (RNA) analysis, hepatic cells were seeded into 12-well plates and treated approximately 3 h after isolation, except HSC that were treated one day after. LSEC, KC, and hepatocytes were treated with free activated simvastatin or PM/FPM-Sim at a concentration of 2.5 µM, while HSC at 5 µM. Control wells received medium or treatment with empty (Ø) micelles depending on the experiment. After O/N treatment (37 ºC, 5% CO$_2$), cells were lysed with a 1:100 dilution of 2-mercaptoethanol (Merck KGaA, Germany) in Buffer RLT (QIAGEN, Venlo, Netherlands), and total RNA was extracted from lysed cells using the RNeasy Mini Kit (QIAGEN, Netherlands) according

to manufacturer's instructions. Extracted RNA was quantified by spectrophotometry in a NanoDrop® ND-1000 Spectrophotometer (Thermo Fisher Scientific, USA).

- From tissue

To extract RNA from tissue, liver samples were collected in RNA*later*™ Stabilization Solution and kept for 1 week at 4 ºC before being stored at -80 ºC. A sample of 20-30 mg of frozen liver was placed in a Lysing Matrix D tube (MP Biomedicals, Irvine, USA) containing 600 µl of Buffer RLT with 2-mercaptoethanol (100:1 dilution). Then, tissue was disrupted in a FastPrep® FP120 homogenizer (Thermo Fisher Scientific, USA) at maximum speed for 20 sec and spun to remove the foam generated. This step was performed three times. After the last spin, the supernatant was collected in a RNase-free microcentrifuge tube and centrifuged at 13,000 rpm for 3 min (4 ºC). The supernatant obtained was ready for RNA extraction by the RNeasy Mini Kit, as abovementioned.

RNA reverse transcription to complementary deoxyribonucleic acid

RNA extracted from liver cells and tissue was converted to complementary deoxyribonucleic acid (cDNA) by reverse transcription with the High-Capacity cDNA Reverse Transcription Kit (Applied Biosystems™, Thermo Fisher Scientific, USA) following manufacturer's instructions (Table 9). The process was performed in an Applied Biosystems™ 2720 Thermal Cycler (Applied Biosystems™, Thermo Fisher Scientific, USA) and at the end of it, the sample was diluted in RNase-free water to obtain a final concentration of approximately 5-10 ng/µl of cDNA.

Table 9. Sample preparation for the High-Capacity cDNA Reverse Transcription Kit.

Reagent	Volume (µl)
10X RT Buffer	2
10X RT Random Primers	2
25X dNTP Mix	0.8
MultiScribe™ Reverse Transcriptase	1
RNase Inhibitor	1
RNase-free H$_2$O	13.2 − x
RNA	x*

dNTP: deoxynucleotide triphosphates, RNA: ribonucleic acid, RT: reverse transcription. * Depending on RNA concentration. Total volume = 20 µl/sample. High-Capacity cDNA Reverse Transcription Kit reagents were from Applied Biosystems™, Thermo Fisher Scientific, USA.

Quantitative reverse transcription polymerase chain reaction

Quantitative reverse transcription polymerase chain reaction (qRT-PCR) was performed on a MicroAmp™ Optical 384-Well Reaction Plate (Applied Biosystems™, Thermo Fisher Scientific, USA) with triplicates for each sample to analyze. For the reaction, 20 ng of cDNA were amplified by a universal TaqMan™ master mix (Table 10) carrying random primers, deoxynucleotide triphosphates (dNTPs), a Taq polymerase enzyme and a TaqMan™ probe (Applied Biosystems™, Thermo Fisher Scientific, USA) specific for each gene of study (Table 11). qRT-PCR was carried out in a 7900HT Fast Real-Time PCR System (Thermo Fisher Scientific, USA). Data were analyzed by relative quantification (RQ) using the Relative Quantification qPCR Application from the Thermo Fisher Connect Platform (Thermo Fisher Scientific, USA).

Table 10. Sample preparation for qRT-PCR.

Reagent	Volume (µl)
TaqMan™ Universal PCR Master Mix	5
TaqMan™ probe	0.5
dH$_2$O	4.5 – x
cDNA	x* (20 ng)

cDNA: complementary deoxyribonucleic acid, dH$_2$O: distilled water, PCR: polymerase chain reaction.
* Depending on cDNA concentration. Total volume = 10 µl/well. TaqMan™ Universal PCR Master Mix and probe were from Applied Biosystems™, Thermo Fisher Scientific, USA.

Table 11. TaqMan™ probes for qRT-PCR.

Gene symbol	Complete gene name	Gene alias	Code
Acta2	Actin alpha 2, smooth muscle	α-SMA	Rn 01759928_g1
Arg1	Arginase-1	ARG-1	Rn 00691090_m1
Col1a1	Collagen type I alpha 1 chain	COL1A1	Rn 01463848_m1
Edn1	Endothelin-1	ET-1	Rn 00561129_m1
Ednra	Endothelin receptor type A	ETA-R	Rn 00561137_m1
Fcgr2b	Fc-gamma receptor IIb	CD32b	Rn 01490232_m1
Gapdh	Glyceraldehyde-3-phosphate dehydrogenase	GAPDH	Rn 99999916_s1
Hmox1	Heme oxygenase-1	HO-1	Rn 01536933_m1
Hnf4a	Hepatocyte nuclear factor 4 alpha	HNF4	Rn 00573309_m1
Il10	Interleukin-10	IL-10	Rn 01483987_m1
Klf2	Krüppel like factor 2	KLF2	Rn 01420496_gH
Nos3	Nitric oxide synthase 3 (endothelial cell)	eNOS	Rn 02132634_s1
Nqo1	NAD(P)H quinone dehydrogenase-1	NQO1	Rn 00566528_m1
Pdgfrb	Platelet derived growth factor receptor beta	PDGFRB	Rn 00709573_m1
Slc22a1	Solute carrier family 22 (organic cation transporter), member 1	OCT-1	Rn 00562250_m1

GAPDH was used as endogenous control to normalize RQ. TaqMan™ probes were from Applied Biosystems™, Thermo Fisher Scientific, USA.

4.4.5. Western blot

Protein extraction

For liver protein analysis, the liver was perfused with saline to remove the blood, fragmented and directly frozen in liquid nitrogen to be stored at -80 ºC. For protein extraction, frozen liver was ground to a fine powder in a vessel cooled by liquid nitrogen and once finished, 2 spoons of powder were introduced in a microcentrifuge tube with 400 µl of radioimmunoprecipitation assay (RIPA) lysis and extraction buffer (see Appendix, section 10.1). When mixed, liver powder and lysis buffer were vortexed and sonicated (3 x 10 sec) in a Bioruptor® UCD-200 (Diagenode, Hologic, Inc., Marlborough, USA). Then, the sample was allowed to cool for 10 min before centrifugation at 14,000 rpm (10 min, 4 ºC) to remove cell detritus in the pellet and obtain the protein extract in the supernatant. This was stored at -20 ºC until use.

Protein quantification

Total protein concentration was quantified by colorimetric detection with the Pierce™ BCA Protein Assay Kit (Thermo Fisher Scientific, USA) according to the manufacturer's instructions. Briefly, 5 µl of protein extract (1:30 dilution) or albumin standard (0, 0.125, 0.25, 0.5, 0.75, 1, 1.5 and 2 mg/ml) were mixed with 100 µl of BCA Working Reagent mix (50:1, Reagent A:B) and vortexed. The samples were then incubated at 37 ºC for 30 min, and allowed to cool on ice before the protein quantification by NanoDrop® ND-1000 Spectrophotometer.

Gel electrophoresis and protein transfer

For one-dimensional electrophoresis in sodium dodecyl sulfate polyacrylamide gels (SDS-PAGE) under denaturing conditions, a XCell SureLock™ Mini-Cell Electrophoresis System (Invitrogen™, Thermo Fisher Scientific, USA) was used on NuPAGE® Bis-Tris 4-12%, 1.0-1.5 mm, Mini Protein Gels (Invitrogen™, Thermo Fisher Scientific, USA). Sample solutions were prepared to load 60 µg of protein as indicated in table 12. The samples

were boiled at 95 ºC for 10 min in a thermoshaker (Thermal Shake *lite*; VWR®, Avantor, Inc., USA) and spin down. Finally, they were loaded 11.5 µl of sample into each well and 7 µl of the protein ladder Precision Plus Protein™ Dual Color Standards (Bio-Rad Laboratories, Hercules, USA). The gels were run in running buffer (see Appendix, section 10.1) at a constant voltage of 200 V (120 mA) for approximately 1 h 50 min at RT.

Table 12. Sample preparation for NuPAGE® electrophoresis gel loading.

Reagent	Volume (µl)
Protein extract	x* (60 µg)
NuPAGE® LDS Sample Buffer (4X)	3
NuPAGE® LDS Sample Reducing Agent (10X)	1.2
dH$_2$O	7.8 – x

dH$_2$O: distilled water. * Depending on protein extract concentration. Total volume = 12 µl/well (11.5 µl/well were loaded). NuPAGE® reagents were from Invitrogen™, Thermo Fisher Scientific, USA.

For protein transfer, separated proteins were blotted onto a polyvinylidene difluoride (PVDF) blotting membrane (Amersham™ Hybond™ P 0.45 PVDF blotting membrane; Cytiva, Marlborough, USA), previously hydrated in methanol (30 sec), dH$_2$O (5 min) and transfer buffer (5 min) (see Appendix, section 10.1). The transfer was conducted in a XCell II™ Blot Module (Invitrogen™, Thermo Fisher Scientific, USA) by the setting of a blotting sandwich assembled in the following order: 4 blotting pads, 2 Whatman™ chromatography papers (GE Healthcare, Chicago, USA), the polyacrylamide gel, the PVDF membrane, 2 Whatman™ chromatography papers and 4-5 blotting pads (bubbles were avoided when assembling the sandwich). The transfer was performed in transfer buffer at 30 V (400 mA) for 60 min on ice.

Once the transfer was performed, to check its efficiency and the presence of the proteins, the blotting membrane was stained with Ponceau S solution (Sigma-Aldrich, Merck KGaA, Germany) for 10 min at RT in agitation. Then, the membrane was washed three times with Tween®-Tris-buffered saline (TTBS) 1X (see Appendix, section 10.1) for 10 min and blocked with 20 ml of 5% bovine serum albumin (BSA; Biowest, France) in TTBS 1X for 1 h at RT.

Immunodetection

For protein detection, the membrane was incubated O/N with the appropriate dilution of the primary antibody (Table 13) at 4 ºC in agitation. After the incubation time, three washes of 10 min with TTBS 1X were performed to remove excess primary antibody. The membrane was then incubated with the corresponding secondary antibody (Table 14) for 1 h stirring at RT. Finally, to remove excess secondary antibody, the membrane was washed again with TTBS 1X (3 x 10 min).

Table 13. Primary antibodies for western blot.

Primary antibodies				
Protein	**MW (kDa)**	**Species**	**Manufacturer**	**Dilution**
Akt	60	Rabbit	Cell Signaling Technology	1:500 in 5% BSA
p-Akt	60	Rabbit	Cell Signaling Technology	1:500 in 5% PhosphoBLOCKER™
eNOS	140	Mouse	BD	1:500 in TTBS 1X
p-eNOS	140	Rabbit	Cell Signaling Technology	1:250 in 5% BSA
GAPDH	36	Mouse	Ambion	1:5,000 in TTBS 1X
KLF2	42	Mouse	Santa Cruz Biotechnology	1:200 in 5% BSA

Akt: protein kinase B (PKB), BSA: bovine serum albumin, eNOS: endothelial nitric oxide synthase, GAPDH: glyceraldehyde-3-phosphate dehydrogenase, KLF2: Krüppel-like factor 2, MW: molecular weight, p: phosphorylated, TTBS: Tween®-Tris-buffered saline. GAPDH was used as internal control for total protein normalization. PhosphoBLOCKER™ Blocking Reagent was from Cell Biolabs, Inc., San Diego, USA.

Table 14. Secondary antibodies for western blot.

Secondary antibodies		
Name	**Manufacturer**	**Dilution**
Anti-mouse IgG	GE Healthcare	1:10,000 or 1:30,000 in TTBS 1X
Anti-rabbit IgG	Cell Signaling Technology	1:10,000 or 1:15,000 in TTBS 1X or PhosphoBLOCKER™

IgG: immunoglobulin G, TTBS: Tween®-Tris-buffered saline. Dilution of anti-mouse IgG 1:10,000 was prepared to detect eNOS and KLF2, and 1:30,000 for GAPDH. Dilution of anti-rabbit IgG 1:10,000 was prepared to detect p-Akt, and 1:15,000 for Akt and p-eNOS. All dilutions were prepared in TTBS 1X, except for p-Akt, which was done in 5% PhosphoBLOCKER™ Blocking Reagent in TTBS 1X.

The electrophoretic band obtained was detected with the chemiluminescent Amersham™ ECL™ Prime Western Blotting Detection Reagents (Cytiva, USA) using an Odyssey® Fc Imaging System (LI-COR Biosciences, Lincoln, USA). For this purpose, the membrane was incubated for 1 min with 1 ml of detection solution containing a luminol enhancer (Solution A) and a peroxidase substrate (Solution B) (solution A:B, 1:1 dilution), followed by digital chemiluminescence development. Exposure time depended on the primary antibody used (maximum 10 min). Protein quantification was done with Image Studio™ Lite software (LI-COR Biosciences, USA) on six to seven animal samples run for each study group.

For the detection of phosphorylated and total protein on the same membrane, the membrane was stripped by incubation with Restore™ PLUS Western Blot Stripping Buffer (Thermo Scientific™, Thermo Fisher Scientific, USA) for 30 min at 55 ºC in agitation. Subsequently, the membrane was washed thrice with TTBS 1X, re-blocked and incubated with the new primary and secondary antibody as described above.

4.5. Statistical analysis

IBM® SPSS® Statistics 20 (IBM, Armonk, USA) was used for statistical analysis. Quantitative results were expressed as mean ± standard error of the mean (SEM), and were compared with analysis of variance followed by unpaired Student's t-test (between two groups) or one-way analysis of variance (ANOVA) with Tukey's HSD post hoc correction (among three or more groups). In case the data were not normally distributed, nonparametric tests were applied, using Mann-Whitney U test to compare two groups and Kruskal-Wallis test for multiple comparisons. For contingency table analyses, a chi-squared test was applied. Pearson correlation coefficient was calculated to show the correlation of two parameters. A p-value ≤ 0.05 was considered statistically significant.

5. RESULTS

5. RESULTS

5.1. First study: Simvastatin-loaded PM in a model of advanced CLD

Characterization and *in vitro* internalization of PM

Prior encapsulation, simvastatin was activated at 8 mg/ml at very high efficiency, with over 99% active simvastatin detected in solution by UPLC-MS/MS (Figure 22A). Active simvastatin was lyophilized and rehydrated at 20 mg/ml. Simvastatin encapsulation with 100 mg Pluronic® F127 was higher than for F108, reaching 99% of EE (Table 15).

Physicochemical properties of the produced PM are depicted in table 15. Mean hydrodynamic diameter was around 21 nm for PM-F127 and 20 nm for PM-F108 with small PDI, in particular for PM-F127 (ranging from 0.18 to 0.27). PM presented slightly negative surface charge close to neutrality. Particle morphology and homogeneity among PM formulations was evaluated by TEM. Each production batch was highly homogeneous and PM displayed spherical shape (Figure 22B). Subsequently, drug release kinetics was studied in PBS under simulated physiological conditions (37 ºC, pH 7.4). The data suggested a small simvastatin release reaching 1.9% for PM-F108-Sim and 3.8% for PM-F127-Sim after 72 h, demonstrating the stability of the delivery system (Figure 22C).

Table 15. Physicochemical properties of PM-F127-Sim and PM-F108-Sim.

PM	Hydrodynamic diameter (nm)	PDI	Zeta potential (mV)	EE (%)
PM-F127-Sim	20.9 ± 9.5	0.27 ± 0.02	-9.10 ± 1.34	99.7
PM-F108-Sim	20.1 ± 0.05	0.58 ± 0.01	-4.03 ± 0.79	96.7

EE: encapsulation efficiency, PDI: polydispersity index, PM: polymeric micelle, Sim: simvastatin. Values are indicated as mean ± SD.
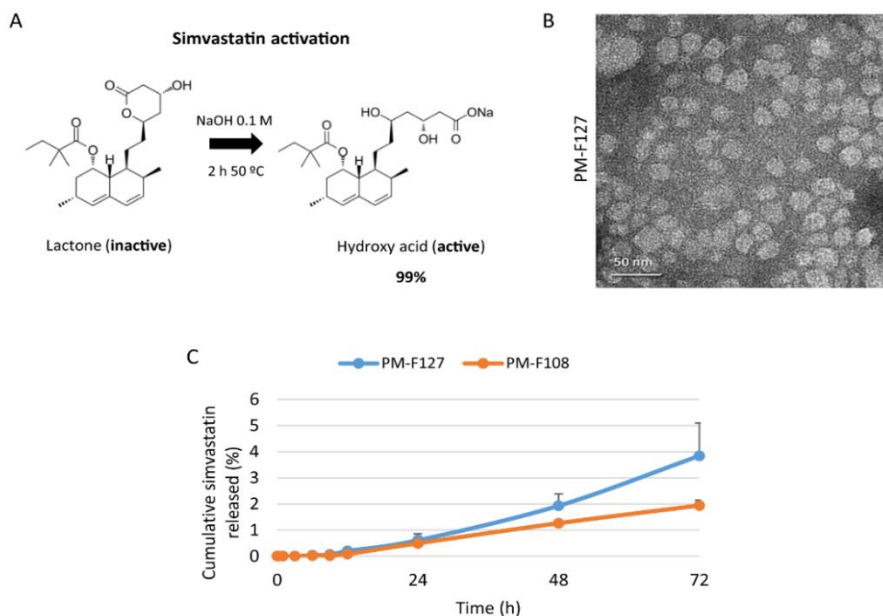
Figure 22. Characterization of PM. (A) Simvastatin activation from its lactone form to the open ring acid conformation. (B) Representative TEM micrograph showing a batch of PM-F127 (scale bar: 50 nm). (C) *In vitro* drug release kinetics under simulated physiological conditions (37 ºC, pH 7.4). Results are plotted as mean ± SEM. n = 2 per experimental condition.

Internalization of PM-F127 and PM-F108 was very fast in LSEC isolated from healthy rats. Most nanoparticles were internalized after 10 min with a maximum of internalized PM at 1 h (Figure 23A). After that, a plateau was established. The percentage of cells internalizing PM was however, significantly higher for PM-F127 (90.7% positive cells) than for PM-F108 (60.2%) after 1 h of incubation. Results were also confirmed by confocal microscopy 2 h after treatment, detecting PM (labelled in green) localized inside cell membranes stained with Cell Mask (red) (Figure 23B). PM-F127 *in vitro* behaviour, the formulation showing higher internalization rates, was further analyzed in the four main liver cell types, LSEC, HSC, KC and hepatocytes, isolated from healthy rats or rats with advanced CLD developed by BDL. LSEC were the cells demonstrating higher internalization capacity, both isolated from healthy and BDL rats (Figure 23C). Healthy HSC also incorporated PM with high efficiency, reaching 65.0% positive cells after 3 h of treatment (Figure 23C left). Nevertheless, internalization capacity of HSC

derived from BDL animals was dramatically reduced with only 37.5% of positivity after 3 h (Figure 23C right). The percentage of positive cells was significantly lower in KC and hepatocytes from both healthy and BDL rats than that observed in LSEC (Figure 23C).
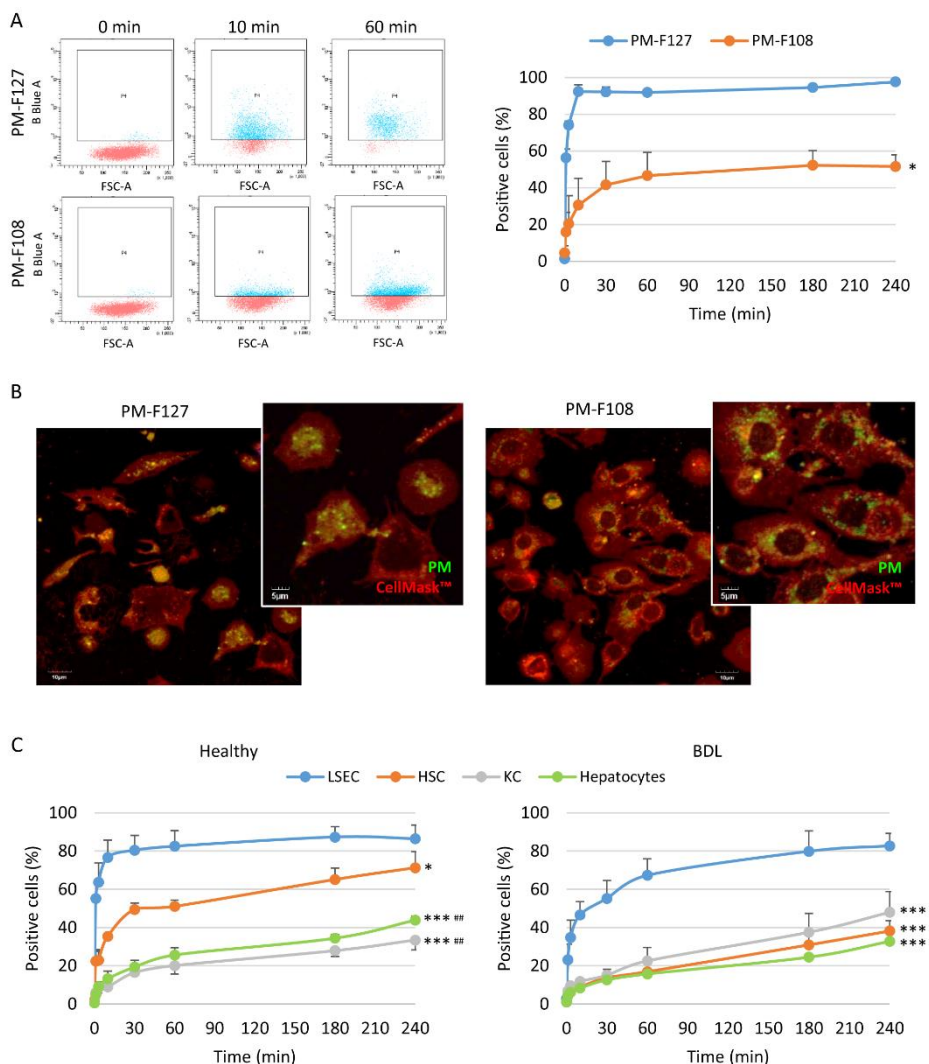
Figure 23. *In vitro* internalization of PM. (A) Internalization of PM evaluated by flow cytometry after *in vitro* treatment with 5-DTAF-PM-F127 or 5-DTAF-PM-F108 at different times from 1 min to 4 h. Representative gates are displayed in the left panel and quantification in the right. Data are expressed as mean ± SEM. n = 2 per condition. * p≤0.05. (B) Internalization of PM confirmed by confocal microscopy 2 h after *in vitro* treatment with PM-F127 (left) or PM-F108 (right). PM are stained with 5-DTAF (green) and cell membranes with CellMask™ (red). All images at 60x. (C) Internalization rate of PM-F127 in the different liver cell types (LSEC, HSC, KC and hepatocytes) isolated from healthy (left) or 3-week BDL rats (right) evaluated by flow cytometry from 1 min to 4 h. Data are expressed as mean ± SEM. n = 3 per condition. * p≤0.05, *** 0.001 vs. LSEC; ## p≤0.01 vs. HSC.

In vitro effect of simvastatin-loaded PM

Viability of LSEC treated with PM-F127-Sim and PM-F108-Sim was not significantly different than that of free simvastatin-treated LSEC, suggesting no toxicity derived from the PM themselves (Figure 24A). None of the PM caused a decrease in cell viability in the working concentration range (2.5-5 µM), and this viability was sustained at concentrations 10 times higher.

Gene expression evaluation of simvastatin target genes KLF2 and eNOS was performed to confirm the effectivity of simvastatin treatment. Both genes were overexpressed in cells treated with PM-F127-Sim and PM-F108-Sim even though detected levels were lower than in cells treated with free simvastatin (Figure 24B). As the gold standard of LSEC phenotype characterization(27), the presence of open fenestrae in the LSEC was evaluated by SEM (Figure 24C). Simvastatin (free and encapsulated) significantly increased fenestrae frequency and endothelial porosity (% area covered by fenestrae), suggesting an improvement of LSEC phenotype (Figure 24D). PM-F127-Sim had slightly better results than PM-F108-Sim.
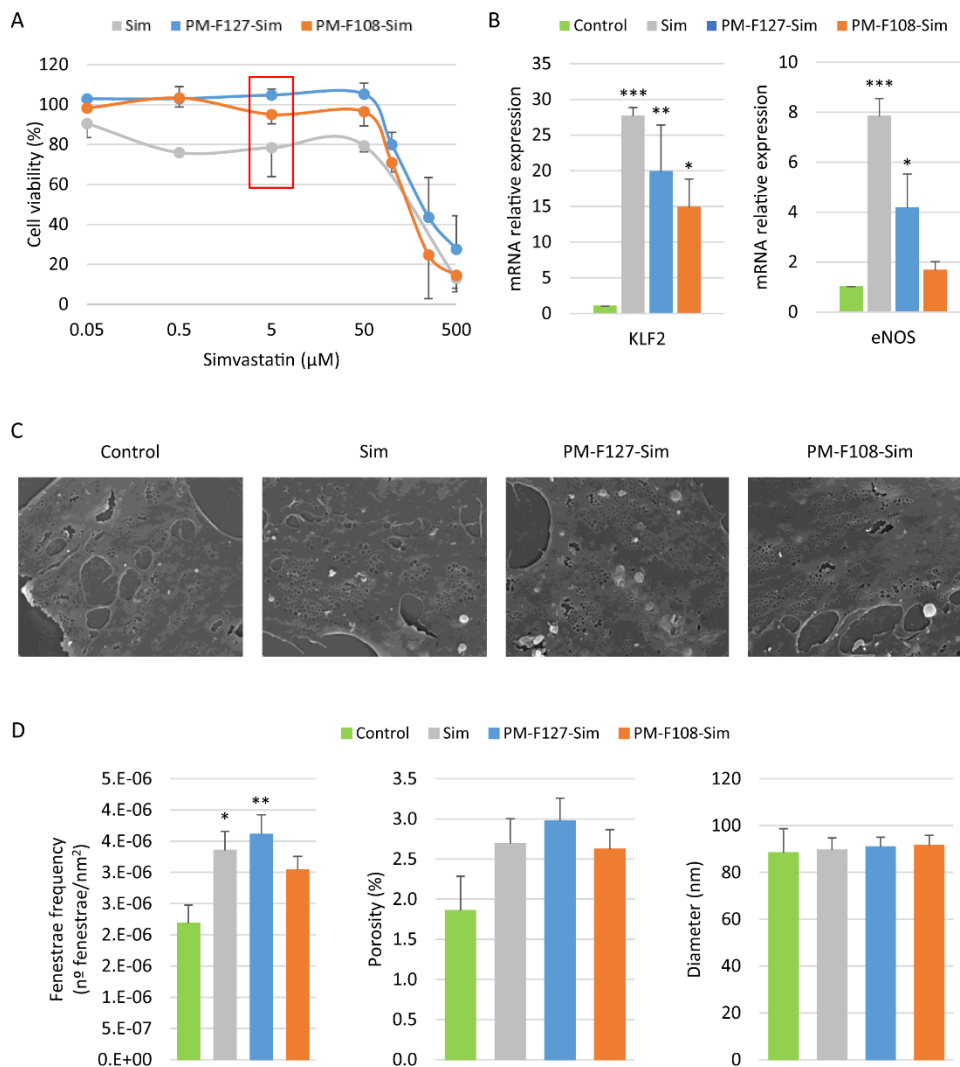
Figure 24. *In vitro* effect of PM-Sim in healthy LSEC. (A) Cell viability determined by PrestoBlue® assay 16 h after treatment with increasing doses of free simvastatin, PM-F127-Sim or PM-F108-Sim (from 0.05 to 500 μM). Red square indicates *in vitro* working concentration. Results are represented as mean ± SEM. n = 3 per condition. (B) Relative mRNA expression levels of KLF2 and eNOS determined by qRT-PCR. GAPDH was used as endogenous control and results were normalized to control cells for both genes separately. mRNA levels are expressed as mean ± SEM. n = 3 animals per experimental condition. * p≤0.05, ** 0.01, *** 0.001 vs. control. (C) Representative SEM images of endothelial fenestrae. (D) Quantification of fenestrae frequency, porosity and mean diameter. Results are represented as mean ± SEM. n = 2 per condition * p≤0.05; ** 0.01 vs control.

Because of the better results achieved by PM-F127-Sim in terms of *in vitro* cell internalization and amelioration of LSEC phenotype, the studies in the CLD experimental model were performed only with this formulation. The *in vitro* effects of the treatments were compared in LSEC, HSC, KC and hepatocytes isolated from healthy or BDL rats by gene expression determination of several genes related to simvastatin administration (e.g. KLF2, eNOS, HO-1, NQO1) or associated with cell phenotype maintenance (e.g. CD32b, ARG-1, HNF4). A significant increase in KLF2 levels was observed in all cell types treated with simvastatin and PM-F127-Sim in a similar extent (Figure 25A and B). In healthy LSEC this was accompanied by an increase in eNOS expression, a target gene of KLF2 and known vasodilator (Figure 25A top left). Further, a slight increase of the antioxidant NQO1 was observed in HSC (Figure 25A bottom left). KC and hepatocytes isolated from healthy animals did not have significant differences in the other genes evaluated (Figure 25A right panels). In cells derived from BDL animals, simvastatin effect was more significant than in the healthy ones. The effect in gene expression was comparable between free simvastatin and PM-F127-Sim (Figure 25B). In summary, LSEC showed improved phenotype by increased levels of eNOS and CD32b (marker of differentiated LSEC), and reduced expression of the vasoconstrictor ET-1 (Figure 25B top left). In HSC, all tested genes associated with fibrosis and collagen deposition were significantly reduced, and results of free simvastatin and PM-F127-Sim showed no significant differences (Figure 25B bottom left). In KC and hepatocytes, only moderate effects in the assessed genes were observed (Figure 25B right panels).
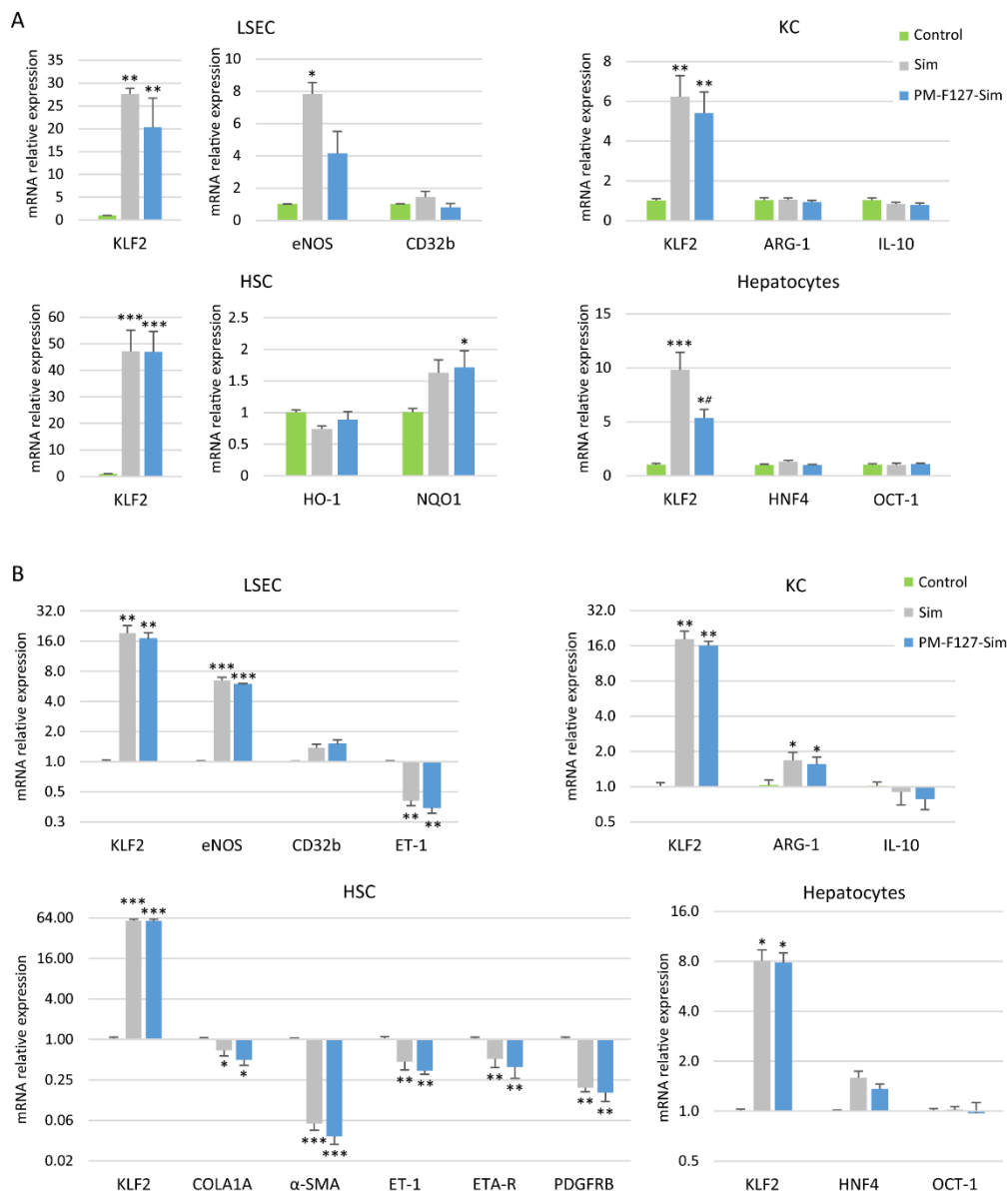
Figure 25. *In vitro* efficacy of PM-Sim in liver cells. Relative mRNA expression levels determined by qRT-PCR in LSEC (KLF2, eNOS, CD32b and ET-1), HSC (KLF2, HO-1, NQO1, COLA1A, α-SMA, ET-1, ETA-R and PDGFRB), KC (KLF2, ARG-1, IL-10) and hepatocytes (KLF2, HNF4, OCT-1) isolated from healthy (A) or BDL (B) rats. GAPDH was used as endogenous control and results were normalized to control cells for each gene separately. mRNA levels are expressed as mean ± SEM. n = 3 animals per experimental condition. * p≤0.05, ** 0.01, *** 0.001 vs. control; # p≤0.05 vs. Sim.

In vivo targeting of PM-F127

In vivo biodistribution studies performed with PM-F127 showed maximum liver accumulation 20-30 min after administration in healthy and BDL rats (Figure 26A and B). Signal was coming mainly from the liver in both models, but an increase in gut accumulation in BDL animals was observed (Figure 26A right). Furthermore, *ex vivo* imaging studies were performed 2 h after PM-F127 administration. About 50% of PM-F127 signal was found in the liver from healthy and cirrhotic animals followed by some spleen and lung accumulation (Figure 26C and D). Importantly, signal in muscle was almost undetectable.
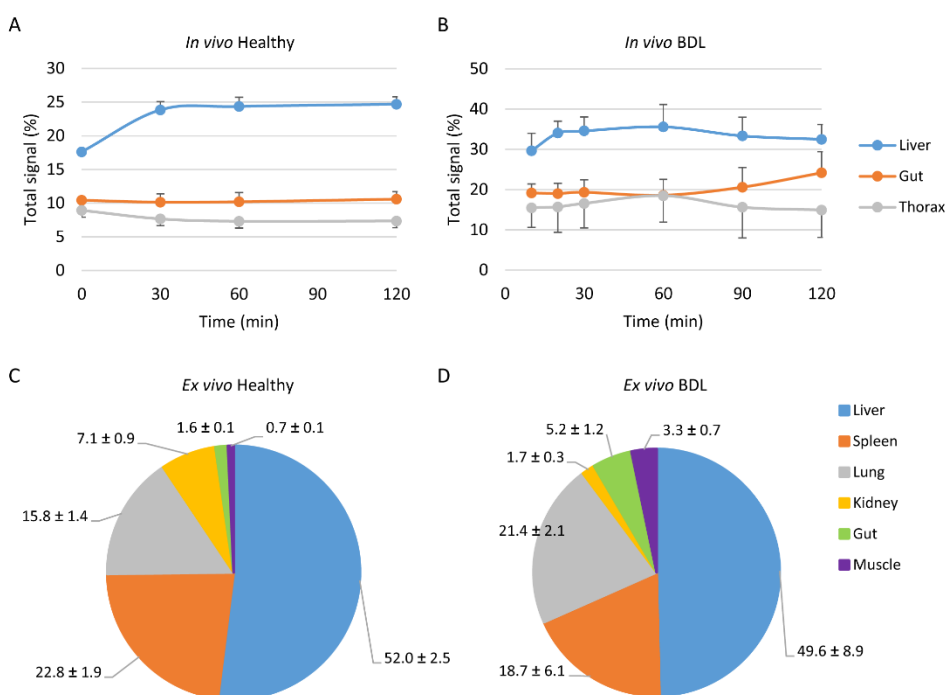
Figure 26. Biodistribution of PM. *In vivo* distribution after IV administration of PM-F127 encapsulating fluorescent lipophilic tracer DiR detected by the IVIS® Spectrum imaging system at different time points from 0 to 120 min in healthy (A) or BDL (B) rats. Images were divided into three regions of interest, corresponding to the areas of the thorax, liver, and gut depicted here. Relative percentage of *ex vivo* fluorescence of different organs from healthy (C) or BDL (D) rats performed 2 h after PM administration. All data are expressed as mean ± SEM. n = 3 animals for each group.

In this line, *ex vivo* localization of IV administered fluorescent PM was further studied by confocal microscopy, confirming that, 2 h after injection, PM-F127 was found in the liver with very little accumulation in kidneys and no detection in muscle tissue (Figure 27A). In a different set of animals, detection of PM accumulation in the liver at different time points (4, 24 and 48 h after administration) was performed. Maximum liver accumulation was observed at 24 h and located near the portal tracts, and 48 h after administration nanoparticles were still detectable in liver, although at lower levels (Figure 27B).
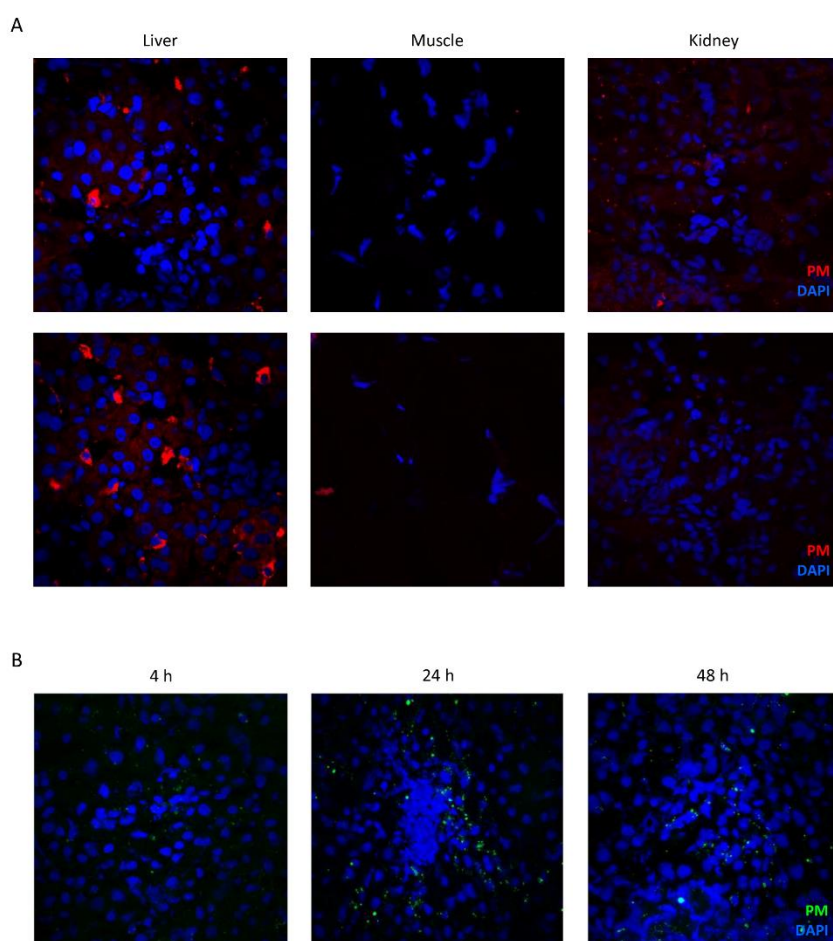
Figure 27. *Ex vivo* localization of PM. (A) Detection of PM-F127 encapsulating fluorescent lipophilic tracer DiR (red) in liver, muscle and kidney tissues 2 h after IV administration. (B) Detection of PM-F127 labelled with 5-DTAF (green) 4, 24 and 48 h after IV administration. For all experiments nuclei were stained with DAPI (blue). All images at 60x.

Within the cirrhotic liver, to determine the co-localization of PM with the different non-parenchymal liver cells an immunofluorescence in BDL rats 16 h after *in vivo* administration was performed. Figure 28A shows PM-F127 (green) internalized by LSEC (stained for its specific marker SE-1, in red) and by liver macrophages (positive for CD68, also in red). Nonetheless, micelles were rarely co-localizing with markers of HSC (desmin) or found inside hepatocytes. The percentage of PM co-localizing with the non-parenchymal cell types was also quantified. The results demonstrated that for LSEC, 86.2% of PM found in each field co-localized with SE-1 specific staining and this value was similar for KC (85.6%), but only 8.6% of total PM co-localized with HSC (Figure 28B).
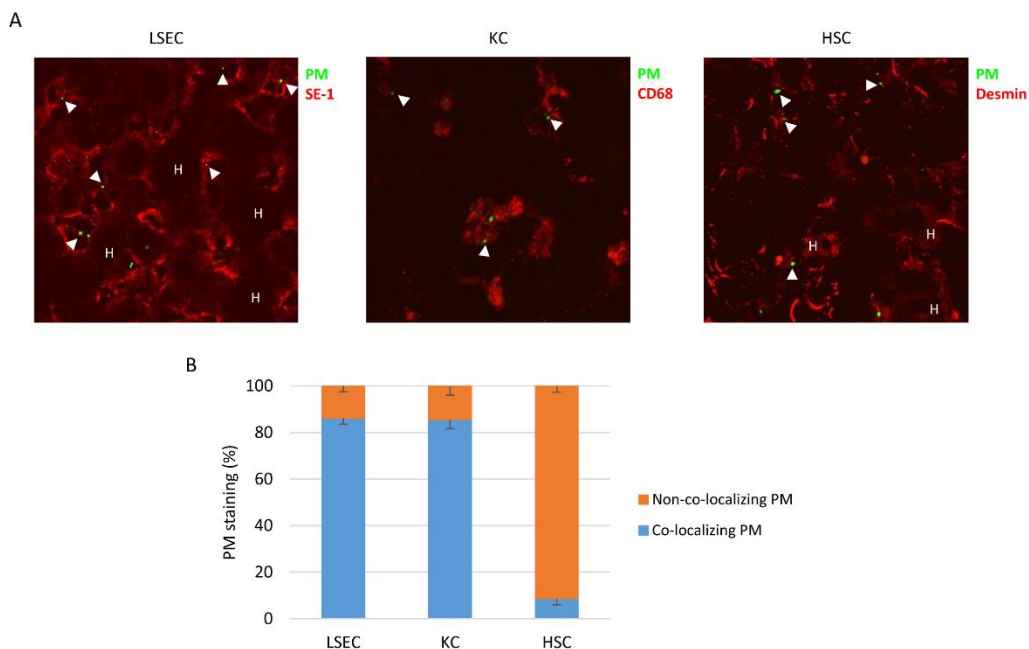
Figure 28. Cellular distribution of PM. (A) Co-localization of IV injected PM-F127 labelled with 5-DTAF (green) with specific cell markers for LSEC (SE-1), KC (CD68) or HSC (desmin) stained with Alexa Fluor® 594 (red). Arrowheads indicate co-localizing PM. Hepatocytes are indicated as "H". All images at 60x. (B) Quantification of percentage of PM co-localizing with specific liver cell markers. Data are represented as mean ± SEM.

In vivo safety and efficacy

MTD was determined in healthy rats administering PM-F127-Sim or PM-F108-Sim 3 days/week during 2 weeks. Simvastatin did not cause any effect in animal behaviour or general health condition, and survival was 100% for all treatments. However, animals' body weight was significantly reduced by oral simvastatin suggesting some toxicity (Figure 29A); this was not observed in the PM-Sim treated groups. In addition, treatments did not cause liver toxicity evaluated by serum AST and ALT levels (Figure 29B).
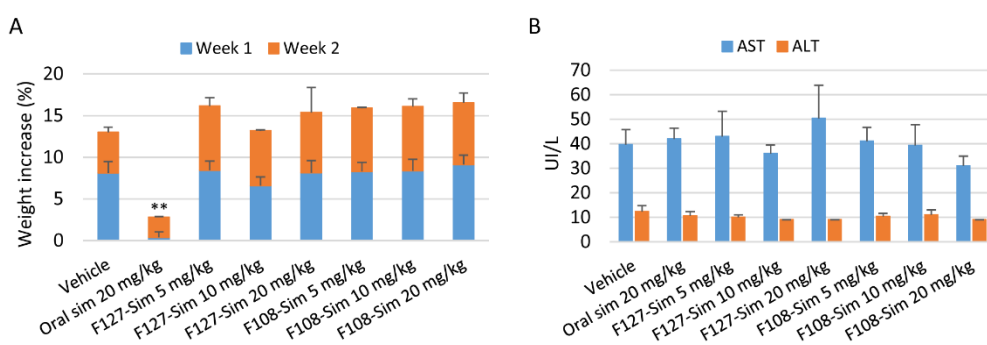
Figure 29. Determination of MTD on healthy rats. (A) Percentage of weight increase respect initial weight after the first and second week of treatment (3 days/week). (B) Serum AST and ALT levels at the end of the study. All results are represented as mean ± SEM. n = 3 per group. ** p≤0.01 vs. vehicle.

After 1 week of daily free simvastatin or PM-Sim treatment in cirrhotic rats developed by 3 weeks of BDL, hemodynamic studies were performed to evaluate the therapeutic effect of the drug. Oral simvastatin caused a significant weight reduction during the week of treatment (Figure 30) and increased plasma ALT and AST levels (Table 16). In particular, 3 of 9 animals (33.3%) developed hepatotoxicity, and ALT and AST mean value in oral simvastatin group was higher than in vehicle rats. Encapsulation of simvastatin in PM resulted in the prevention of body weight decrease and did not cause elevations in transaminases. The *in vivo* effect of our PM-F127-Sim treatment was assessed with respect to PP values. Treatment with oral simvastatin caused a reduction of PP in some individuals, but the effect was not consistent among the group and the

global reduction was not significant (Table 17). Furthermore, no effects in PP were observed when using 1 mg/kg of PM-F127-Sim. Remarkably, IV administration of PM-F127-Sim 5 mg/Kg showed a clinically significant reduction in PP of about 2.2 mmHg in treated animals, being the values much more homogenous than those of oral simvastatin group. Also, efficacy was achieved with no apparent local and systemic toxicities. It is also important to notice that in none of the treatments evaluated extrahepatic effects on systemic hemodynamics (e.g. MAP, SMABF) were observed.
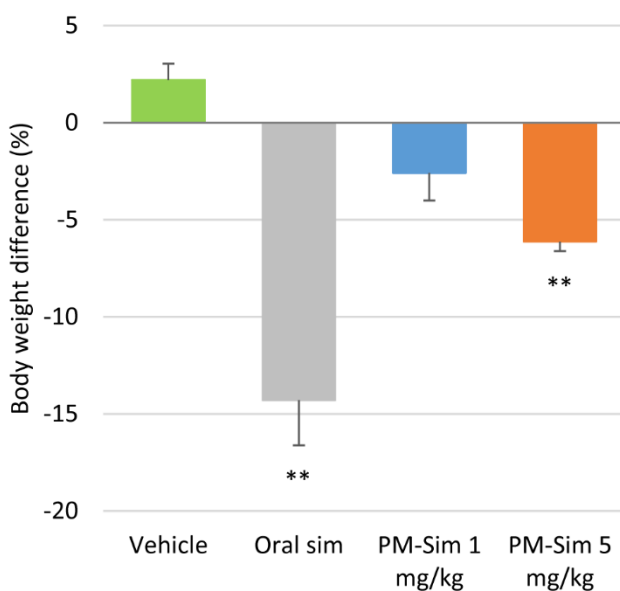
Figure 30. Effect of PM-Sim treatment on BDL rats. Body weight difference after 1 week of daily treatment with vehicle (oral dH$_2$O) (n = 17), oral simvastatin 10 mg/kg (n = 13), PM-F127-Sim 1 mg/kg (n = 9) or PM-F127-Sim 5 mg/kg (n = 15). Data are expressed as mean ± SEM. ** p≤0.01 vs. vehicle.

Table 16. Biochemical parameters of 4-week BDL rats after 1-week daily treatment.

Group	n	Creatinine (mg/dl)	Bilirubin (mg/dl)	AST (IU/L)	ALT (IU/L)	ALP (IU/L)	CK (IU/L)	Albumin (g/dl)
Vehicle	11	0.51 ± 0.03	10.03 ± 1.07	535.64 ± 36.07	54.45 ± 2.90[#]	365.91 ± 23.04	894.45 ± 102.22	2.48 ± 0.05
Oral simvastatin	9	0.44 ± 0.02	9.62 ± 0.69	1,118.44 ± 187.58	135.33 ± 22.45*	641.11 ± 104.46	1,143.22 ± 123.41	2.54 ± 0.09
PM-Sim 1 mg/kg	7	0.56 ± 0.02	10.93 ± 1.07	451.57 ± 30.71[#]	56.71 ± 3.97[#]	465.29 ± 118.76	1,042.86 ± 219.17	2.30 ± 0.11
PM-Sim 5 mg/kg	13	0.53 ± 0.03	9.74 ± 0.24	541.38 ± 56.06	66.31 ± 6.41	428.31 ± 24.35	792.54 ± 85.49[#]	2.25 ± 0.05

ALP: alkaline phosphatase, ALT: alanine aminotransferase, AST: aspartate aminotransferase, CK: creatine kinase, PM: polymeric micelle, Sim: simvastatin. Vehicle group received oral dH$_2$O. Values were taken during fasting and are expressed as mean ± SEM. n = number of rats. * p≤0.05, ** 0.01 vs. vehicle; # p≤0.05 vs. oral simvastatin.

Table 17. Hemodynamic measurements in 4-week BDL rats after 1-week daily treatment.

Group	n	MAP (mmHg)	SMABF ([ml/min]·100 g)	SMAR ([mmHg·min]/[ml·100 g])	PP (mmHg)	Heart rate (BPM)
Vehicle	11	110.35 ± 3.52	5.52 ± 0.37	21.07 ± 1.81	17.02 ± 0.37	346.35 ± 7.38
Oral simvastatin	6	110.45 ± 6.50	4.54 ± 0.41	25.52 ± 3.01	15.38 ± 1.35	343.17 ± 7.67
PM-Sim 1 mg/kg	7	99.34 ± 4.75	4.72 ± 0.67	24.59 ± 4.40	17.09 ± 0.65	351.13 ± 5.65
PM-Sim 5 mg/kg	13	99.34 ± 3.65*	3.93 ± 0.30**	28.04 ± 3.37	14.79 ± 0.42**	344.73 ± 6.22

MAP: mean arterial pressure, PM: polymeric micelle, PP: portal pressure, Sim: simvastatin, SMABF: superior mesenteric artery blood flow, SMAR: superior mesenteric artery resistance. Vehicle group received oral dH$_2$O. Values were taken 90 min after the last dose of treatment and are expressed as mean ± SEM. n = number of rats. * p≤0.05, ** 0.01 vs. vehicle.

5.2. Second study: Functionalization of PM to target LSEC and efficacy evaluation in experimental models of CLD

Optimization of PM targeting LSEC

Synthetic forms of CD32b, CD36 and ITGB3 peptide ligands designed for PM active targeting to LSEC were successfully synthesized using standard Fmoc-SPPS strategy and purified by RP-HPLC, obtaining amino acid sequences suitable for assembly with Pluronic® F127 to form FPM, as well as sequences correctly labelled with FITC for visualization by flow cytometry (Figure 31A). The scrambled versions of CD32b and CD36 sequences, to be used as negative controls for PM targeting to LSEC, were also optimally synthesized with Fmoc-SPPS, generating peptides lacking the recognition site to their respective receptors (Figure 31B).

Analysis of peptide ligands internalization by healthy LSEC in culture showed a great cellular uptake upon *in vitro* treatment. After 1 min of incubation, more than 50% of LSEC internalized CD32b, CD36 and ITGB3 ligands, and the percentage of positive cells in all cases was eventually higher than 80% at 1 h (Figure 31C).
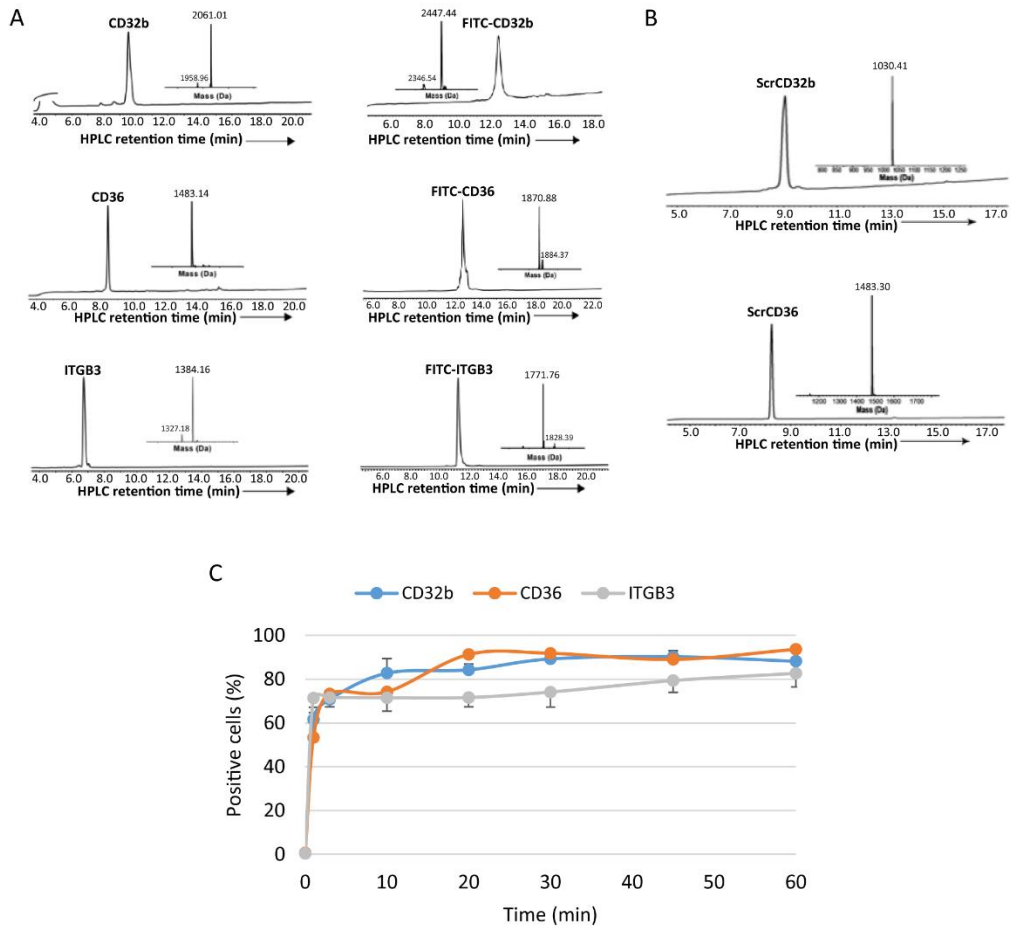
Figure 31. Characterization of peptide ligands. (A) RP-HPLC chromatogram analysis of unlabelled and FITC-labelled specific peptide ligands: CD32b (top), CD36 (middle) and ITGB3 (bottom). (B) RP-HPLC chromatogram of unlabelled scrambled peptide ligands: ScrCD32b (top) and ScrCD36 (bottom). (C) *In vitro* internalization of specific peptide ligands analyzed by flow cytometry after treating LSEC isolated from healthy rats at different times (from 1 to 60 min). Results are plotted as mean ± SEM. n = 2 animals per experimental condition.

Conjugation of the peptide ligands, both original and scrambled, to PM was effectively performed by a peptide bond between the carboxyl group of the polymer and the amide group of the peptide, achieving a correct functionalization of the nanoparticles (Figure 32A) and the generation of FPM with a homogeneous spherical shape and an average size of approximately 20 nm (Figure 32B). The physicochemical properties of FPM are summarized in table 18. The mean hydrodynamic diameter of FPM varied according to the ligand used for functionalization, being approximately 180 nm for FPM-ITGB3 and almost reaching 290 nm for FPM-ScrCD32b. All formulations had mid-range PDI values (ranging from 0.35 to 0.53) and presented a zeta potential close to neutrality, being slightly positive for all nanoparticles except for FPM-ITGB3. Finally, the EE of active simvastatin (20 mg/ml) with FPM (100 mg/mL Pluronic® F127:1 mg/ml peptide) was greater than 95% for all formulations designed. Once loaded, the stability of FPM-Sim in a medium simulating physiological condition was studied by the release kinetics of simvastatin, obtaining a low cumulative percentage of drug released below 1.5% in all types of functionalized micelles, proving to be stable at 37 ºC and pH 7.4 for at least 72 h (Figure 32C).

Table 18. Physicochemical properties of FPM.

FPM	Hydrodynamic diameter (nm)	PDI	Zeta potential (mV)
FPM-CD32b	203.4 ± 3.6	0.44 ± 0.02	7.24 ± 0.21
FPM-CD36	258.2 ± 8.0	0.53 ± 0.12	6.16 ± 0.46
FPM-ITGB3	179.4 ± 0.4	0.41 ± 0.01	-4.55 ± 0.59
FPM-ScrCD32b	288.0 ± 32.4	0.35 ± 0.02	6.88 ± 0.43

FPM: functionalized polymeric micelle, PDI: polydispersity index, Scr: scrambled. Values are indicated as mean ± SD.
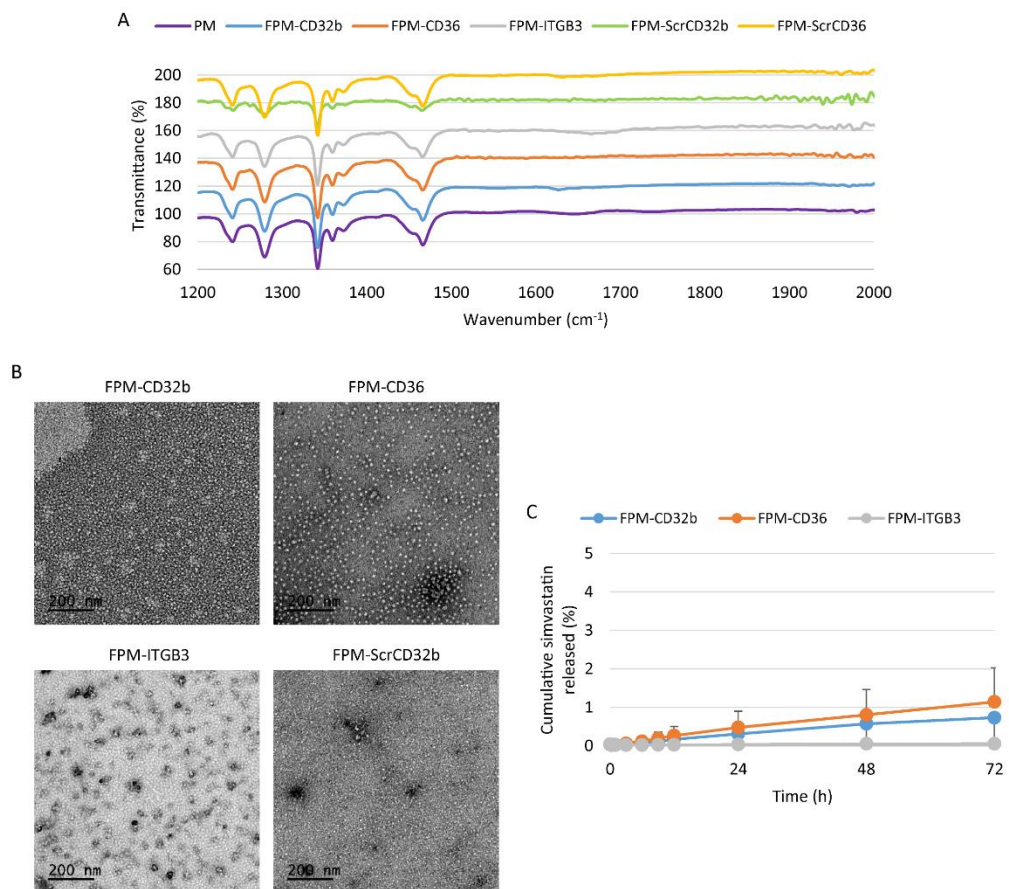
Figure 32. Characterization of FPM. (A) FTIR spectra of PM and FPM with the different peptide ligands (specific and scrambled). (B) Representative TEM micrographs showing different batches of FPM (scale bar: 200 nm). (C) *In vitro* drug release kinetics under simulated physiological conditions (37 ºC, pH 7.4). Data are expressed as mean ± SEM. n = 2 per group.

In vitro internalization of FPM in LSEC isolated from healthy rats was found to be more efficient for nanoparticles functionalized with the specific ligands (CD32b, CD36 and ITGB3) than those functionalized with scrambled versions of these peptides (ScrCD32b and ScrCD36), demonstrating the importance of specific recognition for a correct targeting. Within only 1 min of treatment, at least 20% of LSEC had internalized all types of FPM, but after 5 min a difference in uptake between the two types of functionalization was evident (Figure 33). After 30 min this difference became significant and at 4 h the internalization of specific FPM was over 80% (FPM-CD32b: 81.5%, FPM-CD36: 83.7%, FPM-ITGB3: 86.6%), whereas scrambled FPM were only internalized in 54.8% (FPM-ScrCD36) and 27.6% (FPM-ScrCD32b) of the total LSEC.
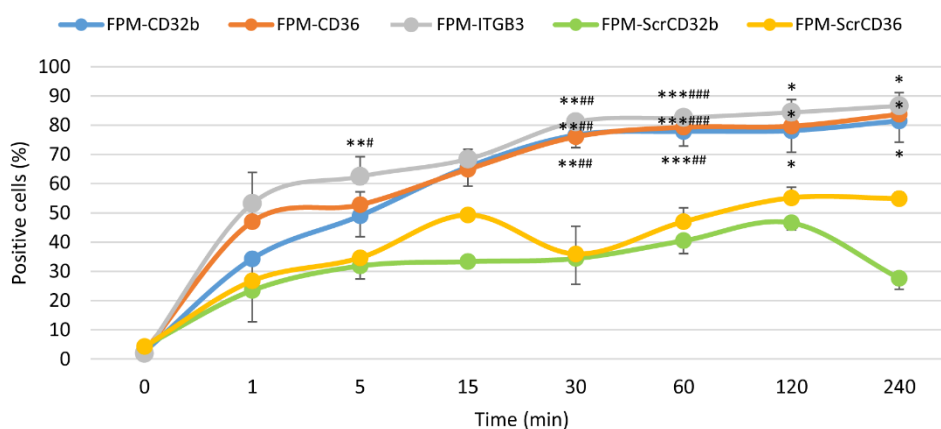
Figure 33. *In vitro* internalization of FPM in healthy LSEC. Internalization percentage of different FPM evaluated by flow cytometry from 1 min to 4 h. Values are represented as mean ± SEM. n = 3 animals for each formulation. * $p \leq 0.05$, ** 0.01, *** 0.001 vs. FPM-ScrCD32b; # $p \leq 0.05$, ## 0.01, ### 0.001 vs. FPM-ScrCD36.

In vitro efficacy of FPM-Sim

The functional effect of simvastatin was measured by the expression of KLF2, a target gene of this drug. In its encapsulated form in FPM, simvastatin was equally effective as the free drug or encapsulated in PM, causing a significant overexpression of KLF2 in healthy LSEC (Figure 34). Specifically, FPM-CD36-Sim was the formulation that achieved the highest overexpression (RQ = 18.1). In contrast, when these endothelial cells were treated with empty nanoparticles (FPM Ø), no changes in gene expression were seen, ruling out any possible functional effect of the FPM themselves.
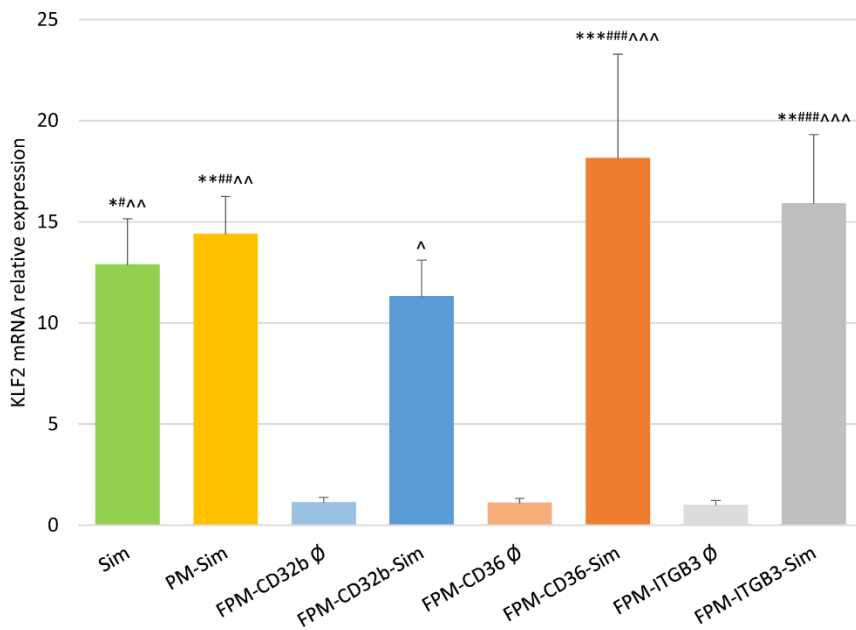
Figure 34. *In vitro* efficacy of FPM-Sim. Relative mRNA expression levels of KLF2 determined by qRT-PCR in treated LSEC isolated from healthy rats. GAPDH was used as endogenous control and results were normalized to FPM-CD36 Ø. mRNA levels are expressed as mean ± SEM. n = 3 animals per experimental condition. * p≤0.05, ** 0.01, *** 0.001 vs. FPM-CD32b Ø; # p≤0.05, ## 0.01, ### 0.001 vs. FPM-CD36 Ø; ^ p≤0.05, ^^ 0.01, ^^^ 0.001 vs. FPM-ITGB3 Ø.

In vivo internalization in liver and determination of simvastatin muscle content

To confirm the active targeting of the specific peptide ligands to their receptors, healthy rats were treated with the three formulations of specific FPM, labelled with 5-DTAF, and their *in vivo* internalization in the four main types of liver cells was compared by flow cytometry with respect to non-functionalized PM.

Binding of specific peptide ligands on the surface of PM led to an increase in the delivery of these nanoparticles to LSEC compared with non-functionalized ones, being taken up by more than 40% of these cells (FPM-CD32b: 42.6%, FPM-CD36: 49.0%, FPM-ITGB3: 46.2%), while PM only entered 2.9% of the total number of endothelial cells (Figure 35A). In KC, there was a significantly higher percentage of positive cells for FPM-CD32b compared with PM (p = 0.041), but the notable difference observed in LSEC was not as great here, because the internalization rate of CD32b micelle did not reach 20% in the liver resident macrophages. The other two specific FPM formulations also produced increases in cellular uptake in KC, but in a more discreet manner. By contrast, in healthy HSC there was virtually no internalization of any kind of nanoparticle after *in vivo* treatment. Finally, in hepatocytes it was found the highest number of internalized FPM-ITGB3 and PM, with a 47.1% and a 23.1% of positive cells, respectively. In the latter case, due to the undesired high internalization of FPM-ITGB3 in hepatocytes, for the following *in vivo* studies this formulation was discarded and only CD32b and CD36 peptide ligands were used, alone (FPM-CD32b and FPM-CD36) or in combination in a mixed functionalization (FPM-CD32b-CD36).

Beyond the *in vivo* internalization of nanoparticles in the liver, their accumulation in muscle was of great interest, because muscle toxicity is known to be the main adverse effect of oral simvastatin. For this purpose, the presence of active simvastatin in muscle was quantified by UPLC-MS/MS comparing free (IV and oral) and encapsulated (PM and FPM) drug administration. Higher amounts of active simvastatin in muscle were observed in the group of animals treated with IV simvastatin, followed by those

receiving oral simvastatin, compared with the scarce values obtained when the drug was loaded in PM and FPM (Figure 35B).
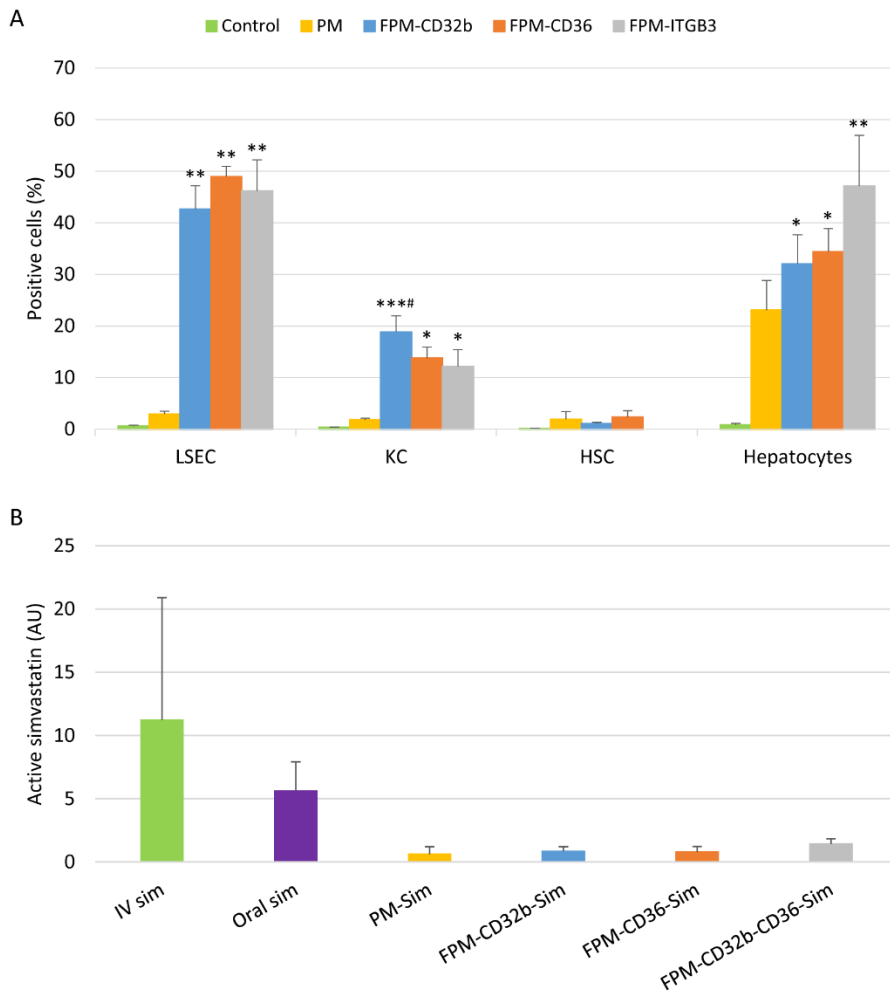
Figure 35. *In vivo* internalization of FPM in liver cells and simvastatin quantitation in muscle. (A) Internalization of nanoparticles in different hepatic cell types (LSEC, KC, HSC and hepatocytes) after IV treatment of healthy rats with PM or FPM. Results are represented as mean ± SEM. n = 3-5 animals per condition. * p≤0.05, ** 0.01, *** 0.001 vs. control; # p≤0.05 vs. PM. (B) Area of active simvastatin determined by UPLC-MS/MS in muscle samples of healthy rats treated with free simvastatin (IV or oral) or encapsulated simvastatin (PM or FPM). Results are represented as mean ± SEM. n = 3 animals per condition.

In vivo safety and toxicity

MTD was determined in healthy mice in a three-phase assay using FPM-CD36 as a reference nanoparticle to assess the toxicity of simvastatin-loaded FPM.

In the first phase, different doses of simvastatin (10, 20 and 50 mg/kg) were tested and their acute toxicity was measured at 4 h, 48 h and 1 week after a single administration. Overall, none of the doses caused behavioural changes in the animals after treatment, nor did they cause a reduction in weight. Nonetheless, at 4 and 48 h, AST and ALT serum levels were elevated in some individuals from each dose, but all parameters normalized 1 week after treatment (Figure 36A). Moreover, doses of 20 and 50 mg/kg caused an increase in CK levels in two individuals, indicating muscle toxicity. Although this effect also disappeared after 1 week, the two higher doses were discarded for the next phases. At the histological level, no major effects were observed in the liver, as only a few individuals in both control and treatment groups (10 and 50 mg/kg) had a score 1 punctuation in relation to lobular inflammation (Figure 36B).
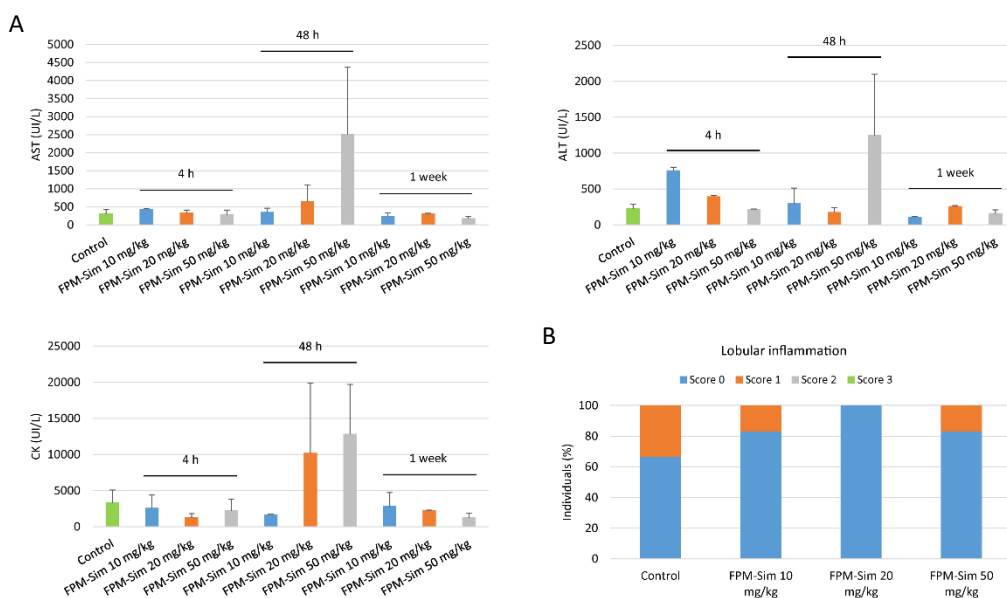
Figure 36. Acute toxicity study (phase 1) of the MTD assay. (A) Serum AST, ALT and CK levels of control (untreated) healthy mice and after a single dose of FPM-CD36-Sim at 10, 20 or 50 mg/kg analyzed at 4 h, 48 h and 1 week. Values are plotted as mean ± SEM. n = 2 per group. (B) Percentage of individuals with lobular inflammation.

In the second phase of the trial, FPM-CD36-Sim at 10 mg/kg was administered 3 days/week during 2 weeks. None of the treated animals exhibited behavioural changes throughout the treatment or significant weight loss (Figure 37A). Regarding the biochemical analysis, after a total of 6 doses administered, serum levels of AST, ALT and CK remained stable and were comparable to those of the control group (Figure 37B). The only significant change observed was a reduction in total cholesterol thanks to the 10 mg/kg dose of encapsulated simvastatin from 111.0 to 91.9 mg/dl (p = 0.034). Histological assessment again showed a maximum score of 1 for lobular inflammation in both study groups, although in a higher percentage of individuals than in phase 1 (Figure 37C).

Finally, a subacute protocol was performed where mice were treated with FPM-CD36-Sim 10 mg/kg for 5 days/week during 3 weeks, and its effect on liver biochemistry and histology was studied. In this case, control animals also received IV injections of saline (vehicle group). As before, animals' behaviour was not altered, but there was a weight loss during the 3 weeks that was similar between the two groups at the end of the study, probably due to the manipulation associated with IV injection (Figure 38A). The subacute study did not result in liver or muscle toxicity (Figure 38B), but a significant reduction in ALP (from 166.8 to 123.0 UI/L, p < 0.000) and total cholesterol (from 91.8 to 84.3 mg/dl, p = 0.018) was achieved with FPM-Sim. Only one individual receiving 10 mg/kg of encapsulated simvastatin showed a higher-scoring lobular inflammation than the vehicle group (Figure 38C).
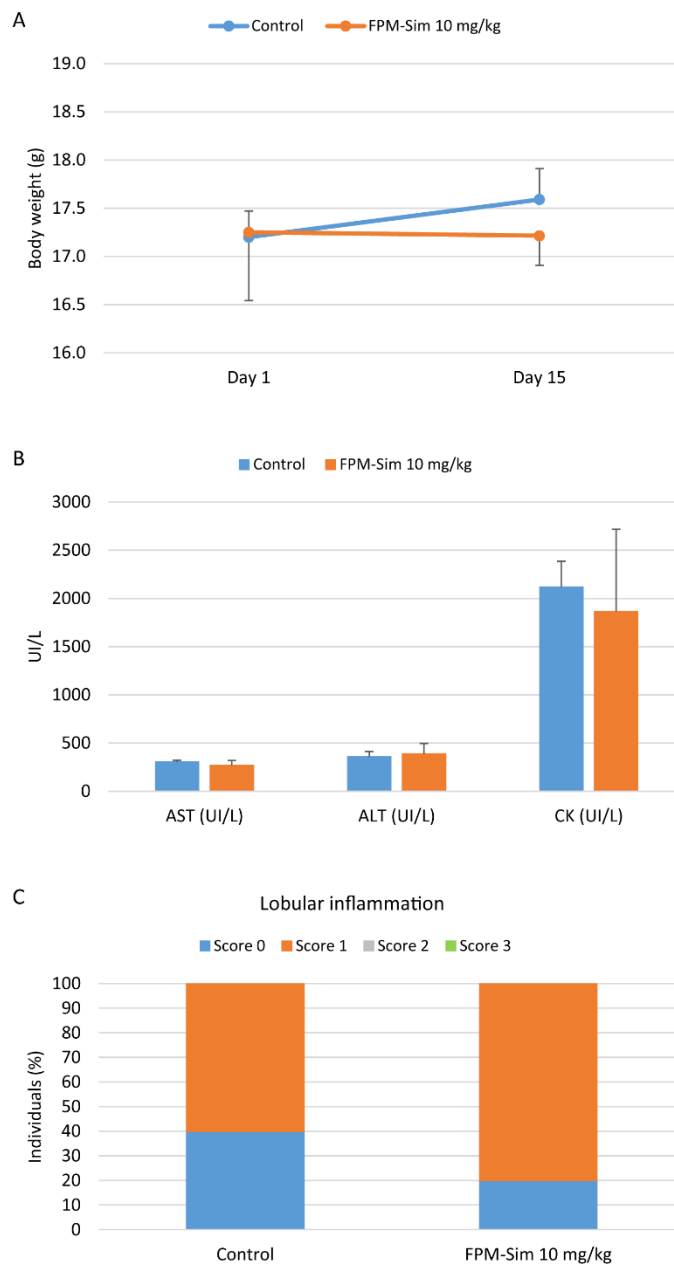
Figure 37. Acute toxicity study (phase 2) of the MTD assay. (A) Evolution of body weight of control (untreated) healthy mice and after treating with IV FPM-CD36-Sim 10 mg/kg for 3 days/week during 2 weeks. (B) Serum AST, ALT and CK levels at the end of the study. All values are expressed as mean ± SEM. n = 5 for each experimental condition. (C) Percentage of individuals with lobular inflammation.
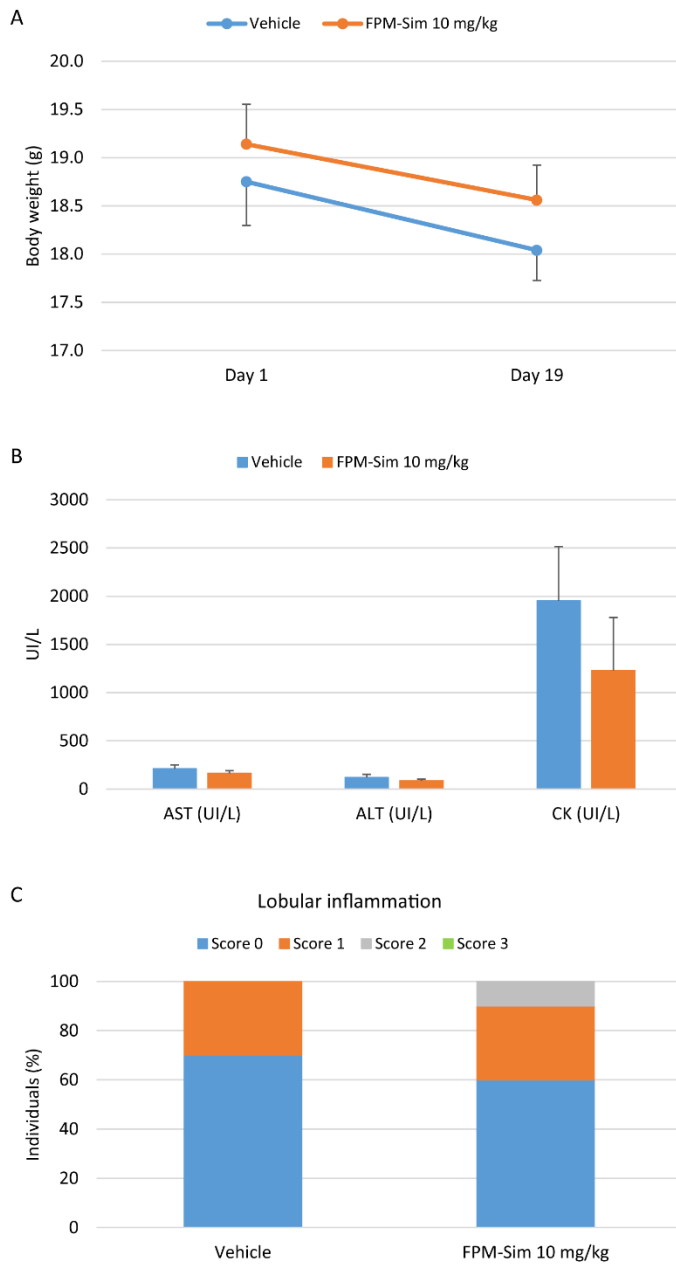
Figure 38. Subacute toxicity study (phase 3) of the MTD assay. (A) Evolution of body weight of healthy mice treated IV with vehicle (saline) or FPM-CD36-Sim 10 mg/kg for 5 days/week during 3 weeks. (B) Serum AST, ALT and CK levels after treatment. All values are expressed as mean ± SEM. n = 10 for each experimental condition. (C) Percentage of individuals with lobular inflammation.

In vivo efficacy

BDL as a model of advanced and decompensated liver disease

In the decompensated liver disease model by BDL, the efficacy of FPM-Sim compared to oral simvastatin and PM-Sim was evaluated after 1 week of daily treatment by hemodynamic studies. After the administration of 7 doses, oral simvastatin caused the most significant body weight decrease compared with untreated BDL animals, being greater than with encapsulated simvastatin, which caused a more moderate weight loss (Figure 39). At the biochemical level, orally administration of simvastatin induced the highest values of AST and ALT, and of CK (Table 19), causing muscle toxicity in 3 of 11 treated rats (27.3%), this being significant with respect to the other groups (Table 20). In contrast, in this advanced cirrhotic model, the use of nanoparticles generated a significant increase in triglycerides and, slightly, in total cholesterol when comparing serum levels with BDL rats that did not receive any type of micelles (control and oral simvastatin groups) (Table 19).
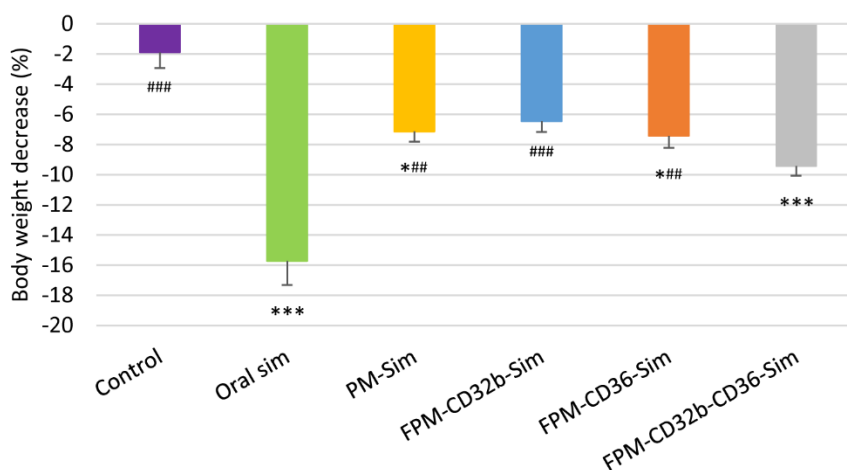
Figure 39. Effect of FPM-Sim treatment on BDL rats. Body weight decrease in rats of the control group (untreated) (n = 9) and after 1 week of daily treatment with oral simvastatin 10 mg/kg (n = 13), PM-Sim 5 mg/kg (n = 9), FPM-CD32b-Sim 5 mg/kg (n = 9), FPM-CD36-Sim 5 mg/kg (n = 12) or FPM-CD32b-CD36-Sim 5 mg/kg (n = 9). Data are represented as mean ± SEM. * p≤0.05, *** 0.001 vs. control; ## p≤0.01, ### 0.001 vs. oral simvastatin.

Table 19. Biochemical parameters of 4-week BDL rats after 1-week daily treatment.

Group	n	Creatinine (mg/dl)	Bilirubin (mg/dl)	AST (IU/L)	ALT (IU/L)	ALP (IU/L)	CK (IU/L)	Cholesterol (mg/dl)	Triglycerides (mg/dl)	Albumin (g/dl)
Control	7	0.59 ± 0.05	11.85 ± 0.72	703 ± 68.75	100 ± 12.38	412 ± 36.13	485 ± 61.13	100 ± 7.60	158 ± 18.18	2.3 ± 0.13
Oral simvastatin	11	0.54 ± 0.07	10.26 ± 0.53	1,426 ± 316.31	187 ± 47.09	439 ± 44.80	974 ± 264.31	158 ± 22.54	195 ± 40.42	2.4 ± 0.11
PM-Sim	9	0.50 ± 0.08	10.97 ± 0.64	915 ± 152.33	112 ± 17.90	360 ± 39.76	461 ± 59.78	171 ± 18.18	406 ± 38.73**###	2.3 ± 0.10
FPM-CD32b-Sim	8	0.59 ± 0.07	11.73 ± 0.48	1,135 ± 267.24	148 ± 25.02	482 ± 35.95	628 ± 115.93	201 ± 19.65	451 ± 56.45**###	2.3 ± 0.10
FPM-CD36-Sim	9	0.60 ± 0.04	11.19 ± 0.98	1,144 ± 355.95	106 ± 29.61	405 ± 23.10	567 ± 64.83	196 ± 25.14	466 ± 51.76***####	2.1 ± 0.07
FPM-CD32b-CD36-Sim	8	0.68 ± 0.10	12.13 ± 1.03	618 ± 86.28	89 ± 16.45	518 ± 56.97	455 ± 49.01	244 ± 33.33**	548 ± 61.22***####	2.2 ± 0.08

ALP: alkaline phosphatase, ALT: alanine aminotransferase, AST: aspartate aminotransferase, CK: creatine kinase, FPM: functionalized polymeric micelle, PM: polymeric micelle, Sim: simvastatin. Control group received no treatment. Values were taken during fasting and are expressed as mean ± SEM. n = number of rats. ** p≤0.01, *** 0.001 vs. control; ## p≤0.01, ### 0.001 vs. oral simvastatin.

Table 20. Percentage of BDL rats with liver and/or muscle toxicity after 1-week daily treatment.

Group	n	Liver toxicity	%	Muscle toxicity	%
Oral simvastatin	11	3	27.3	3	27.3*
PM-Sim	9	1	11.1	0	0.0
FPM-CD32b-Sim	8	1	12.5	2	25.0
FPM-CD36-Sim	9	2	22.2	0	0.0
FPM-CD32b-CD36-Sim	8	0	0.0	0	0.0

FPM: functionalized polymeric micelle, PM: polymeric micelle, Sim: simvastatin. Values are expressed as mean ± SEM. n = number of rats. * p≤0.05.

Regarding the efficacy, oral simvastatin showed a significant reduction in PP in treated animals compared with the untreated control group, with a reduction of 3.92 mmHg (p = 0.004), as well as with respect to PM-Sim, in this case more discreetly (p = 0.037) (Table 21). In turn, a tendency to reduce PP was also observed with functionalized micelles, with FPM-CD32b-CD36-Sim and FPM-CD32b-Sim being the nanoparticle-treated groups with the lowest pressure, but this decrease was not sufficiently consistent with any formulation. The rest of hemodynamic parameters studied (e.g. MAP, IHVR) were not affected in any of the cases.

Table 21. Hemodynamic measurements in 4-week BDL rats after 1-week daily treatment.

Group	n	MAP (mmHg)	SMABF ([ml/min]·100 g)	SMAR ([mmHg·min]/ [ml·100 g])	PP (mmHg)	PBF ([ml/min]·100 g)	IHVR ([mmHg·min]/ [ml·100 g])	Heart rate (BPM)
Control	5	90.75 ± 3.86	4.09 ± 0.82	19.09 ± 2.20	19.73 ± 0.41	3.17 ± 0.71	7.46 ± 1.75	327.2 ± 19.35
Oral simvastatin	5	100.10 ± 7.61	3.60 ± 0.39	23.97 ± 2.19	15.81 ± 0.63**#	2.56 ± 0.32	6.51 ± 0.79	332.5 ± 11.67
PM-Sim	7	97.97 ± 4.90	3.72 ± 0.42	23.86 ± 4.46	18.61 ± 0.51	2.80 ± 0.33	7.44 ± 1.17	345.3 ± 10.89
FPM-CD32b-Sim	6	91.50 ± 4.56	4.28 ± 0.78	20.31 ± 3.42	17.81 ± 0.74	2.62 ± 0.46	7.84 ± 1.30	321.0 ± 8.30
FPM-CD36-Sim	4	89.95 ± 4.14	4.43 ± 0.56	17.26 ± 2.86	18.20 ± 0.68	3.43 ± 0.07	5.31 ± 0.27	332.4 ± 14.32
FPM-CD32b-CD36-Sim	7	92.71 ± 2.58	4.75 ± 0.60	17.74 ± 2.77	17.09 ± 0.67	3.75 ± 0.71	6.13 ± 1.66	326.4 ± 12.34

FPM: functionalized polymeric micelle, IHVR: intrahepatic vascular resistance, MAP: mean arterial pressure, PBF: portal blood flow, PM: polymeric micelle, PP: portal pressure, Sim: simvastatin, SMABF: superior mesenteric artery blood flow, SMAR: superior mesenteric artery resistance. Control group received no treatment. Values were taken 90 min after the last dose of treatment and are expressed as mean ± SEM. n = number of rats. ** $p \leq 0.01$ vs. control; # $p \leq 0.05$ vs. PM-Sim.

TAA as a model of non-decompensated liver disease with advanced fibrosis

In order to see a greater effect on hemodynamics, a less severe liver disease model was generated, such as an 8-week TAA model, with rats receiving treatment 5 days/week during the last 2 weeks of the model. In this intermediate model of cirrhosis, simvastatin did not cause animal weight loss, except in FPM-CD32b and mixed FPM treatment groups. In both cases, a slight reduction in body weight of less than 2% was seen, most likely associated with the stress induced by the manipulation of IV administration rather than the drug itself (Figure 40). A marked overall decrease in liver transaminase levels was observed in this model compared with BDL rats, as well as in triglycerides and cholesterol (Table 22), with only one individual showing liver toxicity in the case of the oral drug, and one individual of oral simvastatin and FPM-CD32b-Sim groups with muscle toxicity (Table 23).
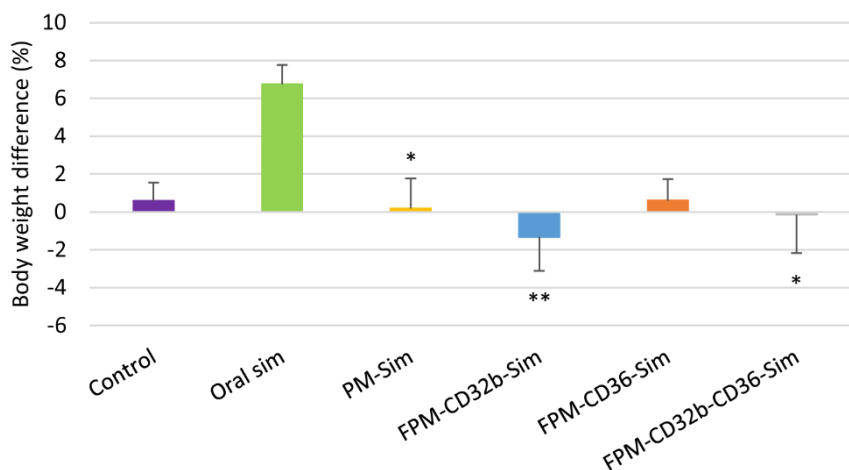
Figure 40. Effect of FPM-Sim treatment on TAA rats. Body weight difference in rats of the control group (untreated) (n = 9) and after 2 weeks of treatment (5 days/week) with oral simvastatin 10 mg/kg (n = 10), PM-Sim 5 mg/kg (n = 10), FPM-CD32b-Sim 5 mg/kg (n = 10), FPM-CD36-Sim 5 mg/kg (n = 10) or FPM-CD32b-CD36-Sim 5 mg/kg (n = 10). Data are represented as mean ± SEM. * p≤0.05, ** 0.01 vs. oral simvastatin.

Table 22. Biochemical parameters in 8-week TAA-induced cirrhotic rats after a 2-week treatment (5 days/week).

Group	n	Creatinine (mg/dl)	Bilirubin (mg/dl)	AST (IU/L)	ALT (IU/L)	ALP (IU/L)	CK (IU/L)	Cholesterol (mg/dl)	Triglycerides (mg/dl)	Albumin (g/dl)
Control	9	0.56 ± 0.03	0.22 ± 0.04	177 ± 18.18	53 ± 6.37	178 ± 12.63	1,074 ± 185.36	62 ± 3.59+	33 ± 1.63	3.0 ± 0.10
Oral simvastatin	10	0.50 ± 0.04	0.16 ± 0.02	275 ± 56.91	67 ± 15.63	218 ± 18.67	1,360 ± 197.30	67 ± 3.94	37 ± 5.52	3.2 ± 0.12
PM-Sim	10	0.50 ± 0.06	0.27 ± 0.05	166 ± 10.65	45 ± 5.84	188 ± 32.07	882 ± 185.70	76 ± 3.78	123 ± 46.65***##	3.1 ± 0.13
FPM-CD32b-Sim	10	0.50 ± 0.05	0.38 ± 0.05*##+	225 ± 34.30	53 ± 4.57	193 ± 25.36	1,515 ± 258.87	62 ± 3.53+	67 ± 9.46***##+	3.0 ± 0.12
FPM-CD36-Sim	10	0.54 ±0.06	0.20 ± 0.02	156 ± 11.76	40 ± 3.20	176 ± 16.96	868 ± 142.94	80 ± 4.55*	43 ± 4.88	3.1 ± 0.10
FPM-CD32b-CD36-Sim	9	0.50 ± 0.03	0.23 ± 0.03	199 ± 19.67	57 ± 5.71	235 ± 30.27	1,055 ± 218.67	59 ± 3.27^++	54 ± 6.62**#	3.2 ± 0.11

ALP: alkaline phosphatase, ALT: alanine aminotransferase, AST: aspartate aminotransferase, CK: creatine kinase, FPM: functionalized polymeric micelle, PM: polymeric micelle, Sim: simvastatin. Control group received no treatment. Values were taken during fasting and are expressed as mean ± SEM. n = number of rats. * p≤0.05, ** 0.01, *** 0.001 vs. control; # p≤0.05, ## 0.01 vs. oral simvastatin; ^ p≤0.05 vs. PM-Sim; + p≤0.05, ++ 0.01 vs. FPM-CD36-Sim.

Table 23. Percentage of TAA rats with liver and/or muscle toxicity after a 2-week treatment (5 days/week).

Group	n	Liver toxicity	%	Muscle toxicity	%
Oral simvastatin	10	1	10.0*	1	10.0
PM-Sim	10	0	0.0	0	0.0
FPM-CD32b-Sim	10	0	0.0	1	10.0
FPM-CD36-Sim	10	0	0.0	0	0.0
FPM-CD32b-CD36-Sim	9	0	0.0	0	0.0

FPM: functionalized polymeric micelle, PM: polymeric micelle, Sim: simvastatin. Values are indicated as mean ± SEM. n = number of rats. * $p \leq 0.05$.

Regarding the hemodynamic determinations, FPM-CD32b-Sim treatment was successful in reducing PP significantly by more than 2 points compared with the untreated control group (p = 0.005) and by more than 1.5 points with respect to oral simvastatin (p = 0.037) and FPM-CD36-Sim (p = 0.014) (Table 24). FPM-CD32b-CD36-Sim and PM-Sim also managed to decrease PP levels, being significant the reduction achieved by the nanoparticles with mixed functionalization regarding the untreated group (p = 0.042). Along with these results, a slight but consistent decrease in IHVR and SMAR in all groups treated with encapsulated simvastatin formulations suggests an overall improvement in PH.

Table 24. Hemodynamic measurements in 8-week TAA-induced cirrhotic rats after a 2-week treatment (5 days/week).

Group	n	MAP (mmHg)	SMABF ([ml/min]·100 g)	SMAR ([mmHg·min]/ [ml·100 g])	PP (mmHg)	PBF ([ml/min]·100 g)	IHVR ([mmHg·min]/ [ml·100 g])	Heart rate (BPM)
Control	7	106.20 ± 5.18	4.60 ± 0.57	22.37 ± 2.86	11.96 ± 0.49	3.84 ± 0.22	3.18 ± 0.24	341.0 ± 9.42
Oral simvastatin	7	100.66 ± 3.43	4.31 ± 0.45	22.12 ± 2.36	11.39 ± 0.76	3.79 ± 0.20	3.11 ± 0.33	332.6 ± 12.52
PM-Sim	6	96.93 ± 3.11	4.84 ± 0.88	20.40 ± 2.84	10.22 ± 0.38	4.70 ± 0.63	2.34 ± 0.27	335.6 ± 6.55
FPM-CD32b-Sim	7	98.62 ± 5.26	5.49 ± 0.89	19.17 ± 3.92	9.64 ± 0.27**#^	4.07 ± 0.53	2.56 ± 0.26	338.1 ± 7.16
FPM-CD36-Sim	7	94.58 ± 3.11	4.71 ± 0.37	18.28 ± 1.63	11.52 ± 0.55	4.41 ± 0.41	2.72 ± 0.21	349.6 ± 7.53
FPM-CD32b-CD36-Sim	6	92.42 ± 3.96	4.19 ± 0.41	20.80 ± 2.54	10.15 ± 0.52*	4.13 ± 0.19	2.47 ± 0.11	321.8 ± 13.25

FPM: functionalized polymeric micelle, IHVR: intrahepatic vascular resistance, MAP: mean arterial pressure, PBF: portal blood flow, PM: polymeric micelle, PP: portal pressure, Sim: simvastatin, SMABF: superior mesenteric artery blood flow, SMAR: superior mesenteric artery resistance. Control group received no treatment. Values were taken 90 min after the last dose of treatment and are expressed as mean ± SEM. n = number of rats. * $p \leq 0.05$, ** 0.01 vs. control; # $p \leq 0.05$ vs. oral simvastatin; ^ $p \leq 0.05$ vs. FPM-CD36-Sim.

To elucidate the possible causes of this reduction in PP and, to a lesser extent, IHVR, the proportion of fibrotic area in the livers of these animals was assessed by detecting collagen fibers (type I and III) with Sirius Red staining. Once quantified, it was observed that TAA rats administered with FPM-CD32b-Sim formulation presented the lowest percentage of fibrotic area in the liver (2.0%) compared with the other groups, being consistent with the improvement in PP caused by this treatment (Figure 41A). In this direction, both parameters, PP and fibrotic area, showed a significantly positive correlation (r = 0.580; p < 0.001), portraying the relationship between the formation of an abnormally large amount of scar tissue in the liver, triggering an elevated IHVR, and PH (Figure 41B). Likewise, analysis of gene expression in total liver samples revealed a down-regulation of COL1A1 gene, encoding the major component of type I collagen, when rats received simvastatin encapsulated in FPM-CD32b (Figure 41C).
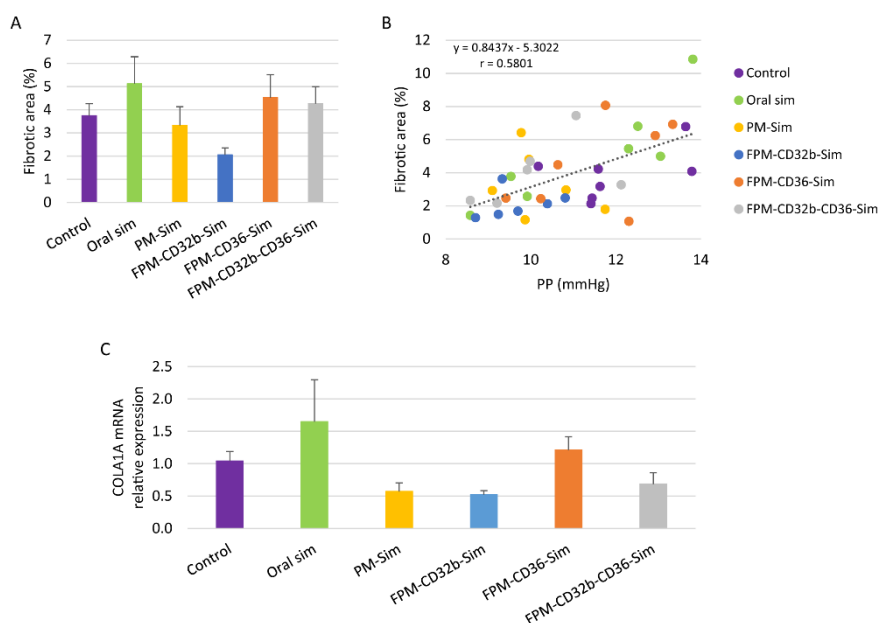
Figure 41. Efficacy of FPM in an experimental model of TAA-induced cirrhosis. (A) Percentage of fibrotic area in the liver of control rats (untreated) (n = 7) and after 2 weeks of treatment (5 days/week) with oral simvastatin 10 mg/kg (n = 7), PM-Sim 5 mg/kg (n = 6), FPM-CD32b-Sim 5 mg/kg (n = 7), FPM-CD36-Sim 5 mg/kg (n = 7) or FPM-CD32b-CD36-Sim 5 mg/kg (n = 6). Values are plotted as mean ± SEM. (B) Correlation between PP value and fibrotic area percentage. Dashed line represents the linear trend, with its equation and R-value displayed on the graph. (C) Relative mRNA expression levels of COLA1A determined by qRT-PCR in total liver. GAPDH was used as endogenous control and results were normalized to the control group (untreated). mRNA levels are plotted as mean ± SEM. n = 5 per group.

Finally, the protein expression levels of intrahepatic endothelial dysfunction markers were assessed through Western blot analyses of total liver samples from TAA rats, showing no significant difference in KLF2 expression between treated and untreated rats (Figure 42). Akt and eNOS activation was also studied by quantifying the phosphorylation levels of these proteins (p-Akt and p-eNOS) and their ratio to total protein expression (Figure 42). For Akt, there was a significant increase in its phosphorylation when rats received FPM-CD36-Sim compared with all groups. Abut eNOS, a target protein of this kinase, its activation was significantly promoted when simvastatin was administered in FPM-CD32b and FPM-CD32b-CD36, as the proportion of p-eNOS doubled and tripled, respectively, compared with rats receiving no treatment, stimulating the synthesis of NO at the endothelial level.
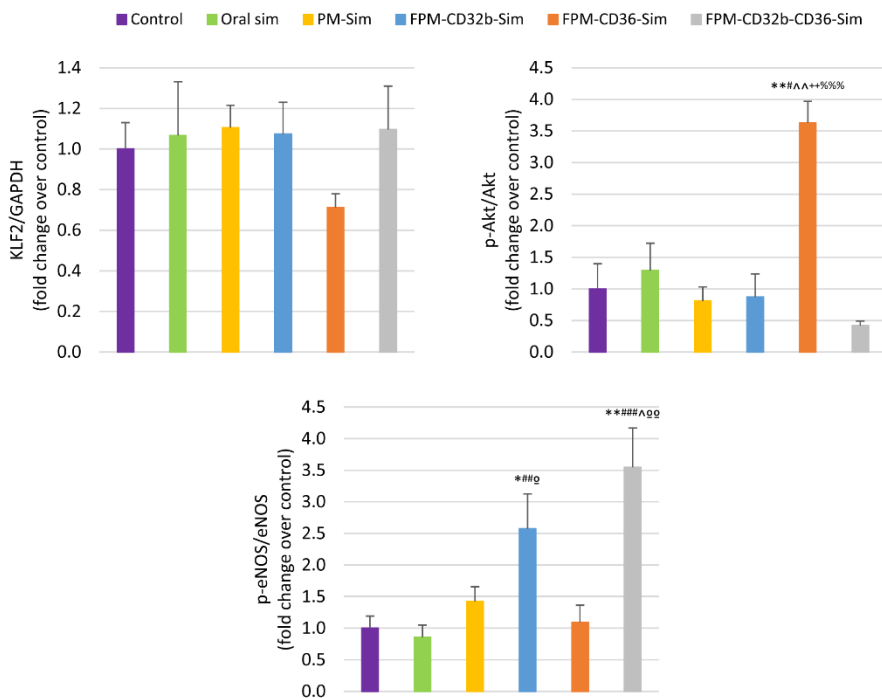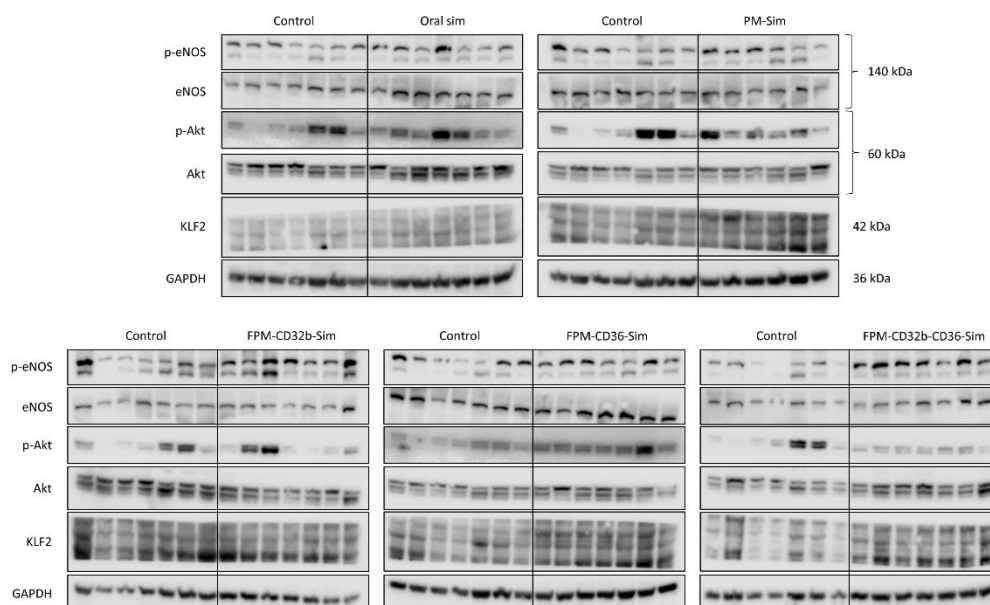
Figure 42. Efficacy of FPM in an experimental model of TAA-induced cirrhosis. Western blot analysis of intrahepatic endothelial dysfunction markers: quantification of KLF2, p-Akt/Akt and p-eNOS/eNOS protein levels in control rats (untreated) (n = 7) and after 2 weeks of treatment (5 days/week) with oral simvastatin 10 mg/kg (n = 7), PM-Sim 5 mg/kg (n = 6), FPM-CD32b-Sim 5 mg/kg (n = 7), FPM-CD36-Sim 5 mg/kg (n = 7) or FPM-CD32b-CD36-Sim 5 mg/kg (n = 7). Corresponding western blots are shown below. Exposure time for chemiluminescence detection was 10 min for p-Akt, eNOS and p-eNOS, 5 min for Akt and KLF2, and 30 sec for GAPDH. GAPDH was used as endogenous control and results were normalized to the control group (untreated). Protein levels are expressed as mean ± SEM. * p≤0.05, ** 0.01 vs. control; # p≤0.05, ## 0.01, ### 0.001 vs. oral simvastatin; ^ p≤0.05, ^^ 0.01 vs. PM-Sim; ++ p≤0.01 vs. FPM-CD32b-Sim; º p≤0.05, ºº 0.01 vs. FPM-CD36-Sim; %%% p≤0.001 vs. FPM-CD32b-CD36.

6. DISCUSSION

6. DISCUSSION

CLD is characterized by being a progressive and long-standing pathology in which the liver undergoes a state of chronic inflammation due to various etiologies, leading to the generation of fibrotic tissue and the development of one of the main complications of the disease: the PH[1,4,5,7,12]. This disease can progress from an asymptomatic phase (compensated cirrhosis) to a symptomatic phase (decompensated cirrhosis) with the development of decompensation events (e.g. oesophageal varices), associated with a deterioration in quality of life and a reduction in the median survival of patients[10,14,16].

There are currently no effective treatments to slow the progression of CLD, except for the elimination of the etiological agent. In fact, the only therapeutic option for patients with CLD are NSBB, which cause splanchnic constriction and reduced hepatic blood flow[71,74]. However, they are not selective for the liver and patients remain unprotected against disease progression[6]. Therefore, any therapy aimed to directly improve IHVR arresting the progression of the disease would have a major health impact due to the high prevalence of CLD[12,15,75].

In this regard, statins have been shown to have multiple pleiotropic effects beyond their cardiovascular protective action, by lowering cholesterol levels, exerting a beneficial effect on the liver for the treatment of fibrosis and PH, directly improving LSEC and HSC phenotype[76,90,97,100,102,107–113,115,118–124]. In clinical trials and animal models of cirrhosis, statins have been shown to have vasoprotective and antifibrotic potential. Nonetheless, those studies have evidenced that, although with low incidence, the individuals with highly deteriorated hepatic function can develop severe adverse events including hepatic and muscle toxicity. These undesirable effects have reduced the therapeutic potential of statins in the field of CLD[90,91,93,121,124–127,130,131].

In an attempt to provide a solution to improve the therapeutic window of statins for use in the treatment of advanced CLD, in the present thesis we have developed a Pluronic®-based PM as a drug delivery system to direct simvastatin towards LSEC, as target cells involved in the early response to liver injury[26], where we want it to exert its

pharmacological effect. To this end, a nanoparticle capable of encapsulating simvastatin has been designed and functionalized for active targeting of LSEC, studying its *in vitro* characteristics in primary cultures of liver cells, as well as the *in vivo* effect in animal models of CLD.

In the first study, we synthesized two formulations of simvastatin-loaded Pluronic® micelles, demonstrating effective encapsulation and stability, as well as high accumulation in the liver, exerting a PP-lowering effect on a cirrhotic liver model by BDL.

PM loaded with statins have been successfully developed and tested in pathologies, such as bone regeneration and various types of cancer, but none of the previous studies were aimed at treating CLD[134–136,212,213]. Here, characterization of the two formulations revealed a high homogeneity in the production with near neutral charge of the PM, which is to be expected since it is well documented that PEG confers hydrophilic and neutral charge to particles and drugs[214].

In the framework of liver diseases, nanoparticles have been mainly designed to target HSC as the producers of collagen and direct contributors to liver fibrosis[151,153,193,215], as well as KC, because of their unspecific uptake of nanoparticles and their role as resident macrophage, maintaining liver immune homeostasis[216]. However, despite the importance of LSEC in the initial response to liver damage and in the progression of fibrosis, they have not attracted much attention in this area of research, being mainly used as a target for nanoparticles aimed at using their antigen-presenting cell function to induce a state of immunological tolerance in cases of autoimmune pathologies or allergies[217–219], or, on the contrary, suppress it to act as immunotherapy for cancer, such as liver metastasis[220]. It has only been more recently that a few studies have focused on using LSEC as target cells for nanoparticles as antifibrotic therapy, either in synergy with other HSC-targeting nanoparticles[221] or to stimulate hepatic stromal remodelling and, again, promote immune cell recruitment to exert an antitumoral effect in fibrotic

HCC[137]. For that reason, the first observation of our study derived from cell internalization analysis of both formulations is of great importance: LSEC were the principal cellular target of PM *in vitro*. They were efficient and fast in incorporating the nanoparticles, and this was confirmed in cells derived from healthy and BDL animals. Even if the uptake results were good in global terms and were expected due to the impressive endocytic capacity of these cells, in BDL-derived LSEC the incorporation was a little slower, which can be explained by the dedifferentiation of these cells during disease progression, where this capacity is gradually lost[31,115,183].

Once the incorporation of our formulations was confirmed, we evaluated the *in vitro* effects of PM-F127-Sim and PM-F108-Sim in LSEC. Accordingly, *in vitro* cytotoxicity studies were performed evidencing no toxicity derived by the PM and, only when simvastatin concentrations were too high, viability started to decrease. Actually, in PM-F127-Sim treated cells viability was sustained at higher doses of the drug, suggesting that the reduced toxicity could be related to the progressive release of simvastatin from the PM[135,140,154,162,214]. Nevertheless, further *in vitro* release or pharmacokinetic experiments are needed to confirm this hypothesis. To further confirm the biological effects of loaded simvastatin in our healthy LSEC, we performed gene expression analysis of KLF2 and eNOS, known to be overexpressed during simvastatin treatments[42,48,76,108–112,120]. While an increase in both genes was observed in PM-Sim groups, gene expression detected levels were lower than in free simvastatin treated cells. Again, this could be caused by the progressive release of the cargo in the PM groups under these experimental conditions. In the other cell types, we only observed increases in KLF2 that were not accompanied by important changes in the other evaluated genes. This result could be explained by the fact that we are treating cells isolated from healthy rats, where simvastatin might not cause changes in the basal gene expression profile. Finally, the evaluation of LSEC phenotype by SEM confirmed the results of previous studies suggesting an increase in endothelial porosity due to simvastatin treatment[114]. Interestingly, PM-F127-Sim had slightly better results than PM-F108-Sim which correlate with the higher level of internalization found *in vitro*.

DISCUSSION

In cells derived from BDL animals, which have marked alterations in their phenotype, the effect of simvastatin was more significant than in the healthy ones. The results of simvastatin (free or encapsulated in PM) were comparable. The main effects were observed in LSEC, with a gene profile more prone to vasodilation due to eNOS increase and ET-1 reduction; and HSC, where treatments caused a reduction in genes associated with fibrosis development. Lower changes in gene expression were observed for hepatocytes and KC, owing to the lower *in vitro* internalization capacity of these two cell types.

Prior to perform *in vivo* studies, the MTD for PM-F127-Sim and PM-F108-Sim was determined in healthy rats and compared with oral *gavage* administration of simvastatin. Treatments were administered 3 days/week during 2 weeks and, not surprisingly, our polymers which have been proven to be two of the least toxic among the Pluronic® family[159,163,165,166] did not cause any kind of toxicity in our animals. Thus, biodistribution studies were safely performed with PM-F127-Sim in healthy and BDL rats after IV administration. The liver was the organ showing higher signal, but it is important to note that some gut accumulation in BDL animals was observed. A possible explanation is the increased permeabilization of the intestinal wall during cirrhotic development[6,222], but further biodistribution studies are needed to finally confirm this. The obtained biodistribution is in accordance with other types of non-targeted nanomaterials after IV administration showing liver accumulation followed by spleen and lung uptake[223]. In fact, the spontaneous liver accumulation of nanoparticles that for other research studies can be an undesired effect, it becomes an advantage for our objectives. In addition, it is worth to mention that in our experiments no muscle accumulation was observed, suggesting a possible reduction in muscle toxicity as a consequence of simvastatin encapsulation in PM.

Most interestingly, PM-F127 was detectable in liver tissue up to 48 h after administration, which point towards the possibility of an active release of the drug at least during two days using our nanocarrier. Co-localization immunofluorescence after

PM administration *in vivo* indicated LSEC and KC accumulation, differing from what was observed in the *in vitro* studies where KC showed poor internalization of PM-F127. It is not clear if this finding could be due to the loss of functionality after cell isolation and culture because of the high sensitivity of these cells. In accordance to this, our co-localization results might indicate that PM-F127 is not totally avoiding the clearance by liver macrophages. Whether direct targeting to LSEC with specific peptides coupled to the micelle's surface might improve the specificity of cell uptake is a possibility that we decided to explore in the second study.

Finally, an *in vivo* effectivity study was designed to compare a new simvastatin formulation based on its encapsulation in PM with the standard of care with proven effectivity in this pathology, oral administration of free inactive simvastatin. In this sense, we performed a 1-week daily treatment in cirrhotic rats developed by 3 weeks of BDL to evaluate the therapeutic performance of PM-F127-Sim. The selection of this particular model was based on the fact that simvastatin is biliary excreted, so BDL rats show signs of high toxicity when treated with statins[76,106]. The dose of oral simvastatin was the one used in previous studies and was compared with two IV doses of PM-F127-Sim (1 and 5mg/kg). The selection of the IV doses was based on previous statin bioavailability data obtained in pharmacokinetic studies, being 5% for simvastatin. With this value, the theoretical blood simvastatin concentration after an oral administration of 10mg/kg would be 0.5mg/kg, and this low systemic concentration already promotes liver and muscle toxicity. So, we selected 1 mg/kg of PM-F127-Sim as the starting point of our efficiency study.

The first observation was an absence of body weight loss or rise in transaminases with our new simvastatin formulation, clearly suggesting a global reduction of simvastatin toxicity. It is widely known that cirrhotic animals have elevated PP, in the context of a hyperdynamic syndrome during CLD development. Simvastatin has shown beneficial effects in different experimental models by reducing PH[76,102,107]. The improved results obtained in the present study with PM-F127-Sim confirm the specific effect in liver

hemodynamics at the higher dose (5 mg/kg), suggesting a strong potential clinical impact of this new drug formulation.

To sum up, we have synthesized two formulations of simvastatin-loaded Pluronic® PM and showed that, although similar, PM-F127 was better in terms of targeting LSEC than PM-F108. In a rat model of advanced CLD, PM-F127-Sim was effective and superior to free simvastatin, significantly reducing PH. Importantly, this effect was achieved without the toxicity caused by free simvastatin. All these results confirm PM-F127 as a potential nanocarrier for drugs directed to the liver, even though some limitations were raised during its development. The incorporation of PM in KC after *in vivo* administration is something to consider and evidences the need to improve the formulation by means of decoration with specific LSEC ligands.

In the second study, we functionalized Pluronic® F127 PM to target LSEC more specifically for the optimization of simvastatin delivery. To this end, we designed peptide ligands for three membrane receptors expressed by these endothelial cells and coupled them to our nanoparticle, resulting in active targeting of this formulation to LSEC and increased therapeutic potential of the loaded drug by reducing PH and liver fibrosis in a non-decompensated CLD animal model.

The use of nanoparticles as vehicles for drug delivery has been widely addressed in the last decade mainly due to their potential to deliver a drug specifically to the desired therapeutic area for controlled release, thus increasing its therapeutic action and, in turn, reducing possible unwanted off-target effects[157,161]. To achieve this, one of the many options available is the use of particles that direct the nanodevices towards the target tissues or cells, one of the most used being surface receptor peptide ligands. In this case, although it is well known that nanoparticles tend to accumulate passively in the liver because of the characteristics of this organ as part of the RES[56,224], this accumulation can occur both in our target cells, LSEC, and to a lesser extent in KC, as

seen in the first study. To prevent PM clearance by resident liver macrophages, we decided to functionalize this type of nanoparticle with peptides that act as ligands for receptors present on the plasma membrane of LSEC for their active targeting, choosing three receptors according to various expression criteria (in both functional and dysfunctional LSEC). Once designed and synthesized, the internalization of the three specific peptides was assessed in primary cultures of LSEC, showing very high uptake rates in all cases, indicating a good affinity of the ligands for their receptors.

The coupling of these peptides on the surface of carboxylated PM-F127 was effective, generating three formulations of FPM with a larger hydrodynamic diameter than non-functionalized PM, due to the size of the peptide ligands themselves, but especially to the increase of functional groups and charges by the carboxylated polymer and the peptides, which attract water molecules to the PM surface when measuring the size distribution profile of these nanoparticles in solution by DLS[225]. But although the hydrodynamic diameter was variable depending on the ligand bound, all FPM presented a homogeneous particle shape and size, and a near neutral charge because of the use of PEG as the surface hydrophilic polymer, which prevents aggregation between the uncharged nanoparticles. Simvastatin was not released under neutral pH conditions, as in the blood circulation, since in a medium at pH 7.4 our micelles are formed and thermodynamically stable[147,158,226], so that practically no drug is released, at least until 72 h.

In the *in vitro* study of FPM uptake, nanoparticles functionalized with the specific ligands for CD32b, CD36 and integrin $\alpha_V\beta_3$ receptors were taken up by a greater number of healthy LSEC than micelles conjugated with scrambled versions of these peptides, probably due to a more affine interaction between the ligand and the receptor binding site, corroborating the usefulness of a specific interaction for better targeting. This interaction was equal for all three specific FPM, since, although in culture the cells gradually begin to dedifferentiate, the three selected receptors are expressed in healthy LSEC to varying degrees.

167

DISCUSSION

Simvastatin has been shown to reduce PH through the putative reduction of IHVR by several mechanisms, including the induction of KLF2 expression, which in turn is related to the stimulation of a vasoprotective phenotype in LSEC[42,112,115,123]. This effect was confirmed by the overexpression of KLF2 in healthy isolated LSEC treated with simvastatin encapsulated in the different three FPM generated, and it was comparable to that observed with the free drug and PM-Sim from the first study. We also ruled out any possible effect of the functionalized nanodevices, acting only as an inert vehicle for the delivery of the loaded drug.

Following *in vitro* characterization, we went on to evaluate the properties of our FPM *in vivo* in order to determine their potential as a therapeutic tool in CLD. The first step was to confirm that, thanks to functionalization, once in circulation our FPM target LSEC more specifically than unfunctionalized micelles, due to active targeting rather than passive accumulation. After O/N treatment of healthy rats with IV doses of the different fluorescent formulations, the internalization capacity of LSEC, as well as KC, hepatocytes and HSC, was studied by flow cytometry. The most remarkable result was that the capture of FPM was clearly superior to that achieved by PM, highlighting the role of LSEC as the liver cells with the highest uptake. In the endothelial cells, all three types of functionalization were equally effective in targeting the micelles, as seen *in vitro*. In conclusion, active specific targeting proved to be a better option for the delivery of drug-loaded PM to LSEC.

However, if we focus on the other cell types, we see that KC and hepatocytes also internalized more FPM than PM. It is worth mentioning that some of the receptors present in LSEC, selected as targets for our nanoparticles, are also expressed in other liver cells. CD32b is an FcγR that confers to LSEC a high endocytic capacity for the efficient elimination of small IgG-antigen immune complexes. However, current studies have shown that, despite what has been thought in recent years, CD32b is not only expressed in LSEC but also in KC, with a liver level expression of 90% and 10%, respectively[29,31]. Regarding CD36, although its expression in the liver is elevated on LSEC,

the rest of hepatic cell types also present this FFAs transporter/scavenger receptor. The liver is the major site for synthesis and metabolism of cholesterol, and both KC and LSEC are responsible for the uptake of ox-LDL from blood, which is subsequently passed on to hepatocytes and HSC, allowing sometimes the accumulation of abnormally high amounts of lipids, leading to the onset of steatosis and accelerating the process of chronic liver injury[33,185,227]. Lastly, a study screening the integrin $\alpha_V\beta_3$ expression in different organs of healthy rats unravelled particularly high levels of expression in the liver, which was then markedly upregulated in BDL rats and correlated with the stage of fibrosis, being found on capillarized LSEC, macrophages and aHSC[191,194,195]. Furthermore, its overexpression has been linked to various pathological processes, one of them being HCC[189]. In our results, a very high uptake of PM functionalized with the integrin-binding ligand ITGB3 was already observed by hepatocytes isolated from healthy rats. For this reason, FPM-ITGB3 was discarded and was no longer used in subsequent studies to avoid undesired internalization of simvastatin in hepatocyte, as the toxic effect of free simvastatin in the liver is mainly on the parenchymal cells due to its metabolism, primarily mediated by the CYP3A4 pathway[91,126,128].

The accumulation of simvastatin in muscle was also a key factor, as avoiding the muscle toxicity associated with this statin was one of the main objectives of this work. As expected, the use of nanoparticles decreased the presence of active drug detected by UPLC-MS/MS in muscle compared to free simvastatin in any of its forms of administration (oral and IV). This effect may be due to the lower uptake of nanoparticles by skeletal muscle compared with the higher natural retention of nanoparticles in the liver, regardless of their functionalization, since both PM and FPM showed an equal reduction in the amount of active simvastatin detected in muscle.

Next, before starting the efficacy studies, we assessed the safety profile of FPM by establishing the MTD in a phased trial in healthy animals, studying the use of different simvastatin doses, as well as different administration patterns. Taking into account the MTD assay from the first study, where we used up to a maximum of 20 mg/kg of

simvastatin loaded in PM, for this new study we increased the dose to be tested based on the hypothesis that the use of a delivery system specifically targeting LSEC would allow us to actively concentrate the drug in these cells, reducing the adverse effects observed in other tissues, mainly the muscle, which our previous results confirmed. Nonetheless, the use of FPM-Sim at high doses of 20 and 50 mg/kg resulted in elevations in liver transaminases, and CK in the first phase of the trial. Although the elevations were transient and only in some individuals, these doses were rejected to avoid possible further toxicity when assessing the effectiveness in animal models. In contrast, the 10 mg/kg dose showed no evidence of toxicity in any of the established phases and was used as a reference to establish the final dose to be administered in subsequent efficacy studies.

For the first efficacy evaluation, the same scheme used in the first study was followed, based on the determination of haemodynamic parameters, after treatment administration in an advanced CLD model such as BDL. In this case, the aim was to improve the PP-lowering effect achieved by PM-encapsulated simvastatin by means of the new functionalized formulations, focusing their action on the main cells involved in the regulation of the response to liver damage. As then, the data showed that encapsulated simvastatin resulted in significantly lower body weight reduction in cirrhotic animals compared to free administration, and lower AST, ALT and CK levels, reducing toxicity rates in all parameters.

At the biochemical level, the use of nanoparticles triggered a significant increase in serum triglycerides and, in a more moderate way, total cholesterol. This can be explained by the fact that the PM is made from Pluronic® F127 (or polaxamer P407), which has been shown to induce a transient hyperlipidemic effect by causing a temporary reduction in the number of fenestrae in LSEC in a dose-dependent manner[228]. In our BDL model, it is understandable that the triglyceride and cholesterol parameters determined in PM-treated individuals were higher than those of control animals or those receiving oral simvastatin, since the baseline BDL-treated animals

already have a more capillarized endothelium and fewer fenestrae due to endothelial dysfunction caused by bile accumulation-induced liver damage[229]. Therefore, in these dysfunctional LSEC, the addition of an extra element that closes the fenestrae, albeit temporarily, leads to impaired transendothelial transfer of lipoproteins from sinusoidal blood to the extracellular space of Disse.

In terms of efficacy, it is worth highlighting the role of oral simvastatin which, although it showed greater toxicity, was the most effective treatment in significantly reducing PP compared to the control group, but also against the PM-Sim, which failed to achieve the same effect as previously observed in the first study. The functionalized nanoparticles came closer to this decrease, causing a greater reduction in PP, especially in the case of FPM-CD32b-CD36 and, to a lesser extent, FPM-CD32b, having a discrete improvement in the effect of simvastatin on hepatic hemodynamics compared to the non-functionalized PM in this model of advanced cirrhosis. At this point it is worth mentioning that, although the BDL model was used in both the first and second study to mimic a decompensated advanced CLD, this model showed variability between both studies, with more severely affected animals in the second study. For example, the control group (untreated) showed a PP up to 2 points higher than the vehicle group of the first study (19.73 and 17.02 mmHg, respectively) and increased liver transaminase values. This reminds us of the difficulty we encounter when working with experimental models due to their inherent individual variability. Thus, these small variations could have a non-negligible effect on the interpretation and extrapolation of the results of the second study, especially considering their magnification when using a small sample size, in this case perhaps leading to a lack of significance in the PP-lowering effect of encapsulated simvastatin in an even more severe model of CLD by BDL.

One of the ideas of this work was to evaluate the effect of the new functionalized micelles loaded with simvastatin in different animal models of CLD, as each of the existing models has its own characteristics, simulating different etiologies and/or different stages of the pathology. In this regard, it was important for us to see whether

the effect of FPM-Sim was different between models recapitulating different stages of CLD, or in other words, between models with a greater or lesser presence of dysfunctional LSEC.

For this reason, we decided to conduct an *in vivo* efficacy study in a new animal model of cirrhosis induced by TAA hepatotoxin, a model widely used for its high reproducibility and homogeneity of results, its low mortality and lower systemic toxicity compared to other chemical substances used for the same purpose[230]. This model was developed for only 8 weeks to represent a moderate CLD stage and the effect of FPM-Sim was again compared with that of PM-Sim and oral simvastatin as in the BDL model, but in this case administered during the last 2 weeks of model generation. In this non-decompensated model of cirrhosis, simvastatin induced lower toxicity in all domains: the body weight of animals was practically not reduced and the slight decrease observed in the groups that received IV treatment can be associated more to the stress caused by the administration route than by the drug itself, since in its oral form the treated rats continued to gain weight normally; transaminases and CK values were also reduced in the overall TAA animals. In addition to these biochemical parameters, the increase in total cholesterol and triglycerides observed in BDL rats was of less magnitude here. These lower values could have their explanation by the fact that the TAA model used in this study, by reproducing a less advanced stage of the disease compared to the BDL model, has an endothelium with a lower degree of capillarization, so its porosity is more preserved and the exchange of lipoproteins between the sinusoid and the liver parenchyma is better maintained.

The reduced toxicity observed in this model was accompanied by a lower PP in the untreated control group compared with the previous BDL model. Treatment with encapsulated simvastatin further reduced the PP, this time with a significant difference accomplished by the FPM-CD32b and FPM-CD32b-CD36 formulations. Notably, FPM-CD32b-Sim achieved such a potent PP-lowering effect that it was also significant versus FPM-CD36-Sim and oral free simvastatin itself. To go beyond these results, we evaluated

different aspects that could explain this reduction. Firstly, PP and fibrosis were shown to be positively correlated, in that the greater the area of liver fibrosis, the greater the liver stiffness and vascular occlusion, leading to an increase in PP, and *vice versa*[6,14]. Likewise, collagen expression followed the same trend, and in the case of treatment with FPM-CD32b-Sim it was reduced by half compared to the untreated TAA group.

Secondly, the state of endothelial dysfunction was analyzed at the molecular level through the quantification of proteins, in total liver, involved in signalling pathways related to vasoprotection induced by statins administration[76,95,98,101,104,109–111]. Determination of protein levels of the transcription factor KLF2 showed no differences between treated and untreated animals; however, Akt phosphorylation was surprisingly increased by FPM-CD36-Sim, being significant in comparison with the other groups. In contrast to these results, but consistent with the results on PP reduction, the p-eNOS/eNOS ratio was significantly elevated by FPM-CD32b-Sim and FPM-CD32b-CD36-Sim, suggesting an amelioration of endothelial dysfunction by stimulating NO production through the targeted release of simvastatin into LSEC of TAA-induced cirrhotic rats.

All in all, it can be proposed that in an earlier model of CLD, and with a lower degree of capillarization and endothelial dysfunction such as the 8-week TAA model, the expression of the scavenger receptor CD32b on LSEC could still be relevant, exerting a significant role in the enhanced targeting. This would be supported by an unpublished study conducted in our laboratory, in which the percentage of CD32b^{+} LSEC was estimated by cell sorting, establishing a higher percentage in animal models at an early/mid stage of the disease compared with a higher loss of this marker in more advanced stages.

In brief, the results of the two studies carried out in this doctoral thesis indicate that the use of a Pluronic® F127-based nanodevice system for the administration of simvastatin

allows controlling the release of the drug for its greater action in the liver, reducing the adverse effects derived from the use of this statin, mainly myopathy, while optimizing its efficacy through the active targeting of the nanoparticle towards LSEC by its specific functionalization. The result has been the improvement of PP in two different models of CLD, reducing one of the primary factors of disease progression. Moreover, the use of FPM for simvastatin encapsulation in a non-decompensated model has been shown to promote the vasoprotective action of the drug, through the stimulation of NO synthesis, as well as its antifibrotic effect, reducing liver fibrosis. Therefore, PM-F127 could be a potential nanotransporter for vasoprotective drug delivery to the liver, especially by means of its functionalization targeting LSEC, being CD32b receptor a potential candidate to increase the therapeutic window of simvastatin in the context of non-decompensated CLD.

7. CONCLUSIONS

7. CONCLUSIONS

- The use of Pluronic® F127 PM enables the encapsulation of hydrophobic drugs such as simvastatin, allowing a more controlled administration into hepatic cells and achieving an enhanced delivery to LSEC, being able to improve their cell phenotype.

- Functionalization of PM with peptide ligands binding LSEC membrane receptors allows to optimize the drug delivery by active targeting these endothelial cells, promoting a greater internalization of the nanoparticle.

- In a model of advanced CLD generated by BDL, the encapsulation of simvastatin in PM, either with and without functionalization, reduces the liver and muscle toxicity derived from its oral administration, although with discrete impact on hepatic hemodynamics.

- In a less severe model of cirrhosis such as the 8-week TAA model (non-decompensated), FPM treatment lowers PP levels relative to the untreated control group, especially with FPM-CD32b formulation, through the reduction of liver fibrosis and promotion of NO synthesis without significant adverse effects.

- The functionalization of PM with a peptide ligand targeting CD32b receptor could be an effective tool for targeting this drug delivery system to LSEC, with the potential to be used for the delivery of any other active pharmaceutical agent in the framework of non-decompensated CLD treatment.

8. FUTURE PERSPECTIVES

8. FUTURE PERSPECTIVES

The results of this thesis have shown that the use of PM consisting of Pluronic® F127 as a vehicle for simvastatin administration could be a new tool for its release in the liver based on its characteristics as a nanoparticulate system, allowing to focus the effects of the drug in the target organ and, therefore, to reduce the dose and the adverse effects of this statin as a potential treatment for CLD. Furthermore, the use of peptide ligands to functionalize the surface of this PM-F127 to actively target LSEC encouraged the beneficial effects of simvastatin, mainly in a non-decompensated model of cirrhosis using CD32b as the target receptor, with improved levels of PP and liver fibrosis.

Nevertheless, despite the results obtained, the need for further research to optimize the targeting of this nanoparticle to LSEC seems to be key to the development of an optimal drug delivery system showing a greater effect at different stages of the disease.

One option would be to perform molecular docking studies to predict the strength of association between different peptide recognition sequences and the binding site of receptors by scoring them, selecting those amino acid sequences with the highest binding affinity for each of the receptors[231].

On the other hand, in this thesis the choice of membrane receptors to act as targets for our PM-F127 was based on pre-existing literature, with no single marker currently described as specific for LSEC, regardless of their functional or dysfunctional state. Thus, in the first instance, a PM could be generated with a mixed functionalization, as with FPM-CD32b-CD36, encompassing some of the other marker combinations known so far[33,34], as well as using two types of FPM to address at the same time active targeting of both functional LSEC and LSEC undergoing capillarization.

In addition, the identification of markers specific of these unique endothelial cells is another line of research to improve the functionalization design. With this idea in mind, our laboratory is carrying out a proteomic study to try to identify new specific surface markers for LSEC in different animal models of CLD, with the aim of obtaining a

membrane protein that ubiquitously increases its expression in cases of pathology, as well as trying to discover a distinctive marker for each of the etiologies or phases of the disease that would allow to generate differential FPM according to the pathological context that we want to treat.

Finally, the development of this drug delivery system for selective administration in LSEC has been fine-tuned using simvastatin encapsulation, but the use of other beneficial drugs could be also evaluated in order to study their effect in these and other animal models.

9. BIBLIOGRAPHY

9. BIBLIOGRAPHY

1. Ginès P, Krag A, Abraldes JG, Solà E, Fabrellas N, Kamath PS. Liver cirrhosis. Lancet. 2021 Oct;398(10308):1359-76.

2. Pellicoro A, Ramachandran P, Iredale JP, Fallowfield JA. Liver fibrosis and repair: Immune regulation of wound healing in a solid organ. Nat Rev Immunol. 2014 Mar;14(3):181-94.

3. Schuppan D, Afdhal NH. Liver cirrhosis. Lancet. 2008 Mar;371(9615):838-51.

4. GBD 2019 Diseases and Injuries Collaborators. Global burden of 369 diseases and injuries in 204 countries and territories, 1990–2019: a systematic analysis for the Global Burden of Disease Study 2019. Lancet. 2020 Oct;396(10258):1204-22.

5. Institute for Health Metrics and Evaluation. Global Health Data Exchange. GBD Results Tool [Internet]. 2023 [cited 2022 Dec 13]. Available from: https://vizhub.healthdata.org/gbd-results/

6. Tsochatzis EA, Bosch J, Burroughs AK. Liver cirrhosis. Lancet. 2014 May;383(9930):1749-61.

7. Cheemerla S, Balakrishnan M. Global Epidemiology of Chronic Liver Disease. Clin Liver Dis (Hoboken). 2021 Jun;17(5):365-70.

8. Asrani SK, Devarbhavi H, Eaton J, Kamath PS. Burden of liver diseases in the world. J Hepatol. 2019 Jan;70(1):151-71.

9. Moon AM, Singal AG, Tapper EB. Contemporary Epidemiology of Chronic Liver Disease and Cirrhosis. Clin Gastroenterol Hepatol. 2020 Nov;18(12):2650-66.

10. Gunarathne LS, Rajapaksha H, Shackel N, Angus PW, Herath CB. Cirrhotic portal hypertension: From pathophysiology to novel therapeutics. World J Gastroenterol. 2020 Oct;26(40):6111-40.

11. Khanna R, Sarin SK. Non-cirrhotic portal hypertension - Diagnosis and management. J Hepatol. 2014 Feb;60(2):421-41.

12. Iwakiri Y, Trebicka J. Portal hypertension in cirrhosis: Pathophysiological mechanisms and therapy. JHEP Reports. 2021 Jun;3(4):100316.

13. Gracia-Sancho J, Laleman W. Mechanisms of portal hypertension: Bench to bedside. Clin Liver Dis (Hoboken). 2016 Dec;8(6):160-66.

14. Engelmann C, Clària J, Szabo G, Bosch J, Bernardi M. Pathophysiology of decompensated cirrhosis: Portal hypertension, circulatory dysfunction, inflammation, metabolism and mitochondrial dysfunction. J Hepatol. 2021 Jul;75(S1):S49-66.

15. García-Pagán JC, Gracia-Sancho J, Bosch J. Functional aspects on the pathophysiology of portal hypertension in cirrhosis. J Hepatol. 2012 Aug;57(2):458-61.

16. D'Amico G, Garcia-Tsao G, Pagliaro L. Natural history and prognostic indicators of survival in cirrhosis: A systematic review of 118 studies. J Hepatol. 2006 Jan;44(1):217-31.

17. Fernández-Iglesias A, Gracia-Sancho J. How to face chronic liver disease: The sinusoidal perspective. Front Med (Lausanne). 2017 Feb;4:7.

18. Ripoll C, Groszmann R, Garcia-Tsao G, Grace N, Burroughs A, Planas R, et al. Hepatic Venous Pressure Gradient Predicts Clinical Decompensation in Patients With Compensated Cirrhosis. Gastroenterology. 2007 Aug;133(2):481-8.

19. Bosch J, Groszmann RJ, Shah VH. Evolution in the understanding of the pathophysiological basis of portal hypertension: How changes in paradigm are leading to successful new treatments. J Hepatol. 2015 Apr;62(S1):S121-30.

20. Mehta G, Gustot T, Mookerjee RP, Garcia-Pagan JC, Fallon MB, Shah VH, et al. Inflammation and portal hypertension - The undiscovered country. J Hepatol. 2014 Jul;61(1):155-63.

21. Ezhilarasan D, Najimi M. Intercellular communication among liver cells in the perisinusoidal space of the injured liver: Pathophysiology and therapeutic directions. J Cell Physiol. 2023 Jan;238(1):70-81.

22. Puche JE, Saiman Y, Friedman SL. Hepatic stellate cells and liver fibrosis. Compr Physiol. 2013 Oct;3(4):1473-92.

23. Li H. Intercellular crosstalk of liver sinusoidal endothelial cells in liver fibrosis, cirrhosis and hepatocellular carcinoma. Dig Liver Dis. 2022 May;54(5):598-613.

24. Poisson J, Lemoinne S, Boulanger C, Durand F, Moreau R, Valla D, et al. Liver sinusoidal endothelial cells: Physiology and role in liver diseases. J Hepatol. 2017 Jan;66(1):212-27.

25. Xu B, Broome U, Uzunel M, Nava S, Ge X, Kumagai-Braesch M, et al. Capillarization of Hepatic Sinusoid by Liver Endothelial Cell-Reactive Autoantibodies in Patients with Cirrhosis and Chronic Hepatitis. Am J Pathol. 2003 Oct;163(4):1275-89.

26. Lafoz E, Ruart M, Anton A, Oncins A, Hernández-Gea V. The Endothelium as a Driver of Liver Fibrosis and Regeneration. Cells. 2020 Apr;9(4):929-54.

27. Deleve LD. Liver sinusoidal endothelial cells in hepatic fibrosis. Hepatology. 2015 May;61(5):1740-6.

28. Szafranska K, Kruse LD, Holte CF, McCourt P, Zapotoczny B. The Whole Story About Fenestrations in LSEC. Front Physiol. 2021 Sep;12:735573.

29. Sørensen KK, Smedsrød B. The Liver Sinusoidal Endothelial Cell: Basic Biology and Pathobiology. In: Arias IM, Alter HJ, Boyer JL, Cohen DE, Shafritz DA, Thorgeirsson SS, Wolkoff AW, editors. The Liver: Biology and Pathobiology. 6th edition. John Wiley & Sons Ltd; 2020. p.422-34.

30. Fraser R, Dobbs BR, Rogers GW. Lipoproteins and the liver sieve: The role of the fenestrated sinusoidal endothelium in lipoprotein metabolism, atherosclerosis, and cirrhosis. Hepatology. 1995 Mar;21(3):863-74.

31. DeLeve LD, Maretti-Mira AC. Liver Sinusoidal Endothelial Cell: An Update. Semin Liver Dis. 2017 Nov;37(4):377-87.

32. Bhandari S, Larsen AK, McCourt P, Smedsrød B, Sørensen KK. The Scavenger Function of Liver Sinusoidal Endothelial Cells in Health and Disease. Front Physiol. 2021 Oct;12:757469.

33. Lalor PF, Lai WK, Curbishley SM, Shetty S, Adams DH. Human hepatic sinusoidal endothelial cells can be distinguished by expression of phenotypic markers

related to their specialised functions *in vivo*. World J Gastroenterol. 2006 Sep;12(34):5429-39.

34. Strauss O, Phillips A, Ruggiero K, Bartlett A, Dunbar PR. Immunofluorescence identifies distinct subsets of endothelial cells in the human liver. Sci Rep. 2017 Mar; 7:44356.

35. Ganesan LP, Kim J, Wu Y, Mohanty S, Phillips GS, Birmingham DJ, et al. FcγRIIb on Liver Sinusoidal Endothelium Clears Small Immune Complexes. J Immunol. 2012 Nov;189(10):4981-8.

36. Mousavi SA, Sporstøl M, Fladeby C, Kjeken R, Barois N, Berg T. Receptor-mediated endocytosis of immune complexes in rat liver sinusoidal endothelial cells is mediated by FcγRIIb2. Hepatology. 2007 Sep;46(3):871-84.

37. Gupta TK, Toruner M, Chung MK, Groszmann RJ. Endothelial dysfunction and decreased production of nitric oxide in the intrahepatic microcirculation of cirrhotic rats. Hepatology. 1998 Oct;28(4):926-31.

38. Iwakiri Y, Kim MY. Nitric oxide in liver diseases. Trends Pharmacol Sci. 2015 Aug;36(8):524-36.

39. Gracia-Sancho J, Marrone G, Fernández-Iglesias A. Hepatic microcirculation and mechanisms of portal hypertension. Nat Rev Gastroenterol Hepatol. 2019 Apr;16(4):221-34.

40. Hide D, Ortega-Ribera M, Garcia-Pagan JC, Peralta C, Bosch J, Gracia-Sancho J. Effects of warm ischemia and reperfusion on the liver microcirculatory phenotype of rats: Underlying mechanisms and pharmacological therapy. Sci Rep. 2016 Feb;6:22107.

41. Gracia-Sancho J, Russo L, García-Calderó H, García-Pagán JC, García-Cardeña G, Bosch J. Endothelial expression of transcription factor Kruppel-like factor 2 and its vasoprotective target genes in the normal and cirrhotic rat liver. Gut. 2011 Apr;60(4):517-24.

42. Marrone G, Russo L, Rosado E, Hide D, García-Cardeña G, García-Pagán JC, et al. The transcription factor KLF2 mediates hepatic endothelial protection and

paracrine endothelial-stellate cell deactivation induced by statins. J Hepatol. 2013 Jan;58(1):98-103.

43.   Marrone G, Shah VH, Gracia-Sancho J. Sinusoidal communication in liver fibrosis and regeneration. J Hepatol. 2016 Sep;65(3):608-17.

44.   Xie G, Wang X, Wang L, Wang L, Atkinson RD, Kanel GC, et al. Role of differentiation of liver sinusoidal endothelial cells in progression and regression of hepatic fibrosis in rats. Gastroenterology. 2012 Apr;142(4):918-27.

45.   Wiest R, Groszmann RJ. The paradox of nitric oxide in cirrhosis and portal hypertension: Too much, not enough. Hepatology. 2002 Feb;35(2):478-91.

46.   Matei V, Rodríguez-Vilarrupla A, Deulofeu R, Colomer D, Fernández M, Bosch J, et al. The eNOS cofactor tetrahydrobiopterin improves endothelial dysfunction in livers of rats with CCl_4 cirrhosis. Hepatology. 2006 Jul;44(1):44-52.

47.   Morales-Ruiz M, Cejudo-Martín P, Fernandez-Varo G, Tugues S, Ros J, Angeli P, et al. Transduction of the liver with activated Akt normalizes portal pressure in cirrhotic rats. Gastroenterology. 2003 Aug;125(2):522-31.

48.   Trebicka J, Hennenberg M, Laleman W, Shelest N, Biecker E, Schepke M, et al. Atorvastatin lowers portal pressure in cirrhotic rats by inhibition of RhoA/Rho-kinase and activation of endothelial nitric oxide synthase. Hepatology. 2007 Jul;46(1):242-53.

49.   Gracia-Sancho J, Laviña B, Rodríguez-Vilarrupla A, García-Calderó H, Bosch J, García-Pagán JC. Enhanced vasoconstrictor prostanoid production by sinusoidal endothelial cells increases portal perfusion pressure in cirrhotic rat livers. J Hepatol. 2007 Aug;47(2):220-27.

50.   Zhang M, Serna-Salas S, Damba T, Borghesan M, Demaria M, Moshage H. Hepatic stellate cell senescence in liver fibrosis: Characteristics, mechanisms and perspectives. Mech Ageing Dev. 2021 Oct;199:111572.

51.   Tsuchida T, Friedman SL. Mechanisms of hepatic stellate cell activation. Nat Rev Gastroenterol Hepatol. 2017 Jul;14(7):397-411.

52.   Zhang W, Conway SJ, Liu Y, Snider P, Chen H, Gao H, et al. Heterogeneity of hepatic stellate cells in fibrogenesis of the liver: Insights from single-cell transcriptomic analysis in liver injury. Cells. 2021 Aug;10(8):2129.

53.   Higashi T, Friedman SL, Hoshida Y. Hepatic stellate cells as key target in liver fibrosis. Adv Drug Deliv Rev. 2017 Nov;121:27-42.

54.   Klein S, van Beuge MM, Granzow M, Beljaars L, Schierwagen R, Kilic S, et al. HSC-specific inhibition of Rho-kinase reduces portal pressure in cirrhotic rats without major systemic effects. J Hepatol. 2012 Dec;57(6):1220-27.

55.   Kitto LJ, Henderson NC. Hepatic Stellate Cell Regulation of Liver Regeneration and Repair. Hepatol Commun. 2020 Nov;5(3):358-70.

56.   Praaning-Van Dalen DP, Brouwer A, Knook DL. Clearance Capacity of Rat Liver Kupffer, Endothelial, and Parenchymal Cells. Gastroenterology. 1981 Dec;81(6):1036-44.

57.   Limmer A, Ohl J, Kurts C, Ljunggren HG, Reiss Y, Groettrup M, Momburg F, Arnold B, Knolle PA. Efficient presentation of exogenous antigen by liver endothelial cells to CD8^{+} T cells results in antigen-specific T-cell tolerance. Nat Med. 2000 Dec;6(12):1348-54.

58.   Limmer A, Ohl J, Wingender G, Berg M, Jüngerkes F, Schumak B, et al. Cross-presentation of oral antigens by liver sinusoidal endothelial cells leads to CD8 T cell tolerance. Eur J Immunol. 2005 Oct;35(10):2970-81.

59.   Heymann F, Tacke F. Immunology in the liver-from homeostasis to disease. Nat Rev Gastroenterol Hepatol. 2016 Feb;13(2):88-110.

60.   Connolly MK, Bedrosian AS, Malhotra A, Henning JR, Ibrahim J, Vera V, et al. In Hepatic Fibrosis, Liver Sinusoidal Endothelial Cells Acquire Enhanced Immunogenicity. J Immunol. 2010 Aug;185(4):2200-8.

61.   Ju C, Tacke F. Hepatic macrophages in homeostasis and liver diseases: From pathogenesis to novel therapeutic strategies. Cell Mol Immunol. 2016 May;13(3):316-27.

62. Zhang J, Li N, Yang L, Xie H, Yang Y, Wang H, et al. Bradykinin contributes to immune liver injury via B2R receptor-mediated pathways in trichloroethylene sensitized mice: A role in Kupffer cell activation. Toxicology. 2019 Mar;415:37-48.

63. Purohit V, Brenner DA. Mechanisms of alcohol-induced hepatic fibrosis: A summary of the Ron Thurman symposium. Hepatology. 2006 Apr;43(4):872-8.

64. Peralta C, Jiménez-Castro MB, Gracia-Sancho J. Hepatic ischemia and reperfusion injury: Effects on the liver sinusoidal milieu. J Hepatol. 2013 Nov;59(5):1094-106.

65. Seo HY, Kim MK, Lee SH, Hwang JS, Park KG, Jang BK. Kahweol ameliorates the liver inflammation through the inhibition of NF-κB and STAT3 activation in primary Kupffer cells and primary hepatocytes. Nutrients. 2018 Jul;10(7):863.

66. Lamatsch S, Sittner R, Tacke F, Engelmann C. Novel drug discovery strategies for the treatment of decompensated cirrhosis. Expert Opin Drug Discov. 2022 Mar;17(3):273-82.

67. Karaa A, Kamoun WS, Clemens MG. Oxidative stress disrupts nitric oxide synthase activation in liver endothelial cells. Free Radic Biol Med. 2005 Nov;39(10):1320-31.

68. Weston CJ, Zimmermann HW, Adams DH. The role of myeloid-derived cells in the progression of liver disease. Front Immunol. 2019 Apr;10:893.

69. Fernandez M. Molecular pathophysiology of portal hypertension. Hepatology. 2015 Apr;61(4):1406-15.

70. Bosch J, García-Pagán JC. Complications of cirrhosis. I. Portal hypertension. J Hepatol. 2000;32(S1):141-56.

71. Garcia-Tsao G. The use of nonselective beta blockers for treatment of portal hypertension. Gastroenterol Hepatol (N Y). 2017 Oct;13(10):617-9.

72. Rose CF, Amodio P, Bajaj JS, Dhiman RK, Montagnese S, Taylor-Robinson SD, et al. Hepatic encephalopathy: Novel insights into classification, pathophysiology and therapy. J Hepatol. 2020 Dec;73(6):1526-47.

73. Kockerling D, Nathwani R, Forlano R, Manousou P, Mullish BH, Dhar A. Current and future pharmacological therapies for managing cirrhosis and its complications. World J Gastroenterol. 2019 Feb;25(8):888-908.

74. Villanueva C, Albillos A, Genescà J, Garcia-Pagan JC, Calleja JL, Aracil C, et al. β blockers to prevent decompensation of cirrhosis in patients with clinically significant portal hypertension (PREDESCI): a randomised, double-blind, placebo-controlled, multicentre trial. Lancet. 2019 Apr;393(10181):1597-608.

75. Rodrigues SG, Mendoza YP, Bosch J. Investigational drugs in early clinical development for portal hypertension. Expert Opin Investig Drugs. 2022 Aug;31(8):825-42.

76. Rodríguez S, Raurell I, Torres-Arauz M, García-Lezana T, Genescà J, Martell M. A Nitric Oxide-Donating Statin Decreases Portal Pressure with a Better Toxicity Profile than Conventional Statins in Cirrhotic Rats. Sci Rep. 2017 Jan;7:40461.

77. Berzigotti A, Bellot P, de Gottardi A, Garcia-Pagan JC, Gagnon C, Spénard J, et al. NCX-1000, a nitric oxide-releasing derivative of UDCA, does not decrease portal pressure in patients with cirrhosis: Results of a randomized, double-blind, dose-escalating study. Am J Gastroenterol. 2010 May;105(5):1094-101.

78. Gracia-Sancho J, Maeso-Díaz R, Fernández-Iglesias A, Navarro-Zornoza M, Bosch J. New cellular and molecular targets for the treatment of portal hypertension. Hepatol Int. 2015 Apr;9(2):183-91.

79. Tateya S, Rizzo NO, Handa P, Cheng AM, Morgan-Stevenson V, Daum G, et al. Endothelial NO/cGMP/VASP signaling attenuates Kupffer cell activation and hepatic insulin resistance induced by high-fat feeding. Diabetes. 2011 Nov;60(11):2792-801.

80. Vilaseca M, Guixé-Muntet S, Fernández-Iglesias A, Gracia-Sancho J. Advances in therapeutic options for portal hypertension. Therap Adv Gastroenterol. 2018 Nov;11:1756284818811294.

81. Weiskirchen R, Weiskirchen S, Tacke F. Recent advances in understanding liver fibrosis: Bridging basic science and individualized treatment concepts. F1000Res. 2018 Jun;7(F1000 Faculty Rev):921.

82. Tsukada S, Parsons CJ, Rippe RA. Mechanisms of liver fibrosis. Clin Chim Acta. 2006 Feb;364(1-2):33-60.

83. Bravo M, Raurell I, Barberá A, Hide D, Gil M, Estrella F, et al. Synergic effect of atorvastatin and ambrisentan on sinusoidal and hemodynamic alterations in a rat model of NASH. Dis Model Mech. 2021 May;14(5):dmm048884.

84. Rosado E, Rodríguez-Vilarrupla A, Gracia-Sancho J, Tripathi D, García-Calderó H, Bosch J, et al. Terutroban, a TP-receptor antagonist, reduces portal pressure in cirrhotic rats. Hepatology. 2013 Oct;58(4):1424-35.

85. Tandon P, Abraldes JG, Berzigotti A, Carlos Garcia-Pagan J, Bosch J. Renin-angiotensin-aldosterone inhibitors in the reduction of portal pressure: A systematic review and meta-analysis. J Hepatol. 2010 Aug;53(2):273-82.

86. Jonsson JR, Clouston AD, Ando Y, Kelemen LI, Horn MJ, Adamson MD, et al. Angiotensin-converting enzyme inhibition attenuates the progression of rat hepatic fibrosis. Gastroenterology. 2001 Jul;121(1):148-55.

87. Harrison SA, Abdelmalek MF, Caldwell S, Shiffman ML, Diehl AM, Ghalib R, et al. Simtuzumab Is Ineffective for Patients With Bridging Fibrosis or Compensated Cirrhosis Caused by Nonalcoholic Steatohepatitis. Gastroenterology. 2018 Oct;155(4):1140-53.

88. Klein S, Frohn F, Magdaleno F, Reker-Smit C, Schierwagen R, Schierwagen I, et al. Rho-kinase inhibitor coupled to peptide-modified albumin carrier reduces portal pressure and increases renal perfusion in cirrhotic rats. Sci Rep. 2019 Feb;9(1):2256.

89. Sauerbruch T, Schierwagen R, Trebicka J. Managing portal hypertension in patients with liver cirrhosis. F1000Res. 2018 May;7(F1000 Faculty Rev):533.

90. Muñoz AE, Pollarsky FD, Marino M, Cartier M, Romero G, Salgado P, et al. Addition of statins to the standard treatment in patients with cirrhosis: Safety and efficacy. World J Gastroenterol. 2021 Jul;27(28):4639-52.

91. Hirota T, Fujita Y, Ieiri I. An updated review of pharmacokinetic drug interactions and pharmacogenetics of statins. Expert Opin Drug Metab Toxicol. 2020 Sep;16(9):809-22.

92. Gazzerro P, Proto MC, Gangemi G, Malfitano AM, Ciaglia E, Pisanti S, et al. Pharmacological actions of statins: A critical appraisal in the management of cancer. Pharmacol Rev. 2012 Jan;64(1):102-46.

93. Pose E, Trebicka J, Mookerjee RP, Angeli P, Ginès P. Statins: Old drugs as new therapy for liver diseases? J Hepatol. 2019 Jan;70(1):194-202.

94. Chong LW, Hsu YC, Lee TF, Lin Y, Chiu YT, Yang KC, et al. Fluvastatin attenuates hepatic steatosis-induced fibrogenesis in rats through inhibiting paracrine effect of hepatocyte on hepatic stellate cells. BMC Gastroenterol. 2015 Feb;15:22.

95. Margaritis M, Channon KM, Antoniades C. Statins as regulators of redox state in the vascular endothelium: Beyond lipid lowering. Antioxid Redox Signal. 2014 Mar;20(8):1198-215.

96. Durai V, Redberg RF. Statin therapy for the primary prevention of cardiovascular disease: Cons. Atherosclerosis. 2022 Sep;356:46-9.

97. Blum A, Shamburek R. The pleiotropic effects of statins on endothelial function, vascular inflammation, immunomodulation and thrombogenesis. Atherosclerosis. 2009 Apr;203(2):325-30.

98. Kureishi Y, Luo Z, Shiojima I, Bialik A, Fulton D, Lefer DJ, et al. The HMG-CoA reductase inhibitor simvastatin activates the protein kinase Akt and promotes angiogenesis in normocholesterolemic animals. Nat Med. 2000 Sep;6(9):1004-10.

99. de Loecker I, Preiser JC. Statins in the critically ill. Ann Intensive Care. 2012 Jun;2(1):19.

100. Janicko M, Drazilova S, Pella D, Fedacko J, Jarcuska P. Pleiotropic effects of statins in the diseases of the liver. World J Gastroenterol. 2016 Jul;22(27):6201-13.

101. Arab JP, Shah VH. Statins and portal hypertension: A tale of two models. Hepatology. 2016 Jun;63(6):2044-7.

102. Tripathi DM, Vilaseca M, Lafoz E, Garcia-Calderó H, Viegas Haute G, Fernández-Iglesias A, et al. Simvastatin Prevents Progression of Acute on Chronic Liver Failure in Rats With Cirrhosis and Portal Hypertension. Gastroenterology. 2018 Nov;155(5):1564-77.

103. Fang D, He Y, Luan Z. Simvastatin augments activation of liver regeneration through attenuating transforming growth factor-β1 induced-apoptosis in obstructive jaundice rats. Exp Ther Med. 2017 Nov;14(5):4839-45.

104. Uschner FE, Ranabhat G, Choi SS, Granzow M, Klein S, Schierwagen R, et al. Statins activate the canonical hedgehog-signaling and aggravate non-cirrhotic portal hypertension, but inhibit the non-canonical hedgehog signaling and cirrhotic portal hypertension. Sci Rep. 2015 Sep;5:14573.

105. Klein S, Klösel J, Schierwagen R, Körner C, Granzow M, Huss S, et al. Atorvastatin inhibits proliferation and apoptosis, but induces senescence in hepatic myofibroblasts and thereby attenuates hepatic fibrosis in rats. Lab Invest. 2012 Oct;92(10):1440-50.

106. Trebicka J, Hennenberg M, Odenthal M, Shir K, Klein S, Granzow M, et al. Atorvastatin attenuates hepatic fibrosis in rats after bile duct ligation via decreased turnover of hepatic stellate cells. J Hepatol. 2010 Oct;53(4):702-12.

107. Abraldes JG, Rodríguez-Vilarrupla A, Graupera M, Zafra C, García-Calderó H, García-Pagán JC, et al. Simvastatin treatment improves liver sinusoidal endothelial dysfunction in CCl$_4$ cirrhotic rats. J Hepatol. 2007 Jun;46(6):1040-6.

108. Marrone G, Maeso-Díaz R, García-Cardena G, Abraldes JG, García-Pagán JC, Bosch J, et al. KLF2 exerts antifibrotic and vasoprotective effects in cirrhotic rat livers: Behind the molecular mechanisms of statins. Gut. 2015 Sep;64(9):1434-43.

109. Wang W, Zhao C, Zhou J, Zhen Z, Wang Y, Shen C. Simvastatin Ameliorates Liver Fibrosis via Mediating Nitric Oxide Synthase in Rats with Non-Alcoholic Steatohepatitis-Related Liver Fibrosis. PLoS One. 2013 Oct;8(10):e76538.

110. Rossoni LV, Wareing M, Wenceslau CF, Al-Abri M, Cobb C, Austin C. Acute simvastatin increases endothelial nitric oxide synthase phosphorylation via AMP-activated protein kinase and reduces contractility of isolated rat mesenteric resistance arteries. Clin Sci (Lond). 2011 Nov;121(10):449-58.

111. Trebicka J, Schierwagen R. Statins, Rho GTPases and KLF2: New mechanistic insight into liver fibrosis and portal hypertension. Gut. 2015 Sep;64(9):1349-50.

112. Liu Z, Zhang X, Xiao Q, Ye S, Lai CH, Luo J, et al. Pretreatment Donors after Circulatory Death with Simvastatin Alleviates Liver Ischemia Reperfusion Injury through a KLF2-Dependent Mechanism in Rat. Oxid Med Cell Longev. 2017;2017:3861914.

113. Kocak FE, Kucuk A, Ozyigit F, Tosun M, Kocak C, Kocak A, et al. Protective effects of simvastatin administered in the experimental hepatic ischemia-reperfusion injury rat model. J Surg Res. 2015 Dec;199(2):393-401.

114. Hide D, Warren A, Fernández-Iglesias A, Maeso-Díaz R, Peralta C, le Couteur DG, et al. Ischemia/reperfusion injury in the aged liver: The importance of the sinusoidal endothelium in developing therapeutic strategies for the elderly. J Gerontol A Biol Sci Med Sci. 2020 Jan;75(2):268-77.

115. Bravo M, Raurell I, Hide D, Fernández-Iglesias A, Gil M, Barberá A, et al. Restoration of liver sinusoidal cell phenotypes by statins improves portal hypertension and histology in rats with NASH. Sci Rep. 2019 Dec;9(1):20183.

116. Athyros VG, Alexandrides TK, Bilianou H, Cholongitas E, Doumas M, Ganotakis ES, et al. The use of statins alone, or in combination with pioglitazone and other drugs, for the treatment of non-alcoholic fatty liver disease/non-alcoholic steatohepatitis and related cardiovascular risk. An Expert Panel Statement. Metabolism. 2017 Jun;71:17-32.

117. Pastori D, Polimeni L, Baratta F, Pani A, del Ben M, Angelico F. The efficacy and safety of statins for the treatment of non-alcoholic fatty liver disease. Dig Liver Dis. 2015 Jan;47(1):4-11.

118. Moctezuma-Velázquez C, Abraldes JG, Montano-Loza AJ. The Use of Statins in Patients With Chronic Liver Disease and Cirrhosis. Curr Treat Options Gastroenterol. 2018 Jun;16(2):226-40.

119. Abraldes JG, Albillos A, Bañares R, Turnes J, González R, García-Pagán JC, et al. Simvastatin Lowers Portal Pressure in Patients With Cirrhosis and Portal Hypertension: A Randomized Controlled Trial. Gastroenterology. 2009 May;136(5):1651-8.

120. Zafra C, Abraldes JG, Turnes J, Berzigotti A, Fernández M, García-Pagán JC, et al. Simvastatin Enhances Hepatic Nitric Oxide Production and Decreases the Hepatic Vascular Tone in Patients with Cirrhosis. Gastroenterology. 2004 Mar;126(3):749-55.

121. Abraldes JG, Villanueva C, Aracil C, Turnes J, Hernandez-Guerra M, Genesca J, et al. Addition of Simvastatin to Standard Therapy for the Prevention of Variceal Rebleeding Does Not Reduce Rebleeding but Increases Survival in Patients with Cirrhosis. Gastroenterology. 2016 May;150(5):1160-70.e3.

122. Abd-Elsalam S, Elwan N, Salah R, Hamisa M, Shady E, Hawash N. Evaluation of portal pressure by doppler ultrasound in patients with cirrhosis before and after simvastatin administration - a randomized controlled trial. F1000Res. 2018 Mar;7:256.

123. Miao Q, Zeng X, Ma G, Li N, Liu Y, Luo T, et al. Simvastatin suppresses the proangiogenic microenvironment of human hepatic stellate cells via the Kruppel-like factor 2 pathway. Rev Esp Enferm Dig. 2015 Feb;107(2):63-71.

124. Sung S, Al-Karaghouli M, Kalainy S, Cabrera Garcia L, Abraldes JG. A systematic review on pharmacokinetics, cardiovascular outcomes and safety profiles of statins in cirrhosis. BMC Gastroenterol. 2021 Mar;21(1):120.

125. Orringer CE, Grant JK, Tokgozoglu L. A Review of Statin Intolerance: a Focus on Statin-Attributed Muscle Symptoms. Curr Atheroscler Rep. 2022 Nov;24(11):839-47.

126. Muñoz-Blanco A, Gómez-Huelgas R, Gómez-Cerezo JF. Statin-associated muscle symptoms: Myth or reality? Rev Clin Esp (Barc). 2022 Dec;222(10):602-11.

127. Camerino GM, Musumeci O, Conte E, Musaraj K, Fonzino A, Barca E, et al. Risk of myopathy in patients in therapy with statins: Identification of biological markers in a pilot study. Front Pharmacol. 2017 Jul;8:500.

128. Golomb BA, Evans MA. Statin adverse effects: A review of the literature and evidence for a mitochondrial mechanism. Am J Cardiovasc Drugs. 2008;8(6):373-418.

129. Janssen L, Allard NAE, Saris CGJ, Keijer J, Hopman MTE, Timmers S. Muscle toxicity of drugs: When drugs turn physiology into pathophysiology. Physiol Rev. 2020 Apr;100(2):633-72.

130. Pose E, Napoleone L, Amin A, Campion D, Jimenez C, Piano S, et al. Safety of two different doses of simvastatin plus rifaximin in decompensated cirrhosis (LIVERHOPE-SAFETY): a randomised, double-blind, placebo-controlled, phase 2 trial. Lancet Gastroenterol Hepatol. 2020 Jan;5(1):31-41.

131. Collins R, Reith C, Emberson J, Armitage J, Baigent C, Blackwell L, et al. Interpretation of the evidence for the efficacy and safety of statin therapy. Lancet. 2016 Nov;388(10059):2532-61.

132. Shu N, Hu M, Ling Z, Liu P, Wang F, Xu P, et al. The enhanced atorvastatin hepatotoxicity in diabetic rats was partly attributed to the upregulated hepatic Cyp3a and SLCO1B1. Sci Rep. 2016 Sep;6:33072.

133. Ward NC, Watts GF, Eckel RH. Statin Toxicity: Mechanistic Insights and Clinical Implications. Circ Res. 2019 Jan;124(2):328-50.

134. Yokoyama R, Ii M, Masuda M, Tabata Y, Hoshiga M, Ishizaka N, et al. Cardiac Regeneration by Statin-Polymer Nanoparticle-Loaded Adipose-Derived Stem Cell Therapy in Myocardial Infarction. Stem Cells Transl Med. 2019 Oct;8(10):1055-67.

135. Taymouri S, Ahmadi Z, Mirian M, Tavakoli N. Simvastatin nanosuspensions prepared using a combination of pH-sensitive and timed-release approaches for

potential treatment of colorectal cancer. Pharm Dev Technol. 2021 Mar;26(3):335-48.

136. Campos-Martorell M, Cano-Sarabia M, Simats A, Hernández-Guillamon M, Rosell A, Maspoch D, et al. Charge effect of a liposomal delivery system encapsulating simvastatin to treat experimental ischemic stroke in rats. Int J Nanomedicine. 2016 Jun;11:3035-48.

137. Yu Z, Guo J, Liu Y, Wang M, Liu Z, Gao Y, et al. Nano delivery of simvastatin targets liver sinusoidal endothelial cells to remodel tumor microenvironment for hepatocellular carcinoma. J Nanobiotechnology. 2022 Jan;20(1):9.

138. Najahi-Missaoui W, Arnold RD, Cummings BS. Safe nanoparticles: Are we there yet? Int J Mol Sci. 2020 Dec;22(1):385.

139. Mitchell MJ, Billingsley MM, Haley RM, Wechsler ME, Peppas NA, Langer R. Engineering precision nanoparticles for drug delivery. Nat Rev Drug Discov. 2021 Feb;20(2):101-24.

140. Weng J, Tong HHY, Chow SF. *In vitro* release study of the polymeric drug nanoparticles: Development and validation of a novel method. Pharmaceutics. 2020 Aug;12(8):732.

141. Patra JK, Das G, Fraceto LF, Campos EVR, Rodriguez-Torres MDP, Acosta-Torres LS, et al. Nano based drug delivery systems: Recent developments and future prospects. J Nanobiotechnology. 2018 Sep;16(1):71.

142. Rodríguez F, Caruana P, de la Fuente N, Español P, Gámez M, Balart J, et al. Nano-Based Approved Pharmaceuticals for Cancer Treatment: Present and Future Challenges. Biomolecules. 2022 Jun;12(6):784.

143. Davis ME, Chen Z, Shin DM. Nanoparticle therapeutics: An emerging treatment modality for cancer. Nat Rev Drug Discov. 2008 Sep;7(9):771-82.

144. Fang J, Nakamura H, Maeda H. The EPR effect: Unique features of tumor blood vessels for drug delivery, factors involved, and limitations and augmentation of the effect. Adv Drug Deliv Rev. 2011 Mar;63(3):136-51.

145. Owens DE, Peppas NA. Opsonization, biodistribution, and pharmacokinetics of polymeric nanoparticles. Int J Pharm. 2006 Jan;307(1):93-102.

146. Peracchia MT, Harnisch S, Pinto-Alphandary H, Gulik A, Dedieu JC, Desmaële D, et al. Visualization of *in vitro* protein-rejecting properties of PEGylated stealth polycyanoacrylate nanoparticles. Biomaterials. 1999 Jul;20(14):1269-75.

147. Oerlemans C, Bult W, Bos M, Storm G, Nijsen JFW, Hennink WE. Polymeric micelles in anticancer therapy: Targeting, imaging and triggered release. Pharm Res. 2010 Dec;27(12):2569-89.

148. Gener P, Gouveia LP, Sabat GR, de Sousa Rafael DF, Fort NB, Arranja A, et al. Fluorescent CSC models evidence that targeted nanomedicines improve treatment sensitivity of breast and colon cancer stem cells. Nanomedicine. 2015 Nov;11(8):1883-92.

149. Ghosh B, Biswas S. Polymeric micelles in cancer therapy: State of the art. J Control Release. 2021 Apr;332:127-47.

150. Surendran SP, Thomas RG, Moon MJ, Jeong YY. Nanoparticles for the treatment of liver fibrosis. Int J Nanomedicine. 2017 Sep;12:6997-7006.

151. Li Y, Pu S, Liu Q, Li R, Zhang J, Wu T, et al. An integrin-based nanoparticle that targets activated hepatic stellate cells and alleviates liver fibrosis. J Control Release. 2019 Jun;303:77-90.

152. Ribera J, Rodríguez-Vita J, Cordoba B, Portolés I, Casals G, Casals E, et al. Functionalized cerium oxide nanoparticles mitigate the oxidative stress and proinflammatory activity associated to the portal vein endothelium of cirrhotic rats. PLoS One. 2019 Jun;14(6):e0218716.

153. Duong HTT, Dong Z, Su L, Boyer C, George J, Davis TP, et al. The use of nanoparticles to deliver nitric oxide to hepatic stellate cells for treating liver fibrosis and portal hypertension. Small. 2015 May;11(19):2291-304.

154. Lin HL, Cheng WT, Chen LC, Ho HO, Lin SY, Hsieh CM. Honokiol/magnolol-loaded self-assembling lecithin-based mixed polymeric micelles (*lb*MPMs) for improving solubility to enhance oral bioavailability. Int J Nanomedicine. 2021 Jan;16:651-65.

155. Shen C, Zhu J, Song J, Wang J, Shen B, Yuan H, et al. Formulation of pluronic F127/TPGS mixed micelles to improve the oral absorption of glycyrrhizic acid. Drug Dev Ind Pharm. 2020 Jul;46(7):1100-7.

156. Kaur J, Gulati M, Jha NK, Disouza J, Patravale V, Dua K, et al. Recent advances in developing polymeric micelles for treating cancer: Breakthroughs and bottlenecks in their clinical translation. Drug Discov Today. 2022 May;27(5):1495-1512.

157. Figueiras A, Domingues C, Jarak I, Santos AI, Parra A, Pais A, et al. New Advances in Biomedical Application of Polymeric Micelles. Pharmaceutics. 2022 Aug;14(8):1700.

158. Arranja A, Schroder AP, Schmutz M, Waton G, Schosseler F, Mendes E. Cytotoxicity and internalization of Pluronic micelles stabilized by core cross-linking. J Control Release. 2014 Dec;196:87-95.

159. Kabanov AV, Batrakova EV, Alakhov VY. Pluronic® block copolymers as novel polymer therapeutics for drug and gene delivery. J Control Release. 2002 Aug;82(2-3):189-212.

160. Bodratti AM, Alexandridis P. Amphiphilic block copolymers in drug delivery: advances in formulation structure and performance. Expert Opin Drug Deliv. 2018 Nov;15(11):1085-104.

161. Ghezzi M, Pescina S, Padula C, Santi P, del Favero E, Cantù L, et al. Polymeric micelles in drug delivery: An insight of the techniques for their characterization and assessment in biorelevant conditions. J Control Release. 2021 Apr;332:312-36.

162. Zhang Y, Zhuo RX. Synthesis and *in vitro* drug release behavior of amphiphilic triblock copolymer nanoparticles based on poly (ethylene glycol) and polycaprolactone. Biomaterials. 2005 Nov;26(33):6736-42.

163. Pitto-Barry A, Barry NPE. Pluronic® block-copolymers in medicine: From chemical and biological versatility to rationalisation and clinical advances. Polym Chem. 2014 Mar;5:3291-7.

164. Singla P, Garg S, McClements J, Jamieson O, Peeters M, Mahajan RK. Advances in the therapeutic delivery and applications of functionalized Pluronics: A critical review. Adv Colloid Interface Sci. 2022 Jan;299:102563.

165. Chiappetta DA, Sosnik A. Poly(ethylene oxide)-poly(propylene oxide) block copolymer micelles as drug delivery agents: Improved hydrosolubility, stability and bioavailability of drugs. Eur J Pharm Biopharm. 2007 Jun;66(3):303-17.

166. Yu J, Qiu H, Yin S, Wang H, Li Y. Polymeric Drug Delivery System Based on Pluronics for Cancer Treatment. Molecules. 2021 Jun;26(12):3610.

167. Öztürk K, Arslan FB, Öztürk SC, Çalış S. Mixed micelles formulation for carvedilol delivery: In-vitro characterization and in-vivo evaluation. Int J Pharm. 2022 Jan;611:121294.

168. Shafiq A, Madni A, Khan S, Sultana H, Sumaira, Shah H, et al. Core-shell Pluronic F127/chitosan based nanoparticles for effective delivery of methotrexate in the management of rheumatoid arthritis. Int J Biol Macromol. 2022 Jul;213:465-77.

169. Rafael D, Gener P, Andrade F, Seras-Franzoso J, Montero S, Fernandez Y, et al. AKT2 siRNA delivery with amphiphilic-based polymeric micelles show efficacy against cancer stem cells. Drug Deliv. 2018 Nov;25(1):961-72.

170. Andrade F, Rafael D, Vilar-Hernández M, Montero S, Martínez-Trucharte F, Seras-Franzoso J, et al. Polymeric micelles targeted against CD44v6 receptor increase niclosamide efficacy against colorectal cancer stem cells and reduce circulating tumor cells *in vivo*. J Control Release. 2021 Mar;331:198-212.

171. Mahmud A, Xiong XB, Aliabadi HM, Lavasanifar A. Polymeric micelles for drug targeting. J Drug Target. 2007 Nov;15(9):553-84.

172. Sahay G, Alakhova DY, Kabanov AV. Endocytosis of nanomedicines. J Control Release. 2010 Aug;145(3):182-95.

173. Sahay G, Batrakova EV, Kabanov AV. Different internalization pathways of polymeric micelles and unimers and their effects on vesicular transport. Bioconjug Chem. 2008 Oct;19(10):2023-9.

174. Torchilin VP. Cell penetrating peptide-modified pharmaceutical nanocarriers for intracellular drug and gene delivery. Biopolymers. 2008 Sep;90(5):604-10.

175. Nag OK, Delehanty JB. Active cellular and subcellular targeting of nanoparticles for drug delivery. Pharmaceutics. 2019 Oct;11(10):543.

176. Majumdar S, Siahaan TJ. Peptide-mediated targeted drug delivery. Med Res Rev. 2012 May;32(3):637-58.

177. Jiang Z, Guan J, Qian J, Zhan C. Peptide ligand-mediated targeted drug delivery of nanomedicines. Biomater Sci. 2019 Jan;7(2):461-71.

178. Drucker DJ. Advances in oral peptide therapeutics. Nat Rev Drug Discov. 2020 Apr;19(4):277-89.

179. Veri MC, Gorlatov S, Li H, Burke S, Johnson S, Stavenhagen J, et al. Monoclonal antibodies capable of discriminating the human inhibitory Fcγ-receptor IIB (CD32B) from the activating Fcγ-receptor IIA (CD32A): Biochemical, biological and functional characterization. Immunology. 2007 Jul;121(3):392-404.

180. Medgyesi D, Uray K, Sallai K, Hudecz F, Koncz G, Abramson J, et al. Functional mapping of the FcγRII binding site on human IgG1 by synthetic peptides. Eur J Immunol. 2004 Apr;34(4):1127-35.

181. March S, Hui EE, Underhill GH, Khetani S, Bhatia SN. Microenvironmental regulation of the sinusoidal endothelial cell phenotype *in vitro*. Hepatology. 2009 Sep;50(3):920-8.

182. Ohmura T, Enomoto K, Satoh H, Sawada N, Mori M. Establishment of a Novel Monoclonal Antibody, SE-1, Which Specifically Reacts with Rat Hepatic Sinusoidal Endothelial Cells. J Histochem Cytochem. 1993 Aug;41(8):1253-7.

183. Géraud C, Schledzewski K, Demory A, Klein D, Kaus M, Peyre F, et al. Liver sinusoidal endothelium: A microenvironment-dependent differentiation program in rat including the novel junctional protein liver endothelial differentiation-associated protein-1. Hepatology. 2010 Jul;52(1):313-26.

184. Rada P, González-Rodríguez Á, García-Monzón C, Valverde ÁM. Understanding lipotoxicity in NAFLD pathogenesis: is CD36 a key driver? Cell Death Dis. 2020 Sep;11(9):802.

185. Liu J, Yang P, Zuo G, He S, Tan W, Zhang X, et al. Long-chain fatty acid activates hepatocytes through CD36 mediated oxidative stress. Lipids Health Dis. 2018 Jul;17(1):153.

186. Scoazec JY, Feldmann G. *In situ* immunophenotyping study of endothelial cells of the human hepatic sinusoid: Results and functional implications. Hepatology. 1991 Nov;14(5):789-97.

187. Scoazec JY, Feldmann G. The cell adhesion molecules of hepatic sinusoidal endothelial cells. J Hepatol. 1994 Feb;20(2):296-300.

188. Couvelard A, Scoazec JY, Feldmann G. Expression of Cell-Cell and Cell-Matrix Adhesion Proteins by Sinusoidal Endothelial Cells in the Normal and Cirrhotic Human Liver. Am J Pathol. 1993 Sep;143(3):738-52.

189. Sun F, Wang J, Sun Q, Li F, Gao H, Xu L, et al. Interleukin-8 promotes integrin β3 upregulation and cell invasion through PI3K/Akt pathway in hepatocellular carcinoma. J Exp Clin Cancer Res. 2019 Nov;38(1):449.

190. Giancotti FG, Ruoslahti E. Integrin Signaling. Science. 1999 Aug;285(5430):1028-32.

191. Li F, Song Z, Li Q, Wu J, Wang J, Xie C, et al. Molecular imaging of hepatic stellate cell activity by visualization of hepatic integrin αvβ3 expression with SPECT in rat. Hepatology. 2011 Sep;54(3):1020-30.

192. Beer AJ, Schwaiger M. Imaging of integrin αvβ3 expression. Cancer Metastasis Rev. 2008 Dec;27(4):631-44.

193. Turaga RC, Satyanarayana G, Sharma M, Yang JJ, Wang S, Liu C, et al. Targeting integrin αvβ3 by a rationally designed protein for chronic liver disease treatment. Commun Biol. 2021 Sep;4(1):1087.

194. Zhou X, Murphy FR, Gehdu N, Zhang J, Iredale JP, Benyon RC. Engagement of $\alpha_V\beta_3$ integrin regulates proliferation and apoptosis of hepatic stellate cells. J Biol Chem. 2004 Jun 4;279(23):23996-4006.

195. Patsenker E, Popov Y, Stickel F, Schneider V, Ledermann M, Sägesser H, et al. Pharmacological inhibition of integrin alphaV beta3 aggravates experimental liver fibrosis and suppresses hepatic angiogenesis. Hepatology. 2009 Nov;50(5):1501-11.

196. Ahmed F, Alexandridis P, Neelamegham S. Synthesis and application of fluorescein-labeled pluronic block copolymers to the study of polymer-surface interactions. Langmuir. 2001 Jan;17(2):537-46.

197. Uray K, Medgyesi D, Hilbert Á, Sármay G, Gergely J, Hudecz F. Synthesis and receptor binding of IgG1 peptides derived from the IgG Fc region. J Mol Recognit. 2004 Feb;17(2):95-105.

198. Hulett MD, Witort E, Brinkworth RI, McKenzie IF, Hogarth PM. Multiple regions of human FcγRII (CD32) contribute to the binding of IgG. J Biol Chem. 1995 Sep;270(36):21188-94.

199. Muro H, Shirasawa H, Kosugi I, Nakamurat S. Defect of Fc Receptors and Phenotypical Changes in Sinusoidal Endothelial Cells in Human Liver Cirrhosis. Am J Pathol. 1993 Jul;143(1):105-20.

200. Li WX, Howard RJ, Leung LL. Identification of SVTCG in Thrombospondin as the Conformation-dependent, High Affinity Binding Site for Its Receptor, CD36. J Biol Chem. 1993 Aug;268(22):16179-84.

201. Leung LL, Li WX, McGregor JL, Albrecht G, Howard RJ. CD36 Peptides Enhance or Inhibit CD36-Thrombospondin Binding. A Two-Step Process of Ligand-Receptor Interaction. J Biol Chem. 1992 Sep;267(25):18244-50.

202. Febbraio M, Hajjar DP, Silverstein RL. CD36: a class B scavenger receptor involved in angiogenesis, atherosclerosis, inflammation, and lipid metabolism. J Clin Invest. 2001 Sep;108(6):785-91.

203. Kar NS, Ashraf MZ, Valiyaveettil M, Podrez EA. Mapping and characterization of the binding site for specific oxidized phospholipids and oxidized low density lipoprotein of scavenger receptor CD36. J Biol Chem. 2008 Mar;283(13):8765-71.

204. Baruch DI, Ma XC, Pasloske B, Howard RJ, Miller LH. CD36 Peptides That Block Cytoadherence Define the CD36 Binding Region for *Plasmodium falciparum*-Infected Erythrocytes. Blood. 1999 Sep;94(6):2121-7.

205. Song Z, Lin Y, Zhang X, Feng C, Lu Y, Gao Y, et al. Cyclic RGD peptide-modified liposomal drug delivery system for targeted oral apatinib administration: Enhanced cellular uptake and improved therapeutic effects. Int J Nanomedicine. 2017 Mar;12:1941-58.

206. Singh SR, Grossniklaus HE, Kang SJ, Edelhauser HF, Ambati BK, Kompella UB. Intravenous transferrin, RGD peptide and dual-targeted nanoparticles enhance anti-VEGF intraceptor gene delivery to laser-induced CNV. Gene Ther. 2009 May;16(5):645-59.

207. Schaffert D, Badgujar N, Wagner E. Novel Fmoc-polyamino acids for solid-phase synthesis of defined polyamidoamines. Org Lett. 2011 Apr;13(7):1586-9.

208. Duro-Castano A, Conejos-Sánchez I, Vicent MJ. Peptide-based polymer therapeutics. Polymers. 2014 Feb;6:515-51.

209. Cistrone PA, Bird MJ, Flood DT, Silvestri AP, Hintzen JCJ, Thompson DA, et al. Native Chemical Ligation of Peptides and Proteins. Curr Protoc Chem Biol. 2019 Mar;11(1):e61.

210. D'Souza S. A Review of *In Vitro* Drug Release Test Methods for Nano-Sized Dosage Forms. Adv Pharm. 2014 Nov;2014:304757.

211. Kleiner DE, Brunt EM, van Natta M, Behling C, Contos MJ, Cummings OW, et al. Design and validation of a histological scoring system for nonalcoholic fatty liver disease. Hepatology. 2005 Jun;41(6):1313-21.

212. Zhu K, Zhao F, Yang Y, Mu W. Effects of simvastatin loaded PLGA microspheres on treatment of rats with intervertebral disk degeneration and on 6-K-PGF1α and HIF-1α. Exp Ther Med. 2020 Jan;19(1):579-84.

213. Wang CZ, Fu YC, Jian SC, Wang YH, Liu PL, Ho ML, et al. Synthesis and characterization of cationic polymeric nanoparticles as simvastatin carriers for enhancing the osteogenesis of bone marrow mesenchymal stem cells. J Colloid Interface Sci. 2014 Oct;432:190-9.

214. Samkange T, D'Souza S, Obikeze K, Dube A. Influence of PEGylation on PLGA nanoparticle properties, hydrophobic drug release and interactions with human serum albumin. J Pharm Pharmacol. 2019 Oct;71(10):1497-1507.

215. Hassan R, Tammam SN, El Safy S, Abdel-Halim M, Asimakopoulou A, Weiskirchen R, et al. Prevention of hepatic stellate cell activation using JQ1- and atorvastatin-loaded chitosan nanoparticles as a promising approach in therapy of liver fibrosis. Eur J Pharm Biopharm. 2019 Jan;134:96-106.

216. Bartneck M, Warzecha KT, Tacke F. Therapeutic targeting of liver inflammation and fibrosis by nanomedicine. Hepatobiliary Surg Nutr. 2014 Dec;3(6):364-76.

217. Liu Q, Wang X, Liu X, Liao YP, Chang CH, Mei KC, et al. Antigen- And Epitope-Delivering Nanoparticles Targeting Liver Induce Comparable Immunotolerance in Allergic Airway Disease and Anaphylaxis as Nanoparticle-Delivering Pharmaceuticals. ACS Nano. 2021 Jan;15(1):1608-26.

218. Carambia A, Gottwick C, Schwinge D, Stein S, Digigow R, Şeleci M, et al. Nanoparticle-mediated targeting of autoantigen peptide to cross-presenting liver sinusoidal endothelial cells protects from CD8 T-cell-driven autoimmune cholangitis. Immunology. 2021 Apr;162(4):452-63.

219. Carambia A, Freund B, Schwinge D, Bruns OT, Salmen SC, Ittrich H, et al. Nanoparticle-based autoantigen delivery to Treg-inducing liver sinusoidal endothelial cells enables control of autoimmunity in mice. J Hepatol. 2015 Jun;62(6):1349-56.

220. Yu X, Chen L, Liu J, Dai B, Xu G, Shen G, et al. Immune modulation of liver sinusoidal endothelial cells by melittin nanoparticles suppresses liver metastasis. Nat Commun. 2019 Feb;10(1):574.

221. Zhang LF, Wang XH, Zhang CL, Lee J, Duan BW, Xing L, et al. Sequential Nano-Penetrators of Capillarized Liver Sinusoids and Extracellular Matrix Barriers for Liver Fibrosis Therapy. ACS Nano. 2022 Sep;16(9):14029-42.

222. Thalheimer U, Triantos CK, Samonakis DN, Patch D, Burroughs AK. Infection, coagulation, and variceal bleeding in cirrhosis. Gut. 2005 Apr;54(4):556-63.

223. Kumar V, Mundra V, Peng Y, Wang Y, Tan C, Mahato RI. Pharmacokinetics and biodistribution of polymeric micelles containing miRNA and small-molecule drug in orthotopic pancreatic tumor-bearing mice. Theranostics. 2018 Jul;8(15):4033-49.

224. Anderson CL. The liver sinusoidal endothelium reappears after being eclipsed by the Kupffer cell: a 20th century biological delusion corrected. J Leukoc Biol. 2015 Dec;98(6):875-6.

225. Bhattacharjee S. DLS and zeta potential - What they are and what they are not? J Control Release. 2016 Aug;235:337-51.

226. Basak R, Bandyopadhyay R. Encapsulation of hydrophobic drugs in Pluronic F127 micelles: Effects of drug hydrophobicity, solution temperature, and pH. Langmuir. 2013 Apr;29(13):4350-6.

227. Couturier J, Nuotio-Antar AM, Agarwal N, Wilkerson GK, Saha P, Kulkarni V, et al. Lymphocytes upregulate CD36 in adipose tissue and liver. Adipocyte. 2019 Dec;8(1):154-63.

228. Cogger VC, Hilmer SN, Sullivan D, Muller M, Fraser R, le Couteur DG. Hyperlipidemia and surfactants: The liver sieve is a link. Atherosclerosis. 2006 Dec;189(2):273-81.

229. Mariotti V, Strazzabosco M, Fabris L, Calvisi DF. Animal models of biliary injury and altered bile acid metabolism. Biochim Biophys Acta Mol Basis Dis. 2018 Apr;1864(4 Pt B):1254-61.

230. Königshofer P, Brusilovskaya K, Schwabl P, Reiberger T. Animal models of portal hypertension. Biochim Biophys Acta Mol Basis Dis. 2019 May;1865(5):1019-30.

231. Ferreira LG, dos Santos RN, Oliva G, Andricopulo AD. Molecular docking and structure-based drug design strategies. Molecules. 2015 Jul;20(7):13384-421.

10. APPENDIX

10. APPENDIX

10.1. Buffers and reagents

Sirius Red staining

0.1% Picro-Sirius Red (500 ml):

- 500 ml saturated aqueous solution of picric acid (1.3% in H_2O)

- 0.5 g Direct Red 80 (0.36 mM) (Sigma-Aldrich, Merck KGaA, Germany)

Store at RT (highly explosive; can be reused several times).

Acidified water (1 L):

- 995 ml dH_2O

- 5 ml glacial acetic acid

Isolation and culture of primary liver cells

Hanks 10X (1 L):

- 80 g sodium chloride (NaCl) (1.4 M)

- 4 g potassium chloride (KCl) (0.05 M)

- 2 g magnesium sulfate heptahydrate ($MgSO_4 \cdot 7H_2O$) (0.01 M)

- 0.6 g potassium dihydrogen phosphate (KH_2PO_4) (4.38 mM)

- 0.43 g disodium hydrogen phosphate (Na_2HPO_4) (3 mM)

- dH_2O upon 1 L

Store at RT.

Hanks HEPES (625 ml):

- 62.5 ml Hanks 10X

- 1.31 g sodium hydrogencarbonate ($NaHCO_3$) (25 mM)

- 1.875 g 2-[4-(2-hydroxyethyl)piperazin-1-yl]ethane-1-sulfonic acid (HEPES) (12 mM)*

- dH_2O upon 625 ml

Gas with carbogen (95% O_2, 5% CO_2) for 20 min (* add HEPES while gassing the buffer).

Adjust pH to 7.4 (7.39-7.45).

Hanks I buffer (250 ml):

- 250 ml Hanks HEPES

- 4 g BSA (0.23 mM)

- 0.057 g egtazic acid (EGTA) (0.6 mM)

- 0.9 ml 1% heparin*

Filter through a 100 µm filter.

Divide Hanks I buffer into 4 centrifuge tubes of 50 ml each (* add 0.9 ml of 1% heparin into the two first centrifuge tubes, 0.5 ml to the first tube and 0.4 ml to the second tube, just before starting the perfusion).

Leave in a water bath at 37 ºC.

Hanks II buffer (300 ml):

- 300 ml Hanks HEPES

- 0.175 g calcium chloride dihydrate ($CaCl_2 \cdot 2H_2O$) (4 mM)

Filter through a 100 µm filter.

Divide Hanks II buffer into an Erlenmeyer flask (200 ml), left in a water bath at 37 ºC for *in vivo* digestion, and a jar (100 ml), left in an incubator at 37 ºC for *ex vivo* digestion.

Krebs 4X (1 L):

- 27.6 g NaCl (0.5 M)

- 8 g $NaHCO_3$ (0.01 M)

- 1.44 g KCl (0.02 M)

- 1.18 g $MgSO_4 \cdot 7H_2O$ (7 mM)

- 0.54 g KH_2PO_4 (4 mM)

- dH$_2$O upon 1 L

Store at RT.

Krebs' buffer (250 ml):

- 62.5 ml Krebs 4X

- 0.093 g CaCl$_2$·2H$_2$O (2.5 mM)

- 1.5 g HEPES (25 mM)*

- dH$_2$O upon 250 ml

Gas with carbogen (95% O$_2$, 5% CO$_2$) for 20 min (* add HEPES while gassing the buffer).

Adjust pH to 7.4 (7.39-7.45).

Leave at 4 ºC.

Filter through a 100 µm filter just before use.

Completed RPMI medium (500 ml):

- 440 ml RPMI 1640 Medium (Biowest, France)

- 50 ml FBS (10%) (Biowest, France)

- 5 ml penicillin-streptomycin (1%) (Biowest, France)

- 5 ml L-glutamine (1%) (Thermo Fisher Scientific, USA)

Supplemented RPMI medium (50 ml):

- 48.5 ml completed RPMI medium

- 0.5 ml amphotericin B (1%) (Labclinics, S.A, Barcelona, Spain)

- 0.5 ml heparin sodium 10 mg/ml (0.1 mg/ml) (Sigma-Aldrich, Merck KGaA, Germany)

- 0.5 ml endothelial cell growth supplement 5 mg/ml (0.05 mg/ml) (Sigma-Aldrich, Merck KGaA, Germany)

Acetic acid 20 mM (50 ml):

- 57 µl glacial acetic acid

- dH$_2$O upon 50 ml

Collagen solution 100 µg/ml (50 ml):

- 47.5 ml acetic acid 20 mM

- 2.5 ml Collagen R solution 0.2 % (SERVA, Heidelberg, Germany)

Completed DMEM medium (500 ml):

- 480 ml DMEM/F-12 (Gibco™, Thermo Fisher Scientific, USA)

- 10 ml FBS (2%)

- 5 ml penicillin-streptomycin (1%)

- 5 ml L-glutamine (1%)

Supplemented DMEM medium (50 ml):

- 45.5 ml completed DMEM medium

- 4 ml FBS (10%)

- 0.5 ml amphotericin B (1%)

- 5 µl dexamethasone 10 mM (1 µM) (Sigma-Aldrich, Merck KGaA, Germany)

- 1 µl insulin 10 mg/ml (0.0002 mg/ml)

Maintenance DMEM medium (50 ml):

- 49.5 ml completed DMEM medium

- 0.5 ml amphotericin B (1%)

- 5 µl dexamethasone 10 µM (1 nM)

- 1 µl insulin 10 mg/ml (0.0002 mg/ml)

Completed IMDM medium (500 ml):

- 440 ml IMDM (Biowest, France)

- 50 ml FBS (10%)

- 5 ml penicillin-streptomycin (1%)

- 5 ml L-glutamine (1%)

Supplemented IMDM medium (50 ml):

- 49.5 ml completed IMDM medium

- 0.5 ml amphotericin B (1%)

SEM

PB 0.2 M:

- 19 ml Buffer A: 13.65 g sodium dihydrogen phosphate (NaH_2PO_4) in 500 ml dH_2O (store at 4 ºC)

- 81 ml Buffer B: 17.8 g disodium hydrogen phosphate dihydrate ($Na_2HPO_4 \cdot 2H_2O$) in 500 ml dH_2O (store at RT protected from light)

Adjust pH to 7.38.

Store at 4 ºC.

Standard fixative (10 ml):

- 5 ml PB 0.2 M

- 3 ml dH_2O

- 1 ml 20% PFA

- 1 ml 25% glutaraldehyde

Store at 4 ºC (up to 1 week).

Maintenance fixative (10 ml):

- 5 ml PB 0.2 M

- 4.5 ml dH$_2$O

- 0.5 ml 20% PFA

Store at 4 ºC (up to 2 months).

Western blot

RIPA lysis and extraction buffer (10 ml):

- 10 ml RIPA Lysis and Extraction Buffer (Thermo Scientific™, Thermo Fisher Scientific, USA)

- 1 tablet cOmplete™ ULTRA Tablets, Mini, *EASY*pack (Roche, Merck KGaA, Gemany)

- 1 tablet PhosSTOP™ *EASY*pack as Protease Inhibitor Cocktail (Roche, Merck KGaA, Germany)

Store at -20 ºC.

Running buffer 1X (1 L):

- 950 ml dH$_2$O

- 50 ml NuPAGE® MES SDS Running Buffer (20X) (Invitrogen™, Thermo Fisher Scientific, USA)

Store at 4 ºC.

Running buffer for gel electrophoresis (200 ml):

- 200 ml running buffer 1X

- 500 µl NuPAGE® Antioxidant (Invitrogen™, Thermo Fisher Scientific, USA)

Transfer buffer (1 L):

- 849 ml dH$_2$O

- 100 ml methanol

- 50 ml NuPAGE® Transfer Buffer (20X) (Invitrogen™, Thermo Fisher Scientific, USA)

- 1 ml NuPAGE® Antioxidant

Store at 4 ºC.

Tris-buffered saline (TBS) 10X (1 L):

- 80 g NaCl (1.4 M)

- 40 g Trizma® hydrochloride (Tris HCl) (254 mM) (Sigma-Aldrich, Merck KGaA, Germany)

- 2 g KCl (27 mM)

- dH$_2$O upon 1 L

Adjust pH to 7.6.

Store at RT.

TTBS 1X (1 L):

- 899 ml dH$_2$O

- 100 ml TBS 10X

- 1 ml Tween® 20 (Sigma-Aldrich, Merck KGaA, Germany) (add in agitation)

Store at RT.

10.2. Fellowship and funding

10.3. Publication

This doctoral thesis has resulted in the following publication:

Hide D, Gil M, Andrade F, Rafael D, Raurell I, Bravo M, Barberá A, Gracia-Sancho J, Vargas V, Augustin S, Genescà J, Schwartz S Jr, Martell M. Simvastatin-loaded polymeric micelles are more effective and less toxic than conventional statins in a pre-clinical model of advanced chronic liver disease. Nanomedicine. 2020 Oct;29:102267. DOI: 10.1016/j.nano.2020.102267. https://doi.org/10.1016/j.nano.2020.102267

Hide D, Gil M, Andrade F, Rafael D, Raurell I, Bravo M, Barberá A, Gracia-Sancho J, Vargas V, Augustin S, Genescà J, Schwartz S Jr, Martell M. Simvastatin-loaded polymeric micelles are more effective and less toxic than conventional statins in a pre-clinical model of advanced chronic liver disease. Nanomedicine. 2020 Oct;29:102267. DOI: 10.1016/j.nano.2020.102267. https://doi.org/10.1016/j.nano.2020.102267

Hide D, Gil M, Andrade F, Rafael D, Raurell I, Bravo M, Barberá A, Gracia-Sancho J, Vargas V, Augustin S, Genescà J, Schwartz S Jr, Martell M. Simvastatin-loaded polymeric micelles are more effective and less toxic than conventional statins in a pre-clinical model of advanced chronic liver disease. Nanomedicine. 2020 Oct;29:102267. DOI: 10.1016/j.nano.2020.102267. https://doi.org/10.1016/j.nano.2020.102267

Hide D, Gil M, Andrade F, Rafael D, Raurell I, Bravo M, Barberá A, Gracia-Sancho J, Vargas V, Augustin S, Genescà J, Schwartz S Jr, Martell M. Simvastatin-loaded polymeric micelles are more effective and less toxic than conventional statins in a pre-clinical model of advanced chronic liver disease. Nanomedicine. 2020 Oct;29:102267. DOI: 10.1016/j.nano.2020.102267. https://doi.org/10.1016/j.nano.2020.102267

Hide D, Gil M, Andrade F, Rafael D, Raurell I, Bravo M, Barberá A, Gracia-Sancho J, Vargas V, Augustin S, Genescà J, Schwartz S Jr, Martell M. Simvastatin-loaded polymeric micelles are more effective and less toxic than conventional statins in a pre-clinical model of advanced chronic liver disease. Nanomedicine. 2020 Oct;29:102267. DOI: 10.1016/j.nano.2020.102267. https://doi.org/10.1016/j.nano.2020.102267

Hide D, Gil M, Andrade F, Rafael D, Raurell I, Bravo M, Barberá A, Gracia-Sancho J, Vargas V, Augustin S, Genescà J, Schwartz S Jr, Martell M. Simvastatin-loaded polymeric micelles are more effective and less toxic than conventional statins in a pre-clinical model of advanced chronic liver disease. Nanomedicine. 2020 Oct;29:102267. DOI: 10.1016/j.nano.2020.102267. https://doi.org/10.1016/j.nano.2020.102267

Hide D, Gil M, Andrade F, Rafael D, Raurell I, Bravo M, Barberá A, Gracia-Sancho J, Vargas V, Augustin S, Genescà J, Schwartz S Jr, Martell M. Simvastatin-loaded polymeric micelles are more effective and less toxic than conventional statins in a pre-clinical model of advanced chronic liver disease. Nanomedicine. 2020 Oct;29:102267. DOI: 10.1016/j.nano.2020.102267. https://doi.org/10.1016/j.nano.2020.102267

Hide D, Gil M, Andrade F, Rafael D, Raurell I, Bravo M, Barberá A, Gracia-Sancho J, Vargas V, Augustin S, Genescà J, Schwartz S Jr, Martell M. Simvastatin-loaded polymeric micelles are more effective and less toxic than conventional statins in a pre-clinical model of advanced chronic liver disease. Nanomedicine. 2020 Oct;29:102267. DOI: 10.1016/j.nano.2020.102267. https://doi.org/10.1016/j.nano.2020.102267

Hide D, Gil M, Andrade F, Rafael D, Raurell I, Bravo M, Barberá A, Gracia-Sancho J, Vargas V, Augustin S, Genescà J, Schwartz S Jr, Martell M. Simvastatin-loaded polymeric micelles are more effective and less toxic than conventional statins in a pre-clinical model of advanced chronic liver disease. Nanomedicine. 2020 Oct;29:102267. DOI: 10.1016/j.nano.2020.102267. https://doi.org/10.1016/j.nano.2020.102267

Hide D, Gil M, Andrade F, Rafael D, Raurell I, Bravo M, Barberá A, Gracia-Sancho J, Vargas V, Augustin S, Genescà J, Schwartz S Jr, Martell M. Simvastatin-loaded polymeric micelles are more effective and less toxic than conventional statins in a pre-clinical model of advanced chronic liver disease. Nanomedicine. 2020 Oct;29:102267. DOI: 10.1016/j.nano.2020.102267. https://doi.org/10.1016/j.nano.2020.102267

Hide D, Gil M, Andrade F, Rafael D, Raurell I, Bravo M, Barberá A, Gracia-Sancho J, Vargas V, Augustin S, Genescà J, Schwartz S Jr, Martell M. Simvastatin-loaded polymeric micelles are more effective and less toxic than conventional statins in a pre-clinical model of advanced chronic liver disease. Nanomedicine. 2020 Oct;29:102267. DOI: 10.1016/j.nano.2020.102267. https://doi.org/10.1016/j.nano.2020.102267

Hide D, Gil M, Andrade F, Rafael D, Raurell I, Bravo M, Barberá A, Gracia-Sancho J, Vargas V, Augustin S, Genescà J, Schwartz S Jr, Martell M. Simvastatin-loaded polymeric micelles are more effective and less toxic than conventional statins in a pre-clinical model of advanced chronic liver disease. Nanomedicine. 2020 Oct;29:102267. DOI: 10.1016/j.nano.2020.102267. https://doi.org/10.1016/j.nano.2020.102267

Hide D, Gil M, Andrade F, Rafael D, Raurell I, Bravo M, Barberá A, Gracia-Sancho J, Vargas V, Augustin S, Genescà J, Schwartz S Jr, Martell M. Simvastatin-loaded polymeric micelles are more effective and less toxic than conventional statins in a pre-clinical model of advanced chronic liver disease. Nanomedicine. 2020 Oct;29:102267. DOI: 10.1016/j.nano.2020.102267. https://doi.org/10.1016/j.nano.2020.102267